

Novel roles of the *C. elegans* central apoptotic pathway in asymmetric cell division

DISSERTATION ZUR ERLANGUNG DES DOKTORGRADES DER
NATURWISSENSCHAFTEN DOCTOR RERUM NATURALIUM (DR. RER. NAT.)
AN DER FAKULTÄT FÜR BIOLOGIE DER
LUDWIG-MAXIMILIANS-UNIVERSITÄT MÜNCHEN



Nikhil Mishra

29.08.2019

-
- 1. Gutachter:** Prof. Dr. Barbara Conradt
 - 2. Gutachter:** Prof. Dr. Christof Osman

Tag der Abgabe: 29.08.2019

Tag der mündlichen Prüfung: 25.11.2019

Eidesstattliche Versicherung

Ich versichere hiermit an Eides statt, dass die vorgelegte Dissertation mit dem Titel ‘Novel roles of the *C. elegans* central apoptotic pathway in asymmetric cell division’ von mir selbständig und ohne unerlaubte Hilfe angefertigt ist.

Nikhil Mishra (München. den 29.08.2019)

Erklärung

Hiermit erkläre ich, dass die Dissertation mit dem Titel ‘Novel roles of the *C. elegans* central apoptotic pathway in asymmetric cell division’ nicht ganz oder in wesentlichen Teilen einer anderen Prüfungskommission vorgelegt worden ist. Ich habe mich nicht anderweitig einer Doktorprüfung ohne Erfolg unterzogen.

Nikhil Mishra (München. den 29.08.2019)

Publication originating from this work

Mishra, N., et al. (2018). *Caenorhabditis elegans ced-3* Caspase is required for asymmetric divisions that generate cells programmed to die. *Genetics* **210**(3): 983.

Acknowledgements

As is often said, a tree owes its growth to water from multiple rainfalls. Therefore, to begin with, it is important that I acknowledge the fact that many people have contributed to the process that reaches a key milestone today with the submission of this doctoral thesis. It is humanly impossible to mention each and every contributor here. So, I write this with a realization that I will unfortunately miss a few significant names.

First, I would like to thank Barbara, who has been a source of constant support, guidance and encouragement for me. I still remember how motivated I was to join her lab for my doctorate when I came across a paper describing a ‘negative’ result from her lab. The motivation stemmed from her willingness to publish even negative results, which showed that she respected the effort each stakeholder had put in that study. The initial phase of my doctoral study was tough since almost none of my experiments used to work. Barbara, however, stuck with me and guided me out of that difficult phase, which reinforced my belief in the idea that she watched out for her students; that results did matter, but efforts mattered even more. I shall always be grateful to her for not only helping me grow as a scientist, but also for setting an example for how a leader should conduct him/herself.

My thesis advisory committee meetings with Hendrik Korswagen, Ilona Grunwald Kadow and Thomas Ott were always very insightful and played a significant role in advancing my work.

Further, I would like to thank Sayantan and Ryan, who helped me with both scientific and non-scientific aspects of my stay here in Munich on several occasions while they were in the lab and have still continued to do so now when they are not. Simon, Fabian, Laura, Jennifer, Elisabeth, Jimei and Adi, among others, have always been awesome company. It was never anything but fun to hang out with them, especially during meals. All members of the lab I have overlapped with together created a positive atmosphere, which made working in the lab something I looked forward to most mornings.

The LSM graduate school organized and sponsored several courses, workshops, and my conference visits, which aided my scientific development. Francisca was always available and

ready to help. On a couple of occasions, in fact, her offer to help preceded my realization for a need for it.

Two of my closest friends, Amrita and Bikash, were always encouraging. Without even one of them, this day would probably not be possible. My family – my mom, dad, brother, uncle and grandma – has contributed significantly to this thesis. They have all sacrificed different necessities and pleasures in their lives so as to enable me to achieve my goal today. It is difficult to articulate how thankful I am to them, but their being with me has made an indelible impression on my life and career.

I would also like to thank all my teachers from all stages of my academic career. Many of them were also extremely generous in making resources available to me, especially in some cases where they were difficult for me to afford. I would not be me, as a person, without any single one of them and I cannot thank them enough. Finally, I would like to thank everyone who has made a positive contribution to my life and career, but whom I may have missed mentioning here.

Contents

Eidesstattliche Versicherung.....	ii
Erklärung	ii
Publication originating from this work	iii
Acknowledgements	iv
ABSTRACT.....	1
Chapter I: INTRODUCTION	5
1.1 Programmed Cell Death.....	6
1.2 <i>Caenorhabditis elegans</i> is an excellent model organism to study programmed cell death .	7
1.2.1 <i>C. elegans</i> as a model to study development.....	7
1.2.2 <i>C. elegans</i> as a model to study programmed cell death	9
1.3 The corpse engulfment pathways in <i>C. elegans</i>	11
1.4 Engulfment genes promote apoptosis	13
1.5 Apoptosis and asymmetric cell division are functionally linked.....	15
Chapter II: MATERIALS AND METHODS	19
2.1 Strains and genetics.....	20
2.2 Plasmid construction	20
2.2.1 pBC1565 ($P_{toe-2gfp}$).....	20
2.2.2 pBC1591 ($P_{hyp7gfp}$) and pBC1681 ($P_{hyp7ced-1::gfp}$)	20
2.2.3 pBC1805 ($P_{toe-2ced-1::mKate2}$).....	21
2.2.4 pBC1807 ($P_{toe-2mKate2::tac-1}$)	21
2.3 Microinjection and plasmid integration	23
2.3.1 <i>bcIs133</i> ($P_{toe-2gfp}$)	23

2.3.2	<i>bcEx1277</i> ($P_{hyp7ced-1::gfp}$)	23
2.3.3	<i>bcEx1334</i> ($P_{toe-2ced-1::mKate2}$)	23
2.3.4	<i>bcSi82</i> ($P_{toe-2mKate2::tac-1}$)	23
2.4	PVM neuron counting	24
2.5	CED-1 localization	24
2.6	Live imaging of QL.a and QL.p divisions	24
2.7	QL.pp survival	24
2.8	QL.pp division	25
2.9	Embryonic lethality	25
2.10	Cell area measurements	25
2.11	Cleavage furrow position	27
2.12	mKate2::TAC-1 ratio	27
2.13	NSM neuroblast daughter cell sizes	28
2.14	NMY-2::GFP quantification	28
2.15	Metaphase plate position	28
2.16	Anaphase chromosome migration	29
2.17	Statistical tests	29
Chapter III: RESULTS		32
Part I: The <i>C. elegans ced-3</i> caspase promotes asymmetric division of cells that produce apoptotic daughters		32
3.1	Lack of <i>ced-1</i> and <i>ced-3</i> lead to the generation of extra PVM neurons	33
3.2	QL.p division asymmetry	36
3.2.1	<i>ced-3</i> promotes size-asymmetry in QL.p division	36
3.2.2	Protease function of CED-3 is required for the regulation of size-asymmetry in QL.p division	37
3.2.3	<i>ced-3</i> is required for posterior positioning of the cleavage furrow during QL.p division	38
3.3	QL.pp death	40
3.3.1	The engulfment gene <i>ced-1</i> promotes QL.pp death	40
3.3.2	<i>ced-1</i> acts in parallel to <i>pig-1</i> to promote QL.pp death	41

3.3.3	CED-1 is in asymmetric contact with QL.p and promotes QL.pp death cell non-autonomously	42
3.3.4	<i>ced-1</i> is required to establish/maintain a gradient of active CED-3 in QL.p	44
3.4	QL.pp division	46
3.4.1	<i>ced-3</i> prevents division of undead QL.pp	46
3.4.2	Protease function of CED-3 is required to prevent the division of undead QL.pp.....	48
3.4.3	<i>ced-3</i> prevents QL.pp division independently of QL.pp size.....	48
3.4.4	<i>ced-1</i> may not be required to prevent QL.pp division	51
3.5	Role of <i>ced-3</i> in cell division in other cell lineages.....	52
3.5.1	<i>ced-3</i> promotes size-asymmetry during QL.a division	52
3.5.2	<i>ced-3</i> promotes size-asymmetry in NSM neuroblast division.....	53
3.5.3	<i>ced-3</i> may play an important role across cell lineages during <i>C. elegans</i> embryonic development.....	55
Part II: Mechanistic insights into the regulation of asymmetric cell division by <i>ced-3</i> caspase.....		57
3.6	Spindle is symmetrically positioned during QL.p metaphase	58
3.7	<i>ced-3</i> may not be required for spindle positioning during QL.p metaphase	60
3.8	Chromosomes migrate unequally during QL.p anaphase	60
3.9	<i>ced-3</i> may not be required to regulate chromosome migration during QL.p anaphase	63
3.10	NMY-2 localizes anisotropically during QL.p metaphase	63
3.11	Size asymmetry during QL.p division arises during anaphase.....	65
3.12	Release of NMY-2 from the anterior cortex may cause its expansion	66
3.13	<i>ced-3</i> may not control NMY-2 dynamics.....	66
3.14	NMY-2 anisotropy may dictate spindle positioning.....	68
3.15	<i>ced-3</i> may link NMY-2 anisotropy with spindle positioning during QL.p division.....	69
3.16	CED-3 physically interacts with ECT-2, a regulator of NMY-2 contractility	72
Chapter IV: DISCUSSION.....		75
4.1	Novel non-apoptotic roles of the <i>C. elegans ced-3</i> caspase	76
4.1.1	The regulation of size-asymmetry in cell divisions by <i>ced-3</i>	76
4.1.2	The regulation of fate-asymmetry in cell divisions by <i>ced-3</i>	77

4.2 NMY-2 (Myosin) as a regulator of cell behaviors.....79

4.3 NMY-2 may play an important role in the asymmetric division of the QL.p neuroblast. .81

4.4 Several mechanisms may act partially redundantly of each other to regulate asymmetry in cell divisions.83

4.5 The organization of an active CED-3 gradient by engulfment genes is a general phenomenon.85

REFERENCES.....89

CURRICULUM VITAE101

ABSTRACT

Throughout an animal's life, new cells are constantly being produced. However, old and worn-out cells and those that are damaged or produced in excess need to be simultaneously eliminated. This elimination of cells is accomplished through a process referred to as programmed cell death. Cells undergoing programmed death do so, as the name suggests, in a programmed and controlled manner. One widely studied type of programmed cell death is apoptosis. Apoptosis plays a key role during and after animal development, and misregulated apoptosis can severely impact animal health and may even result in death. Therefore, to understand this process is of critical importance.

A significant part of our understanding of apoptosis and the molecular players that regulate and execute it comes from studies carried out using an excellent genetic model, *Caenorhabditis elegans*. In *C. elegans*, apoptosis is executed by a linear central pathway, comprising of four conserved genes: *egl-1* (egg-laying defective), *ced-9*, *ced-4* and *ced-3* (cell death abnormal). The expression and activity of each of these players are tightly regulated so as to prevent ectopic cell death, which can cause lethality. During *C. elegans* development, exactly 131 somatic cells die; most of these 131 cells die by apoptosis. Interestingly, nearly all 131 cells are products of asymmetric cell divisions. More specifically, they are the smaller daughter cells obtained from the division of mother cells that produce two unequal-sized daughters. It is known that a defect in this asymmetry of the mother cell division can influence the fate its daughter cells adopt. For instance, in mutants where the mother cell divides symmetrically rather than asymmetrically, the otherwise smaller daughter cell often survives. Therefore, asymmetric cell division and apoptosis are functionally linked, such that asymmetric cell division influences apoptosis.

Initially, it was believed that the apoptotic pathway is activated only in cells programmed to die. However, further investigation revealed that the pathway is, in fact, already active in the mothers of cells that undergo apoptosis. Considering that the mother cells do not die, this surprising observation led to the hypothesis that the apoptotic pathway may play non-apoptotic roles in the mother cells. In my thesis, I have attempted to understand what role(s) the apoptotic pathway plays in those cells.

Using mainly the postembryonic QL.p lineage as model, I showed that the central apoptotic pathway is active in the mother cell and that it performs an important function in its asymmetric division. Specifically, I found that loss-of-function (lf) mutations in *egl-1*, *ced-4* or *ced-3* lead to

a reduced asymmetry in the mother cell division. This suggests that the apoptotic pathway promotes asymmetry in the mother cell division. In addition, similar observations were also made for the division of another postembryonic neuroblast, QL.a and for that of an embryonic neuroblast, NSM (NeuroSecretory Motorneuron). Furthermore, I present data that suggest that the apoptotic pathway also functions to prevent the division of cells fated to die; it accomplishes this not only by killing those cells but also by potentially preventing the segregation of mitotic fate determinants into them.

Further analyses carried out specifically with *ced-3(lf)* animals have provided key insights into the mechanism through which the apoptotic pathway may regulate at least the size-asymmetry during mother cell divisions. My results suggest that QL.p divides asymmetrically through two mechanisms, which may not be mutually exclusive. It employs both an asymmetric spindle and anisotropic NMY-2 (myosin) localization, which potentially cooperate to produce two unequal-sized daughters. While in *ced-3(lf)* animals, neither spindle asymmetry nor NMY-2 dynamics was found to be affected, interestingly, the coordination between the two was lost. Furthermore, my results also suggest that in *ced-3(lf)* animals, NMY-2 activity may be reduced and that spindle asymmetry may therefore play a larger role to ensure that QL.p divides asymmetrically. Another observation further strengthens this idea: Together with Hai Wei, another doctoral student in the lab, I have identified the Rho-GEF ECT-2, which is a positive regulator of NMY-2 activity, as an interactor of CED-3 in a yeast two-hybrid screen. We speculate that ECT-2 acts downstream of CED-3 and facilitates the regulation of NMY-2 activity by CED-3.

In summary, my thesis has uncovered two novel non-apoptotic roles of the apoptotic pathway in asymmetric cell divisions: 1. It promotes division asymmetry by size, potentially by promoting NMY-2 activity via ECT-2, and 2. It promotes division asymmetry by fate, whereby it prevents the division of cells fated to die, probably by preventing the segregation of mitotic fate determinants into the cell at the time of its birth. In other words, while asymmetric cell division influences the specification/execution of the apoptotic fate in the daughter cells, the apoptotic pathway also, in turn, controls asymmetry in mother cell division. Considering that both asymmetric cell division and cell death are processes of fundamental importance, this crosstalk between the two processes can be key to gaining further insights into their regulation.

Chapter I: INTRODUCTION

1.1 Programmed Cell Death

Throughout animal life, new cells are constantly being produced. However, at the same time, a large number of cells are also eliminated in a controlled manner in order to maintain homeostasis or to shape organs and tissues during development (Vogt 1842; Wagener 1879; Flemming 1885). This process, which is responsible for controlled elimination of cells, is called programmed cell death (Ellis *et al.* 1991b; Clarke and Clarke 1995, 1996). Programmed cell death plays key roles during development. For instance, during development of higher vertebrates, ‘extra cells’ between the future digits, referred to as

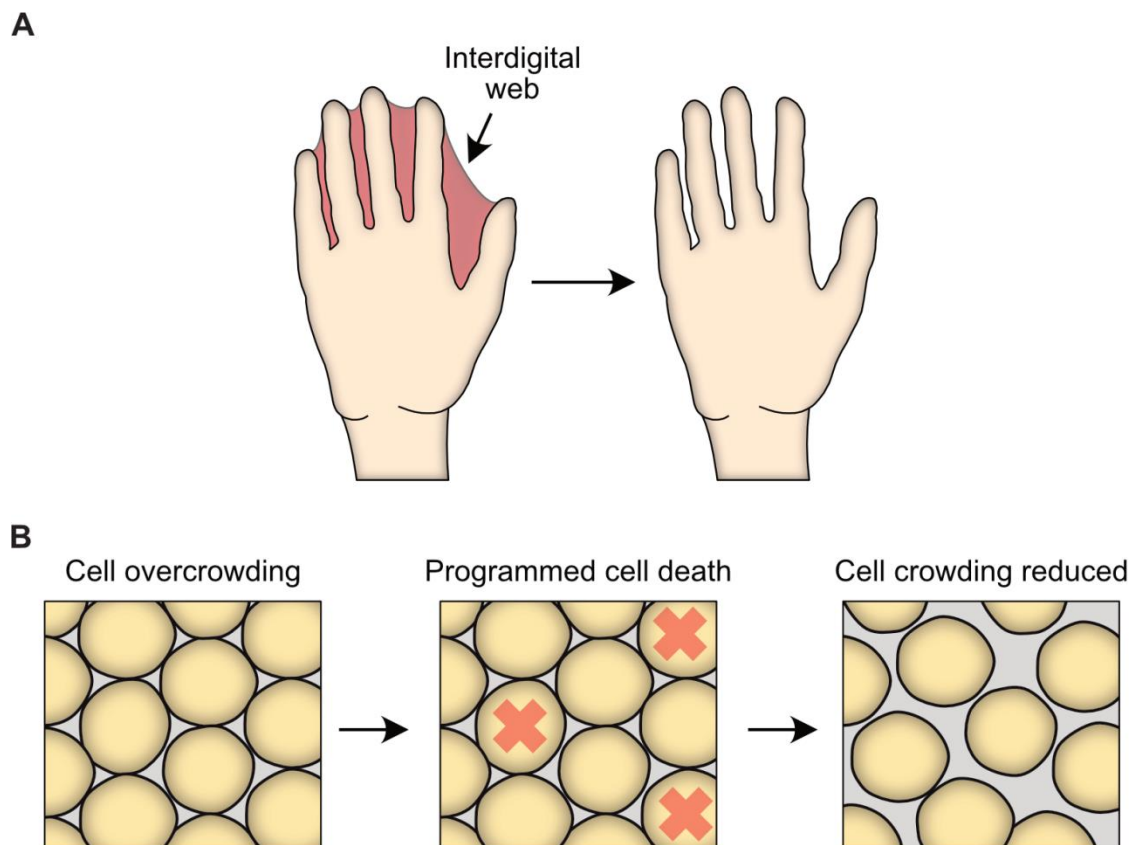


Figure 1.1: Programmed Cell Death plays important roles during development and in tissue homeostasis

(A) During limb development in higher vertebrates, interdigital webs are eliminated through programmed cell death, which gives rise to well-separated digits. (B) Programmed cell death also selectively eliminates cells from a crowded tissue to restore homeostasis.

interdigital webs, undergo programmed cell death (**Fig. 1.1A**) (Saunders 1966; Hernández-Martínez and Covarrubias 2011). This elimination of cells is necessary for the formation of well-separated digits. Programmed cell death also plays a key role in maintaining tissue homeostasis and also as a force generator for cell migration during development – for example, during dorsal closure in *Drosophila melanogaster* (**Fig. 1.1B**) (Rosenblatt et al. 2001; Toyama et al. 2008; Gorfinkiel et al. 2009). It is an important process, a misregulation of which is implicated in several serious conditions; for instance, increased programmed cell death is often associated with neurodegenerative disorders, such as Parkinson’s disease, whereas decreased programmed cell death can result in the development of tumors (Anglade 1997; Tompkins *et al.* 1997; Tatton *et al.* 1998; Soengas *et al.* 1999; Hartmann *et al.* 2001). Given the serious consequences of the misregulation of programmed cell death, it is, therefore, key that we understand how programmed cell death is controlled.

1.2 *Caenorhabditis elegans* is an excellent model organism to study programmed cell death

1.2.1 *C. elegans* as a model to study development

C. elegans is a nematode, which was first introduced as a genetic model by Sydney Brenner (Brenner 1974). It has a short life cycle, which spans three days at 25°C (**Fig. 1.2**). In addition, it is amenable to genetic manipulations and is easy to grow in laboratory conditions. Furthermore, it is a transparent organism, which makes it an excellent model for optical analysis. Within a decade of the introduction of *C. elegans* as model, investigators – especially John Sulston – carried out a comprehensive analysis of the somatic cell lineage of *C. elegans*. They mapped the entire somatic cell lineage of *C. elegans* both during embryonic and postembryonic development (Sulston and Horvitz 1977; Sulston et al. 1983). Unarguably the most exciting finding from the analysis was that the nematodes have an invariant somatic cell lineage – i.e. across animals, the patterns and timing of cell divisions, the fate each cell adopts and the timings at which the fate is specified and executed remain almost exactly the same (Sulston and Horvitz 1977; Sulston et al. 1983). As a result, the number of somatic cells making up an individual nematode also remains constant across animals. Specifically,

an adult wild-type hermaphrodite has exactly 959 somatic cells. However, during the development of these hermaphrodites, a total of 1090 somatic cells are produced, out of which 131 cells reproducibly undergo programmed cell death. The identities of these 131

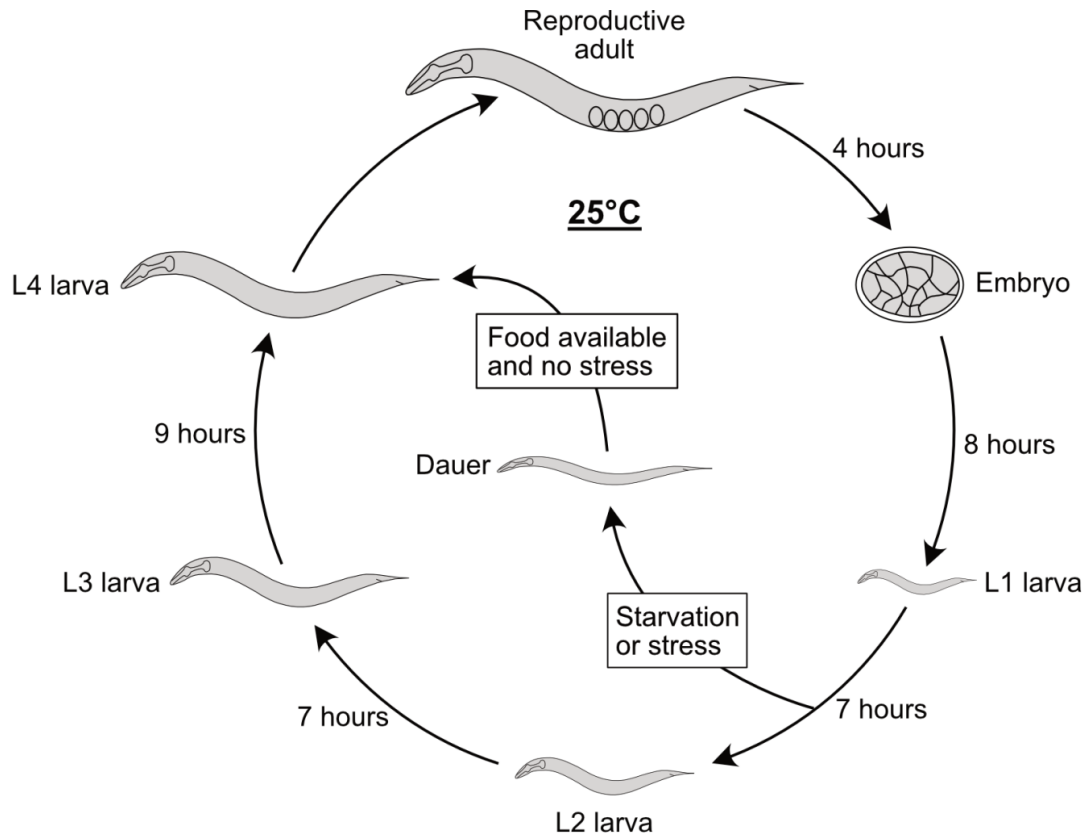


Figure 1.2: Life cycle of *C. elegans* at 25°C

A schematic representation of the life cycle of a *C. elegans* hermaphrodite at 25°C. Adult hermaphrodites lay eggs approximately 4 hours after fertilization. Embryonic development continues for another 8 hours, after which time, the embryos hatch to release L1-stage larvae. L1 larvae develop into adults by passing through L2, L3 and L4 stages in the process. In cases where the food supply is limited or where the environmental conditions are unfavorable, larvae enter a dauer stage, as indicated. When food is available again or when the environmental conditions turn favorable, dauers develop into L4 larvae and re-enter the normal cycle.

cells that are programmed to die and the timings of their deaths remain the same across individuals. Therefore, considering that it is feasible to track the biology of specific cells in *C. elegans* with an advanced knowledge of their eventual fates and the time at which those fates will be executed, *C. elegans* is an excellent model organism to study programmed cell

death, which is also a cell fate. More generally, *C. elegans* can also be effectively employed to understand several other processes, especially during development.

1.2.2 *C. elegans* as a model to study programmed cell death

Robert Horvitz and his team, in particular, combined and exploited two of the main strengths of *C. elegans* as model – somatic cell lineage invariance and optical accessibility - to advance our understanding of one key type of programmed cell death – apoptosis (Kerr *et al.* 1972). Apoptosis is a type of programmed cell death that occurs largely without inducing an immunological response. Cells undergoing apoptosis show characteristic morphological changes, such as cell shrinkage, nuclear fragmentation and plasma membrane blebbing (Kerr *et al.* 1972). Apoptosis occurs in a manner dependent on a linear pathway referred to as the central apoptotic pathway. This pathway comprises of four evolutionarily conserved genes – *ced-3* (*ced*: cell death abnormal) (Caspase), *ced-4* (Apaf-1), *ced-9* (Bcl-2) and *egl-1* (egg-laying defective) (BH3-only) (Ellis and Horvitz 1986; Hengartner *et al.* 1992; Conradt and Horvitz 1998) (**Fig. 1.3A**). *ced-3*, *ced-4* and *ced-9* were identified as cell-death regulators through genetic screens. Animals with loss-of-function mutations in *ced-3* or *ced-4* or a gain-of-function mutation in *ced-9* show reduced cell death (Ellis and Horvitz 1986; Hengartner *et al.* 1992). This leads to the presence of ‘extra’ cells – i.e. cells that normally undergo apoptosis in wild-type but fail to die in the mutants. These observations established that *ced-3* and *ced-4* are required to promote apoptosis, whereas *ced-9* is required to prevent apoptosis. In addition, another gene, *egl-1* (*egl*: egg-laying defective), which was originally identified in a screen for animals with defects in egg-laying, was also assigned a function in apoptosis as a positive regulator of the process (Conradt and Horvitz 1998). Further epistatic analyses placed the four genes in a linear pathway in which *egl-1* is the most upstream gene, and *ced-3* the most downstream gene (**Fig. 1.3A**). *ced-3* is activated by *ced-4*. *ced-9* inhibits *ced-4* and is inhibited by *egl-1* itself (**Fig. 1.3A**).

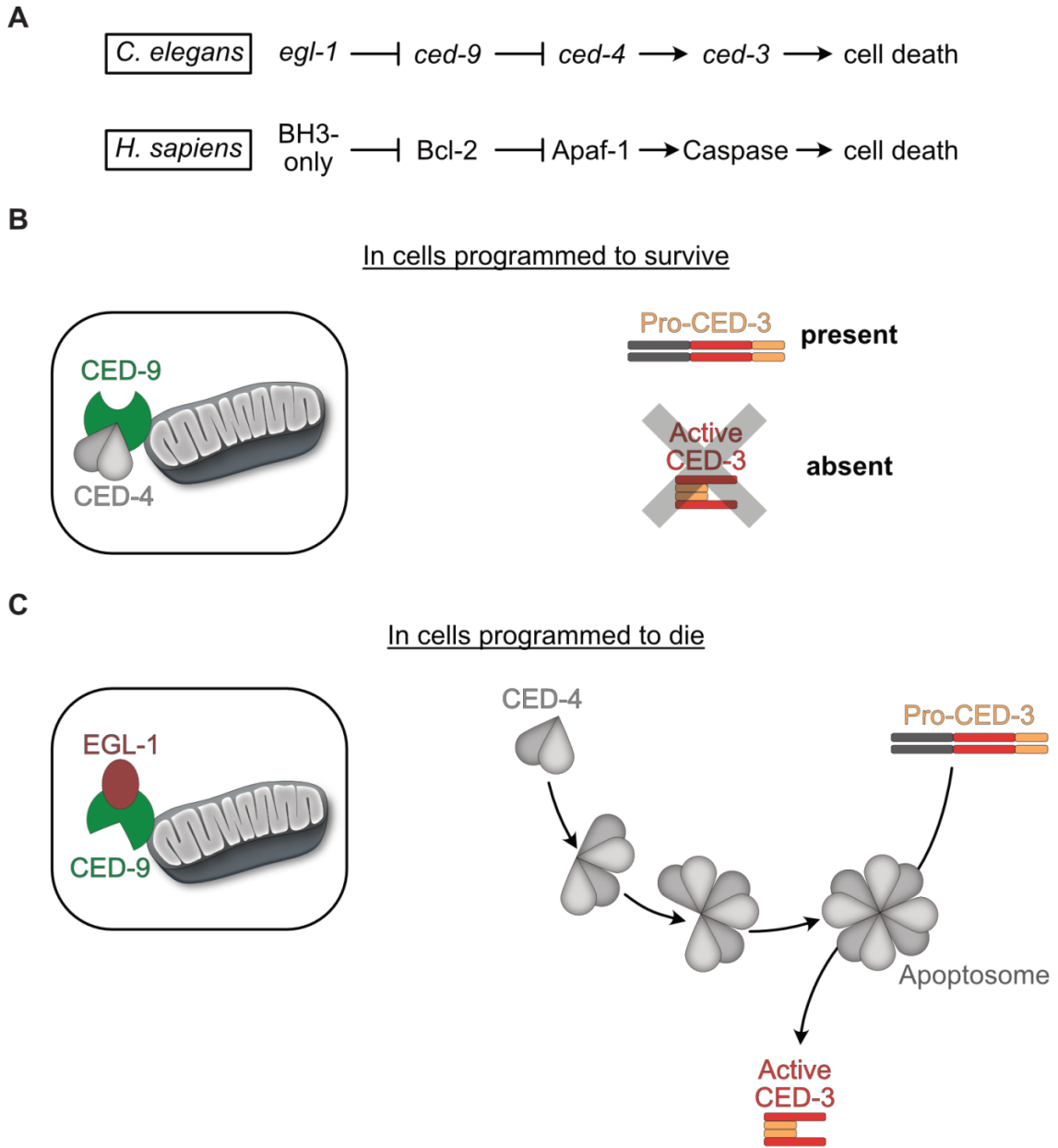


Figure 1.3: The central apoptotic pathway in *C. elegans*

(A) The genetic pathways of apoptosis in *C. elegans* and in *H. sapiens*. In *C. elegans*, *egl-1*, *ced-4* and *ced-3* are proapoptotic genes, and *ced-9* is the sole antiapoptotic gene. (B) In living cells, the antiapoptotic protein CED-9 remains bound to (and thus, sequesters) a dimer of the proapoptotic protein CED-4 on the outer mitochondrial membrane. Since an octamer of CED-4 is required for the activation of CED-3, which is necessary for the execution of apoptosis, in these cells, apoptosis is averted. (C) In cells that are programmed to die, another proapoptotic protein, EGL-1, is up-regulated. It binds to CED-9, which induces a conformational change in CED-9. As a result, CED-4 is released from the complex with CED-9. CED-4 octamerizes to form the apoptosome, which facilitates the conversion of pro-CED-3 (inactive) to active CED-3. Once active, CED-3 swiftly executes apoptosis, and the cell dies.

More specifically, in cells programmed to live, CED-9 protein remains bound in a complex with a dimer of CED-4 on the outer mitochondrial membrane (**Fig. 1.3B**) (Hengartner *et al.* 1992; Yuan and Horvitz 1992; Hengartner and Horvitz 1994; Chinnaiyan *et al.* 1997; Spector *et al.* 1997; Yan *et al.* 2005). However, in cells that are programmed to die, EGL-1 is produced, and it binds to CED-9, inducing a conformational change in CED-9 in the process, which results in the release of the CED-4 dimer from the complex (**Fig. 1.3C**) (Conradt and Horvitz 1998). Once released, CED-4 forms an octamer – apoptosome – which facilitates the full maturation of CED-3, which is a protease (**Fig. 1.3C**) (Yuan *et al.* 1993; Del Peso *et al.* 1998; Bao and Shi 2007). CED-3 matures (becomes active) by the cleavage of its N-terminus, and this ‘active’ CED-3 then cleaves several target proteins and executes apoptosis (Xue *et al.* 1996; Del Peso *et al.* 1998; Shaham *et al.* 1999). The unavailability of apoptosome for CED-3 maturation in living cells due to the sequestering of CED-4 by CED-9 is, therefore, key to the survival of the cell and the means through which CED-9 prevents apoptosis. In summary, *egl-1*, *ced-4* and *ced-3* promote apoptosis and are classified as proapoptotic genes, whereas *ced-9* prevents apoptosis and is classified as an antiapoptotic gene. For their contributions, Sydney Brenner, John Sulston and Robert Horvitz were awarded the Nobel Prize in Physiology and Medicine in the year 2002.

Apoptosis is an evolutionarily well-conserved biological process. Likewise, as mentioned earlier, the genes that regulate apoptosis are also highly conserved (**Fig. 1.3A**). In fact, much of our understanding of this process in mammals is a result of studies performed using *C. elegans*. For instance, *ced-3* was the first gene found to encode a caspase, and *ced-4*, which encodes a CED-3-activator protein, was also discovered before its mammalian orthologs. Such discoveries underline the fact that *C. elegans* is a simple, yet effective, model to understand apoptosis and its regulation in higher animals.

1.3 The corpse engulfment pathways in *C. elegans*

When cells undergo apoptosis in *C. elegans*, they assume a refractile, button-like morphology (**Fig. 1.4**) (Hedgecock *et al.* 1983). At this stage, a cell is referred to as a cell corpse, and it is easily distinguishable from living cells. In living cells, phosphatidyl serine

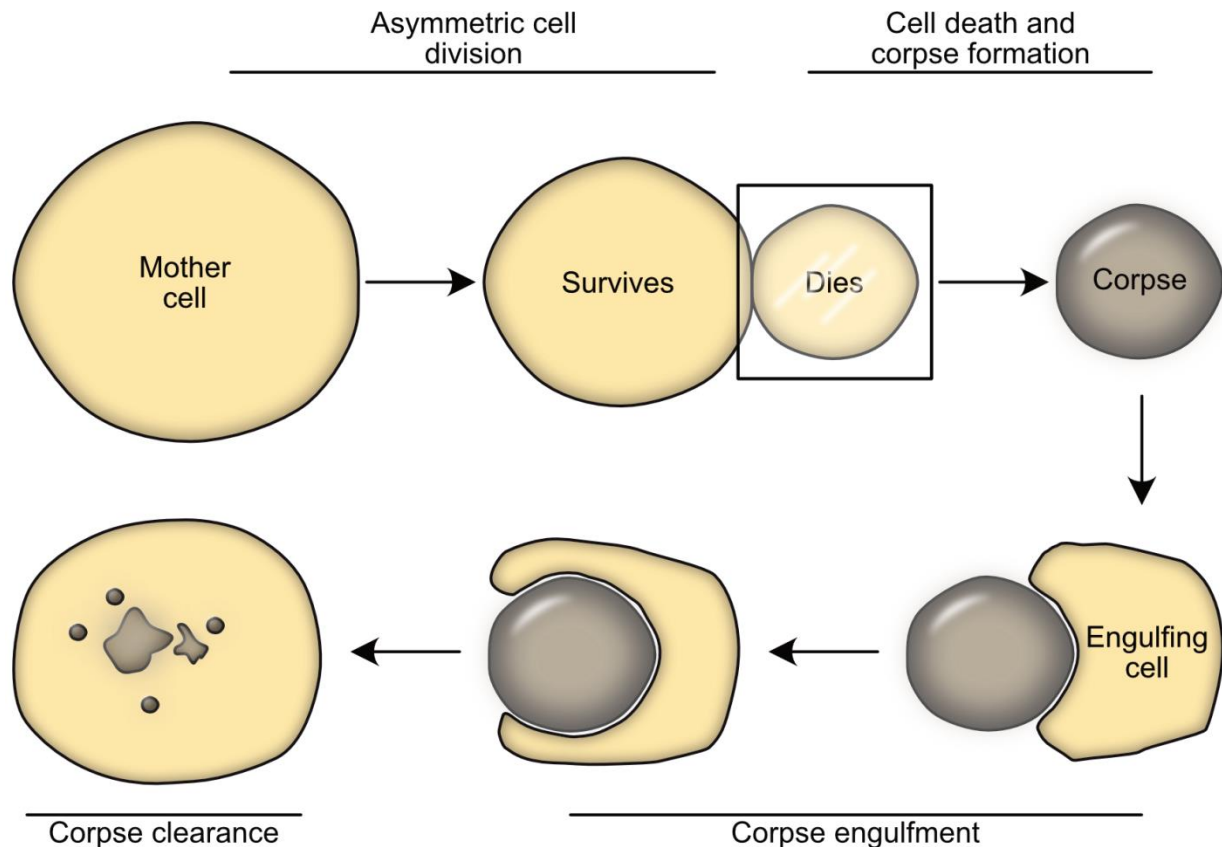


Figure 1.4: Apoptosis and engulfment in *C. elegans*

Mother cell divides asymmetrically by both size and fate to produce a larger daughter cell, which survives, and a smaller daughter cell, which undergoes apoptosis. The smaller daughter dies within 30 minutes of its birth in most cases. Upon death, it assumes a characteristic button-like morphology, at which point, it is referred to as a cell corpse. This corpse is then engulfed by a neighboring cell in most cases since *C. elegans* lacks specialized phagocytes. Upon engulfment, the engulfing cell clears the cell corpse through autophagy.

(PS) is restricted to the inner leaflet of the plasma membrane (**Fig. 1.5A**). On the contrary, a key feature of cell corpses is that they expose PS on the outer leaflet of their plasma membrane (**Fig. 1.5B**) (Fadok *et al.* 1992a; b; Chen *et al.* 2013). This exposed PS serves as an ‘eat me’ signal for the neighboring cells, one of which recognizes the cell as being dead and clears it. The exposed PS on the corpse is recognized by a receptor protein, CED-1, which is present on the plasma membrane of the neighboring cells (**Fig. 1.5B**) (Hedgecock *et al.* 1983; Zhou *et al.* 2001b). Upon detecting the exposed PS, CED-1 clusters and activates a downstream engulfment pathway, comprising of three additional genes – *ced-6*, *ced-7* and *dyn-1* (**Fig. 1.5C**) (Ellis *et al.* 1991a; Yu *et al.* 2008). In addition, another pathway,

comprising of the genes *ced-2*, *ced-5*, *ced-10* and *ced-12*, acts partially redundantly with the *ced-1*-pathway, and both pathways promote the engulfment of the cell corpse (**Fig. 1.5C**) (Ellis *et al.* 1991a; Gumienny *et al.* 2001; Zhou *et al.* 2001a). Like the apoptotic genes, the engulfment genes are also evolutionarily conserved. Their mammalian orthologs have been indicated in **figure 1.5C**. In addition, except *ced-7*, which functions in both the dying and the engulfing cell, all of the above-mentioned engulfment genes function in the engulfing cell in order to promote corpse engulfment.

1.4 Engulfment genes promote apoptosis

The first engulfment genes – *ced-1* and *ced-2* – were discovered in the early 1980s, and the rest followed within the next two decades (Hedgecock *et al.* 1983; Ellis *et al.* 1991a; Gumienny *et al.* 2001; Zhou *et al.* 2001a). However, contrary to the belief at the time the roles of these genes in engulfment were first defined, two studies published in 2001 showed that they also play additional roles - in the execution of cell death (Hoepfner *et al.* 2001; Reddien *et al.* 2001). Specifically, in multiple cell lineages in animals where apoptosis was partially compromised, the lack of engulfment genes was found to enhance the failure of cell death. In addition, in some lineages, the lack of engulfment genes alone in an otherwise wild-type background was sufficient to prevent cell death. These observations established that the role of the engulfment genes was not limited to the clearance of dead cells. Rather, they were also required for the actual death of those cells.

In 2015, Sayantan Chakraborty, a former doctoral student in the lab, showed that the engulfment genes help organize/maintain a gradient of proapoptotic factors in the mother of the apoptotic daughter cell (Chakraborty *et al.* 2015). The gradient is organized in such a manner that it presumably favors a disproportionate segregation of proapoptotic factors into the apoptotic daughter cell and likely promotes its death. Importantly, it seems likely that this gradient of proapoptotic factors may not be necessary for cell death, except in a few cell lineages, but that it may function to make death-fate specification more robust.

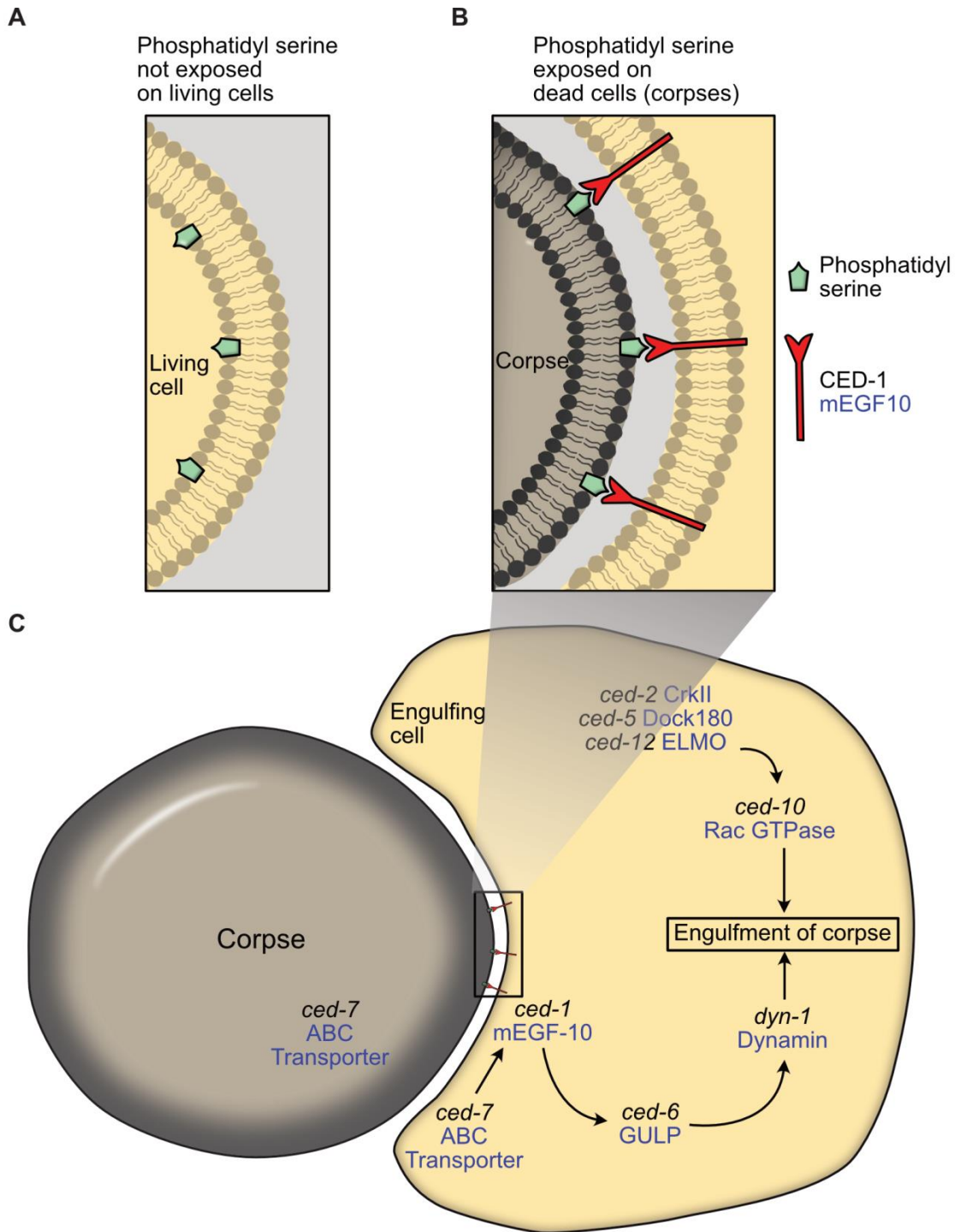


Figure 1.5: Cell corpse clearance in *C. elegans*

(A) Phosphatidyl serine is sequestered on the inner leaflet the plasma membrane of living cells. (B) In corpses, phosphatidyl serine is exposed on the outer leaflet. CED-1, an engulfment receptor protein on the neighboring cell, recognizes this 'eat me' signal and activates the engulfment machinery. (C) Two engulfment pathways, one comprising of *ced-1*, *ced-6* and *dyn-1* and the other comprising of *ced-2*, *ced-5*, *ced-10* and *ced-12* function partially redundantly of each other in the engulfing cell and promote corpse engulfment. Mammalian orthologs of the *C. elegans* genes have been mentioned in blue.

1.5 Apoptosis and asymmetric cell division are functionally linked

Exactly 131 somatic cells undergo programmed cell death during *C. elegans* development (Sulston and Horvitz 1977; Sulston et al. 1983). Interestingly, nearly all of these cells are smaller daughters of mother cells that divide asymmetrically by both size and fate. The larger daughter cell survives, whereas the smaller daughter cell invariably dies (**Fig. 1.6A**). It has been shown previously that this asymmetry in mother cell division is critical for the specification of the death fate in its daughter cell (Cordes *et al.* 2006; Hatzold and Conrardt 2008; Singhvi *et al.* 2011; Gurling *et al.* 2014). For instance, in animals, such as *pig-1(lf)*

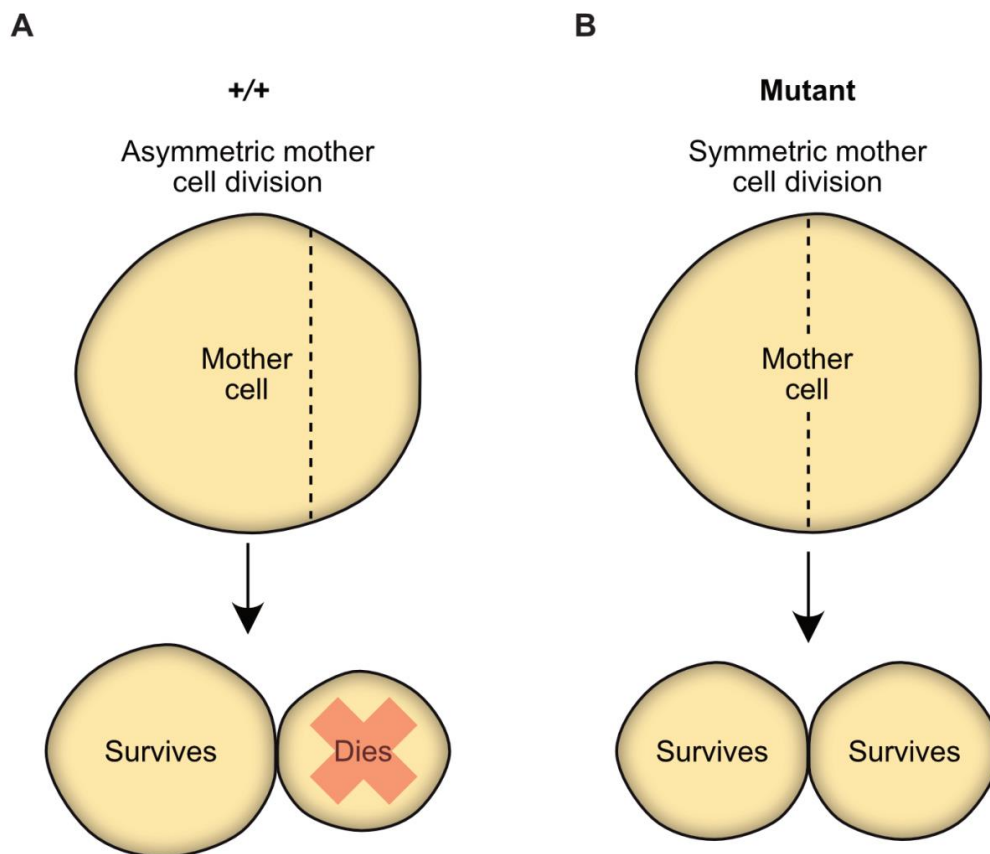


Figure 1.6: Apoptosis and asymmetric cell division are functionally linked

(A) In wild type animals, apoptotic cells are produced through asymmetric division of mother cells. Dotted line denotes the position of the cleavage furrow. The smaller daughter invariably undergoes apoptosis (red cross), whereas the larger daughter survives. (B) In mutants where the mother cell instead divides symmetrically, both daughter cells are of a similar size. In such cases, the daughter cell that is otherwise fated to die in wild type, often survives, thus leading to the presence of extra cells.

(*par-1(i)*-like gene) animals, where the mother cell divides symmetrically, rather than asymmetrically, the daughter cell normally programmed to die instead survives (**Fig. 1.6B**) (Cordes *et al.* 2006). Furthermore, in many such cases, it also mimics its sister in terms of cell fate.

This thesis mainly focuses on the division of one particular cell - QL.p. At the time of hatching, each L1 larva has two Q neuroblasts – one on the left, QL, and one on the right, QR (**Fig. 1.7A**) (Sulston and Horvitz 1977). Both neuroblasts delaminate from the neuroepithelium and, at 3.5 hours post-hatching at 20°C, undergo a division to produce two daughters each, which are similar in size – QL produces QL.a and QL.p, whereas QR produces QR.a and QR.p (**Fig. 1.7B**). QL.a and QR.a are the anterior daughters of QL and QR, respectively. On the other hand, QL.p and QR.p are the posterior daughters. QL.p, the cell used as model for my study, then undergoes a division at 5.5 hours post-hatching that produces two unequal-sized daughter cells – a larger anterior daughter cell, QL.pa, and a smaller posterior daughter cell, QL.pp (**Fig. 1.7B**). QL.pp dies by apoptosis shortly after its birth, whereas QL.pa divides again and produces a PVM and an SDQL neuron (Sulston and Horvitz 1977; Ellis and Horvitz 1986). Further, unlike other cells of the Q lineage, QL.p is a non-migratory cell.

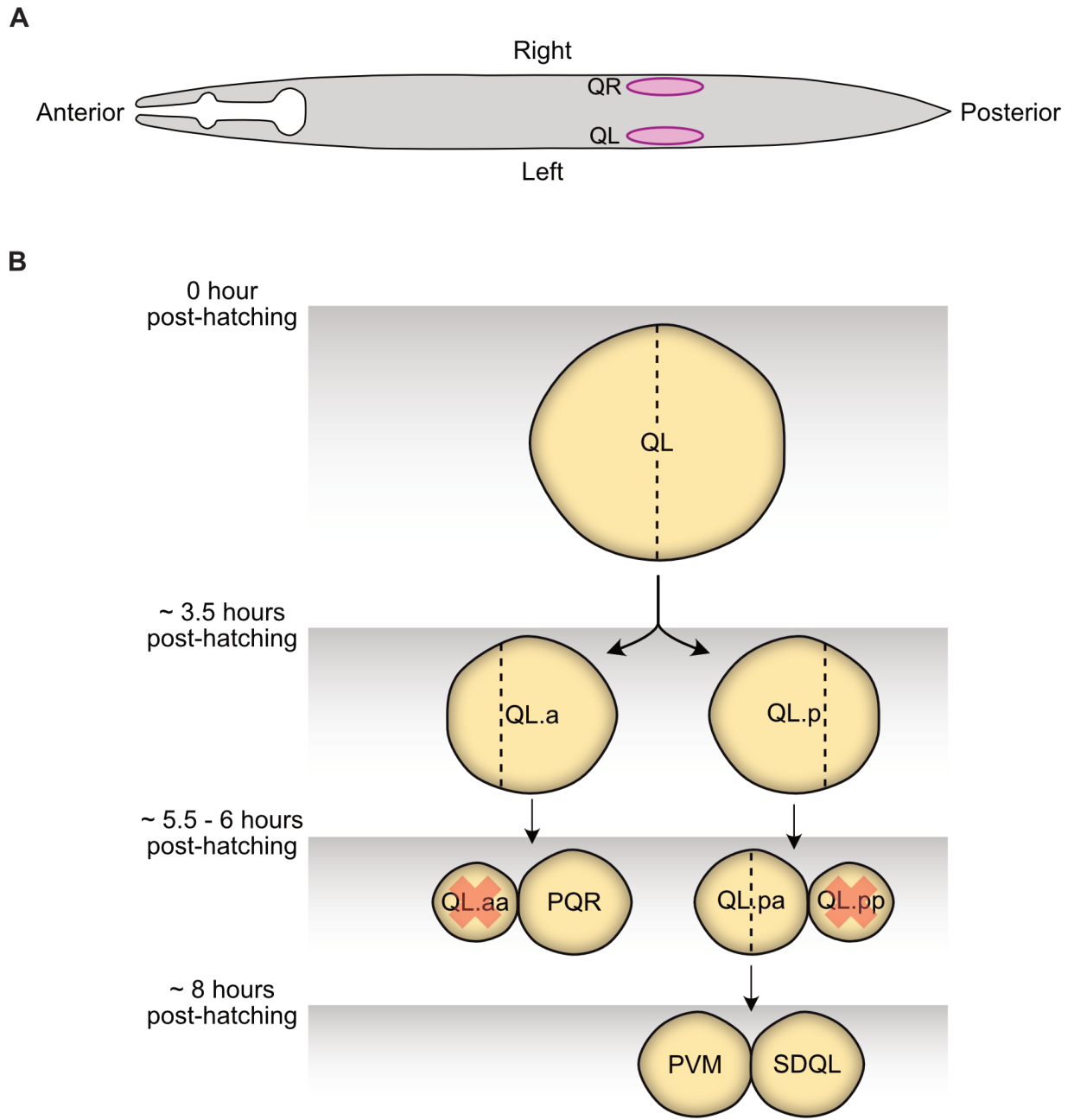


Figure 1.7: The Q lineage

(A) At the time of hatching, two Q neuroblasts - QL and QR - are present on the left and the right side of the L1 larva, respectively. (B) QL divides symmetrically to produce QL.a and QL.p, both of which divide asymmetrically. The approximate timings for all divisions at 20°C are indicated on the left. Three neurons - PQR, PVM and SDQL - are generated upon the completion of the QL lineage development. QR lineage cells also divide in a manner similar to the QL lineage cells and produce AQR, AVM and SDQR neurons. The red cross indicates that the cell undergoes apoptosis.

***Chapter II: MATERIALS AND
METHODS***

2.1 Strains and genetics

All *C. elegans* strains were cultured on Nematode Growth Medium (NGM) and maintained at 25°C for experiments unless mentioned otherwise. Mutant alleles and transgenes used in this study are: LGI: *ced-1(e1735)* (Hedgecock *et al.* 1983); LGIII: *ced-4(n1162)* (Ellis and Horvitz 1986), *ced-6(n1813)* (Ellis *et al.* 1991a), *rdvIs1(P_{egl-17mCherry::TEV-S::his-24}, P_{egl-17myristoylated mCherry}, P_{egl-17mig-10::yfp})* (Ou *et al.* 2010), *unc-119(ed3)* (Maduro and Pilgrim 1995); LGIV: *ced-2(1994)* (Hedgecock *et al.* 1983), *ced-3(n717)* (Ellis and Horvitz 1986), *ced-3(n2433)* (Shaham *et al.* 1999), *ced-3(n2427)* (Shaham *et al.* 1999), *pig-1(gm344)* (Cordes *et al.* 2006), *bcSi82 (P_{toe-2mKate2::tac-1})* (this study); LGV: *egl-1(n3330)* (Sherrard *et al.* 2017), *bzIs190 (P_{mec-4gfp})* (M. Driscoll; personal communication), *ltIs44 (P_{pie-1mCherry::ph^{PLCδ}})* (Audhya *et al.* 2005), *enIs1 (P_{ced-1ced-1ΔC::gfp})* (Zhou *et al.* 2001b) and *zuIs45 (P_{nmy-2nmy-2::gfp})* (Nance 2003). Additional transgenes used in this study are: *bcIs133 (P_{toe-2gfp})* (this study), *bcEx1277 (P_{hyp7ced-1::gfp})* (this study), *bcEx1334 (P_{toe-2ced-1::mKate2})* (this study).

2.2 Plasmid construction

Sequences of all primers mentioned in this section can be found in table 2.1.

2.2.1 pBC1565 (P_{toe-2gfp})

2117 bp immediately upstream of the *toe-2* start site was amplified by PCR using N2 genomic DNA and restriction sites for AgeI and SacI were introduced at the ends of the PCR product. This was used as the *toe-2* promoter (P_{toe-2}). P_{toe-2} was amplified using the primers SacIP_{toe-2-F} and AgeIP_{toe-2-R}. This PCR amplicon and plasmid pBC1408 (P_{ces-2gfp::unc-54 3'UTR} in pBluescript) were digested with AgeI and SacI (which eliminates P_{ces-2} from pBC1408), and the digested PCR amplicon was introduced into the pBC1408 backbone using T4 ligation to obtain pBC1565 (P_{toe-2gfp}).

2.2.2 pBC1591 (P_{hyp7gfp}) and pBC1681 (P_{hyp7ced-1::gfp})

2910 bp immediately upstream of the start site of the gene Y37A1B.5 was used as P_{hyp7} (Hunt-Newbury *et al.* 2007). P_{hyp7} was amplified by PCR using N2 genomic DNA as

template and P_{hyp7}-F and P_{hyp7}-R as primers, which introduced restriction sites for AgeI and SacI at the ends of the PCR product. This amplicon was used to replace P_{toe-2} in pBC1565 using restriction digestion with AgeI and SacI followed by T4 ligation to obtain the plasmid pBC1591 (P_{hyp7gfp}). A *ced-1* minigene was amplified using the plasmid pZZ610 (P_{ced-1ced-1::gfp}) as template by PCR using the primers AgeIced-1-F and *ced-1*-R (Zhou *et al.* 2001b). The resulting amplicon and pBC1591 were digested with AgeI and the *ced-1* minigene was inserted by T4 ligation into the linearized pBC1591 to generate the plasmid pBC1681 (P_{hyp7ced-1::gfp}).

2.2.3 pBC1805 (P_{toe-2ced-1::mKate2})

P_{toe-2} was amplified using the primers pBSKptoe-2-F and *ced-1*ptoe-2-R, and pBC1565 as template. A *ced-1* minigene was amplified by PCR in two parts using pZZ610 as template: Fragment 1: amplified using the primers P_{toe-2ced-1_fwd} and *ced-1_mini_(1)_rev*. Fragment 2: amplified using the primers *ced-1_mini_(2)_fwd* and *ced-1_mini_(2)_rev* (Zhou *et al.* 2001b). *mKate2::tbb-2* 3'UTR was amplified using the plasmid pEZ167 (P_{mex-5fkbp12::mKate2::tbb-2 3'UTR; personal communication: Esther Zanin) as template and the primers mK_tbb-2_fwd and mK_tbb-2_rev (Turek *et al.* 2013). EcoRV-digested pBluescript II KS(+) was used as backbone, and all the above fragments were assembled using Gibson assembly to obtain pBC1805 (P_{toe-2ced-1::mKate2}) (Gibson *et al.* 2009).}

2.2.4 pBC1807 (P_{toe-2mKate2::tac-1})

Primers NM1 and NM2, and pBC1565 (template for PCR) were used to amplify P_{toe-2}. *mKate2::tac-1* was obtained by PCR amplification using plasmid TMD34 (P_{mex-5mKate2::tac-1::tbb-2 3'UTR; personal communication: Tamara Mikeladze-Dvali) as template and the primers NM3 and NM4. Similarly, the *unc-54* 3'UTR was also amplified by PCR using pBC1565 as template and the primers NM5 and NM6. These fragments were then inserted into StuI-digested pCFJ909 using Gibson assembly to generate pBC1807 (P_{toe-2mKate2::tac-1}) (Gibson *et al.* 2009; Frøkjær-Jensen *et al.* 2014).}

Plasmid name	Features	Primers	Primer sequence (5'→3')
pBC1565	$P_{toe-2} gfp$	SacIP _{toe-2} -F	AAAAAGAGCTCTTATCTGTACCACAAAT TCC
		AgeIP _{toe-2} -R	AAAAAACC GGTTTTT GACCTGAGGACA TGATG
pBC1591	$P_{hyp7} gfp$	P_{hyp7} -F	AAAGAGCTCAAAC TTTATTAGACGTCG CAATT
		P_{hyp7} -R	AAAACCGGTTTTGGTTTTGGGATTTTT GATC
pBC1681	$P_{hyp7} ced-1::gfp$	AgeIced-1-F	AAAACCGGTATGCGTCTCATTCTCCTTG TGCTAC
		ced-1-R	TTTTTCTACCGGTACTTGAATTCCT
pBC1805	$P_{toe-2} ced-1::mKate2$	pBSKP _{toe-2} -F	ATCCCCCGGGCTGCAGGAATTCGATTT ATCTGTACCACAAATTCCTTG
		ced-1P _{toe-2} -R	GAATGAGACGCATTTTTGACCTGAGGA CATG
		P _{toe-2} ced-1_fwd	CCTCAGGTCAAAAATGCGTCTCATTCTC CTTG
		ced-1_mini_(1)_rev	CCGGGTCACAGTTGGCTCCATTTTCAC AGTC
		ced-1_mini_(2)_fwd	TGAAAATGGAGCCAAC TGTGACCCGGA ACTC
		ced-1_mini_(2)_rev	CCTTGATGAGCTCGGATTTTTCTACCG GTACTTGAATTC
		mK_tbb-2_fwd	ACCGGTAGAAAAATCCGAGCTCATCAA GGAG
		mK_tbb-2_rev	GGTCGACGGTATCGATAAGCTTGATCA ATGAGACTTTTTCTTGGC
pBC1807	$P_{toe-2} mKate2::tac-1$	NM1	GAGCTCTGGTACCCTCTAGTCAAGGTT ATCTGTACCACAAATTCCTTG
		NM2	TGAGCTCGGACATTTTTGACCTGAGGACATG
		NM3	CCTCAGGTCAAAAATGTCCGAGCTCAT CAAG
		NM4	AATTCTACGAATGTTATGCATCCGTCGA AATAAC
		NM5	GACGGATGCATAACATTCGTAGAATTC CAACTG
		NM6	AGTCCGTAATACGACTCACTTAAGGAA ACAGTTATGTTGGTATATTGG

Table 2.1: List of plasmids and primers

2.3 Microinjection and plasmid integration

2.3.1 *bcIs133* ($P_{toe-2gfp}$)

bcIs133 was obtained by injecting pBC1565 (20 ng/μL) + pRF4 (80 ng/μL) into the gonads of young N2 adult hermaphrodites, followed by the integration of the resulting extrachromosomal array by UV-irradiation. The animals carrying the integrated transgene were 5x-backcrossed with N2 before use for experiments.

2.3.2 *bcEx1277* ($P_{hyp7ced-1::gfp}$)

pBC1681 (51 ng/μL) + IR101 (10 ng/μL) ($P_{rps-0HygR::gpd-2/gpd-3::mCherry::unc-54}$ 3'UTR) was injected into the gonads of young *ced-1(e1735); ced-3(n2427); bcIs133* adult hermaphrodites to obtain *ced-1(e1735); ced-3(n2427); bcIs133; bcEx1277* (Radman et al. 2013).

2.3.3 *bcEx1334* ($P_{toe-2ced-1::mKate2}$)

pBC1805 (26 ng/uL) + pCFJ90 ($P_{myo-2::mCherry::unc-54}$ 3'UTR) (2.6 ng/uL) + pBluescript II KS(+) (60 ng/uL) was injected into the gonads of young *ced-1(e1735); ced-3(n2427); bcIs133* adult hermaphrodites in order to obtain *ced-1(e1735); ced-3(n2427); bcIs133; bcEx1334* (Frøkjær-Jensen et al. 2014).

2.3.4 *bcSi82* ($P_{toe-2mKate2::tac-1}$)

bcSi82 was generated by miniMOS integration of pBC1807 ($P_{toe-2mKate2::tac-1}$). 10 ng/uL of pBC1807 was injected into the gonads of HT1593 (*unc-119(ed3)*) animals along with pCFJ601 (50 ng/ul), pGH8 (10 ng/ul), pCFJ90 (2.5 ng/ul) and pCFJ104 (5 ng/ul) (Frøkjær-Jensen et al. 2014). Worms were allowed to starve for a week, after which wild-type movers were examined for a miniMOS integration of the pBC1807 transgene.

2.4 PVM neuron counting

PVM neurons were visualized using the transgene $P_{mec-4gfp}$ (*bzIs190*). In these animals, all mechanosensory neurons are labeled with GFP (Mitani *et al.* 1993). L4 larvae of the desired genotype were anaesthetized in a Sodium azide solution (30 mM in M9 buffer) and mounted on a 2% agarose pad on a glass slide. PVM neurons were visualized using a 100X/1.3 NA oil-immersion objective lens on a Zeiss Imager.M2 epifluorescence microscope.

2.5 CED-1 localization

CED-1 localization was analyzed using the transgene $P_{ced-1ced-1\Delta C::gfp}$ (*enIs1*). L1 larvae anaesthetized with levamisole (0.1 mM in M9 buffer) were mounted on 3% agarose pads on glass slides and imaged using a 63X/1.4 NA oil-immersion objective on a Leica SP5 inverted confocal microscope. Q lineage cells were identified with the help of the transgene $P_{egl-17mCherry::TEV-S::his-24}$, $P_{egl-17myristoylated mCherry}$, $P_{egl-17mig-10::yfp}$ (*rdvIs1*).

2.6 Live imaging of QL.a and QL.p divisions

L1 larvae immobilized using Polybead® microsphere suspension (0.1 μ m diameter, 2.5% w/v, Catalog no. 00876, Polysciences, Inc.) were mounted on a 10% agarose pad (agarose was dissolved in 67% M9 buffer) and covered with an 18mm X 18mm glass coverslip (**Fig. 2.1A-D**). The vacant area surrounding the agarose pad under the coverslip was filled with paraffin oil so as to prevent dehydration (**Fig. 2.1E**). Image Z-stacks were acquired with a temporal resolution of three minutes and a spatial resolution of one micrometer along the XZ axis using a 63X/1.4 NA oil-immersion objective lens on the UltraVIEW VoX spinning disk microscope (Perkin Elmer).

2.7 QL.pp survival

$P_{10e-2gfp}$ (*bcIs133*), a transgene that labels all cells of the Q lineage, was used to visualize QL.pp (Gurling *et al.* 2014). When grown at at 25°C, in wild-type animals, QL.pp dies

within 17 hours after egg laying, during the L1 stage (Sulston and Horvitz 1977). Therefore, to avoid false positives due to delayed cell death, I used L2 larvae for the analysis of QL.pp death. L2-stage larvae, immobilized with levamisole solution (10 mM in M9 buffer), were mounted on a 2% agarose pad on a glass slide. $P_{toe-2gfp}$ was visualized with the help of a 100X/1.3 NA oil-immersion objective lens on a Zeiss Imager.M2 epifluorescence microscope. Only those larvae were considered for assessing QL.pp survival in which QL.pa division was complete, and its daughters (PVM and SDQL neurons) had produced visible neurite extensions at the time of the analysis. This ensured that even slow-growing strains were analyzed at a developmental time point similar to that of wild-type animals.

2.8 QL.pp division

QL.pp was visualized using the $P_{toe-2gfp}$ (*bcIs133*) transgene. L2 larvae were mounted on glass slides as explained for QL.pp survival. Larvae were examined only after QL.pa division was complete and its daughters - PVM and SDQL neurons – had formed visible neurite outgrowths.

2.9 Embryonic lethality

Five L4 larvae of each genotype were placed on seeded NGM plates – one larva on each plate. Eggs were allowed to be laid for the next 30 hours. During this period, the worms were maintained at 20°C. Two days later, the numbers of larvae and dead eggs were counted, and the percentage embryonic lethality for each genotype was calculated.

2.10 Cell area measurements

Q lineage cells have been previously shown to have a relatively flat morphology (Cordes *et al.* 2006). Thus, cell areas measured in a single plane would suffice to provide a reliable estimation of cell sizes. Therefore, the image Z-stacks of the QL.a and QL.p daughters acquired using the transgene $P_{toe-2gfp}$ (*bcIs133*) were converged to obtain maximum intensity

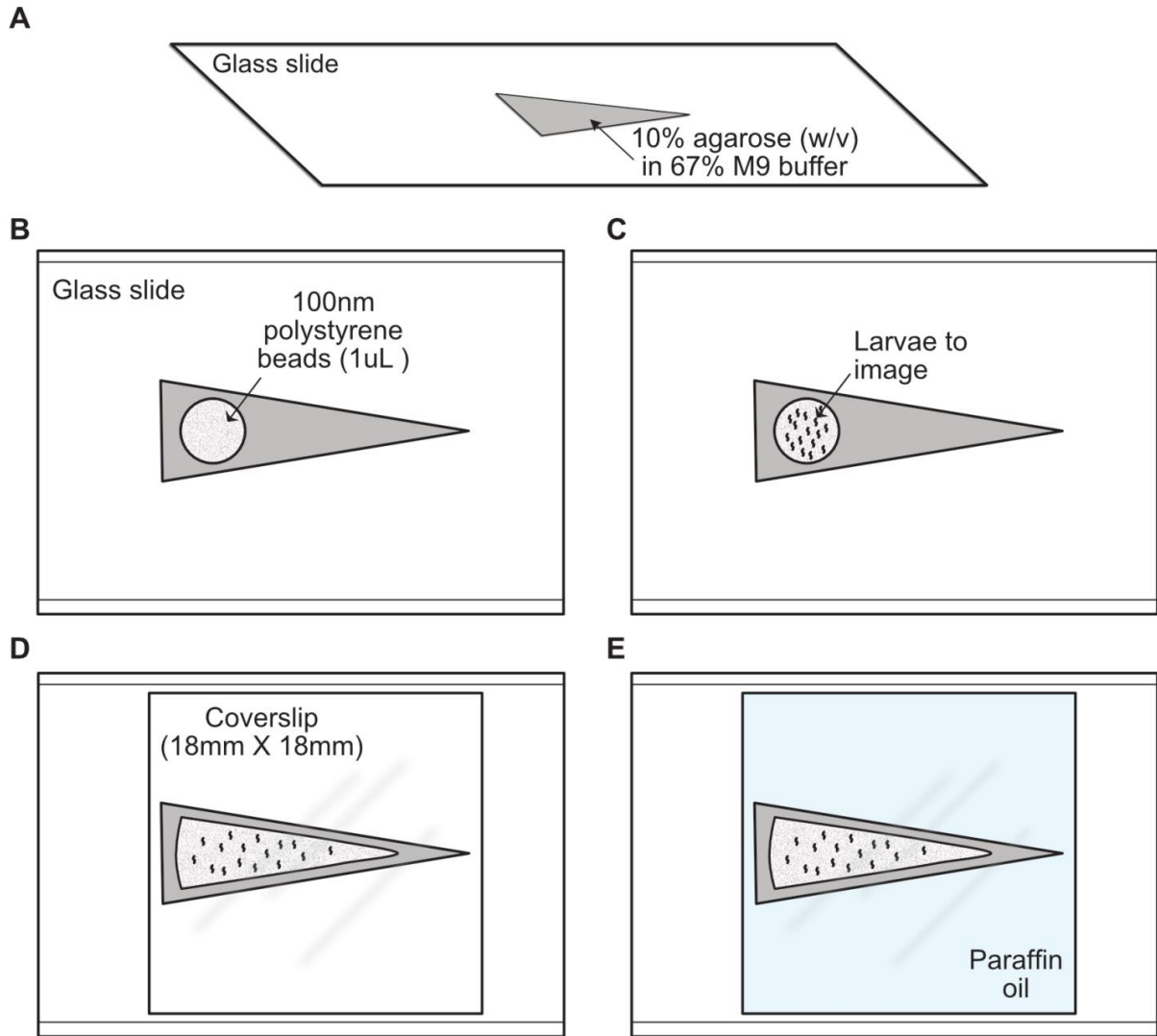


Figure 2.1: Preparation of L1 larvae for live imaging

(A) A triangular pad with a 10% agarose solution (in 67% M9 buffer) is made on a glass slide. (B) A 1 μ L drop of 100nm polystyrene beads is placed in the wider half of the agarose pad. (C) L1-stage larvae are then placed in this drop. Due to the presence of the polystyrene beads, there is an increased amount of friction, which minimizes movement of the larvae. (D) A glass coverslip (18mm X 18mm) is placed on the agarose pad. The drop and the worms spread out on the agarose pad once the coverslip is placed. (E) Fill the vacant area surrounding the agarose pad underneath the coverslip with paraffin oil to prevent dehydration. The slide is now ready to be used for live imaging.

Z-projections. In cases where the *rdvIs1* transgene ($P_{egl-17}mCherry::TEV-S::his-24$, $P_{egl-17}myristoylated\ mCherry$, $P_{egl-17}mig-10::yfp$) was used instead to measure QL.p daughter cell sizes, single-plane movies of QL.p division were generated with a temporal resolution of 15 seconds. In both cases, cell boundaries were circumscribed in the first image captured

after the completion of cytokinesis and their areas measured to obtain the daughter cell size ratio.

2.11 Cleavage furrow position

QL.p division was captured using *bcIs133* ($P_{toe-2gfp}$) as reporter as described in the ‘Live imaging of QL.a and QL.p divisions’ section. The time point at which QL.p was found to be undergoing cytokinesis was used to estimate the position of the cleavage furrow. The distance between the cleavage furrow and the anterior pole of QL.p was determined and presented as a percentage of the total length of the cell (distance between the anterior and the posterior poles) (**Fig. 3.5A**). All distances were measured using FiJi (Schindelin *et al.* 2012).

2.12 mKate2::TAC-1 ratio

TAC-1 was visualized with the help of the *bcSi82* transgene ($P_{toe-2mKate2::tac-1}$) in animals expressing *bcIs133* ($P_{toe-2gfp}$), which enables the visualization of QL.p. L1-stage larvae, cultured at 20°C, were immobilized in Polybead® microsphere suspension as described earlier. Image Z-stacks were acquired with a temporal resolution of five minutes and a spatial resolution of 0.5 micrometer along the XZ axis using a 100X/1.4 NA oil-immersion objective lens on the UltraVIEW VoX spinning disk microscope (Perkin Elmer). When the two centrosomes were positioned at the opposite poles during QL.p metaphase, the amount of TAC-1 associated with each centrosome was determined using FiJi (Schindelin *et al.* 2012). This quantification was performed as described previously. A region of the same size on a part of the slide which did not have any sample was considered as background, and its intensity was deducted from the measured intensities of centrosomal TAC-1.

2.13 NSM neuroblast daughter cell sizes

Imaging of the NSMnb division and the measurements of the sizes of its daughters were performed as previously described (Hatzold and Conradt 2008; Chakraborty *et al.* 2015; Wei *et al.* 2017).

2.14 NMY-2::GFP quantification

L1-stage larvae expressing the *rdvIs1* ($P_{egl-17mCherry::TEV-S::his-24}$, $P_{egl-17myristoylated\ mCherry}$, $P_{egl-17mig-10::yfp}$) and *zuIs45* ($P_{nmy-2nmy-2::gfp}$) transgenes were prepared by immobilization using polystyrene beads as described in the previous sections (Nance 2003; Ou *et al.* 2010). The larvae were imaged using a 100X/1.4 NA oil-immersion objective lens on the UltraVIEW VoX spinning disk microscope (Perkin Elmer). Single-plane images were acquired with a temporal resolution of 15 seconds. NMY-2 concentrations at the anterior and the posterior cortices were quantified by marking the regions in FiJi and measuring mean pixel intensity values (Schindelin *et al.* 2012). The chromosomes and the cleavage furrow were used to define the boundary between the anterior and the posterior parts of the cell.

2.15 Metaphase plate position

Movies generated for NMY-2::GFP quantification were used to analyze the position of the metaphase plate. In these animals (expressing *rdvIs1*), both the plasma membrane and the chromosomes are labeled with mCherry (Ou *et al.* 2010). Therefore, different phases of mitosis can be easily identified. The last time point when QL.p was at metaphase (<15 seconds before anaphase onset) was used to determine the position of the metaphase plate. Position was determined by measuring the distance of the metaphase plate from the anterior periphery of QL.p and dividing it by the total distance between the anterior and the posterior poles of the cell. Distances were measured using FiJi (Schindelin *et al.* 2012).

2.16 Anaphase chromosome migration

Movies generated for NMY-2::GFP quantification were used to analyze chromosome migration during anaphase. In these animals (expressing *rdvIs1*), the chromosomes are labeled with mCherry (Ou et al. 2010). Therefore, different phases of mitosis can be easily identified. Kymographs were generated using Fiji to track the position of the chromosomes during QL.p division (Schindelin et al. 2012). Metaphase and anaphase can also be easily identified in the kymographs based on the number of tracks visible. When at metaphase, the chromosomes are aligned at the metaphase plate, and therefore, a single track is visible (**Fig. 3.14A and B**). On the other hand, at anaphase, when the chromosomes migrate toward opposite poles, two tracks moving in opposite directions can be seen (**Fig. 3.14A and B**). The distance covered by each track from the position of the metaphase plate along the anterior-posterior axis until the beginning of the constriction of the cleavage furrow was measured as the anaphase chromosome migration distance (**Fig. 3.14A and B**). These distances were also measured using Fiji (Schindelin et al. 2012).

2.17 Statistical tests

Fisher's Exact Test was used to compare proportions, and the obtained p values were adjusted using the Benjamini and Hochberg test for multiple comparisons (Benjamini and Hochberg 1995). Wherever applicable, data were tested for normal distribution using the D'Agostino and Pearson normality test (D'Agostino and Pearson 1973). When data were found to be distributed normally, Student's t-test or parametric One-way ANOVA was performed to determine statistical significance between groups assuming that the groups had unequal standard deviations, and Tukey's or Benjamini and Hochberg multiple comparisons test was applied (Student 1908; Fisher 1921; Tukey and Anonymous 1949). When comparing variables with a standard value, such as 1.0 or 50.0, Wilcoxon Signed-Rank test was used to determine if the groups were statistically different (Wilcoxon 1945). The Mann-Whitney test was used in order to compare the ratios of QL.a daughter cell sizes in wild-type animals with those in *ced-3(n717)* animals (Mann and Whitney 1947). Correlations between variables were analyzed by Pearson and Spearman correlation analyses, and the corresponding

correlation coefficients and p values are indicated wherever relevant (Spearman 1904; Pearson 2006).

Chapter III: RESULTS

Part I: The C. elegans ced-3 caspase promotes asymmetric division of cells that produce apoptotic daughters.

3.1 Lack of *ced-1* and *ced-3* lead to the generation of extra PVM neurons

pig-1 (*par-1* (*i*)-like *gene*) encodes a serine-threonine kinase that is orthologous to mammalian MELK (**M**aternal **E**mbryonic **L**euclidean-zipper **K**inase (Cordes *et al.* 2006). It has been shown to play a necessary role in asymmetric cell divisions in several cell lineages during *C. elegans* development (Cordes *et al.* 2006). One such lineage is the postembryonic QL.p lineage. In wild-type animals, QL.p divides asymmetrically by size to produce a larger anterior daughter, QL.pa, and a smaller posterior daughter, QL.pp (**Fig. 3.1**) (Sulston and Horvitz 1977). In addition, QL.p division is also asymmetric by fate – QL.pa survives and

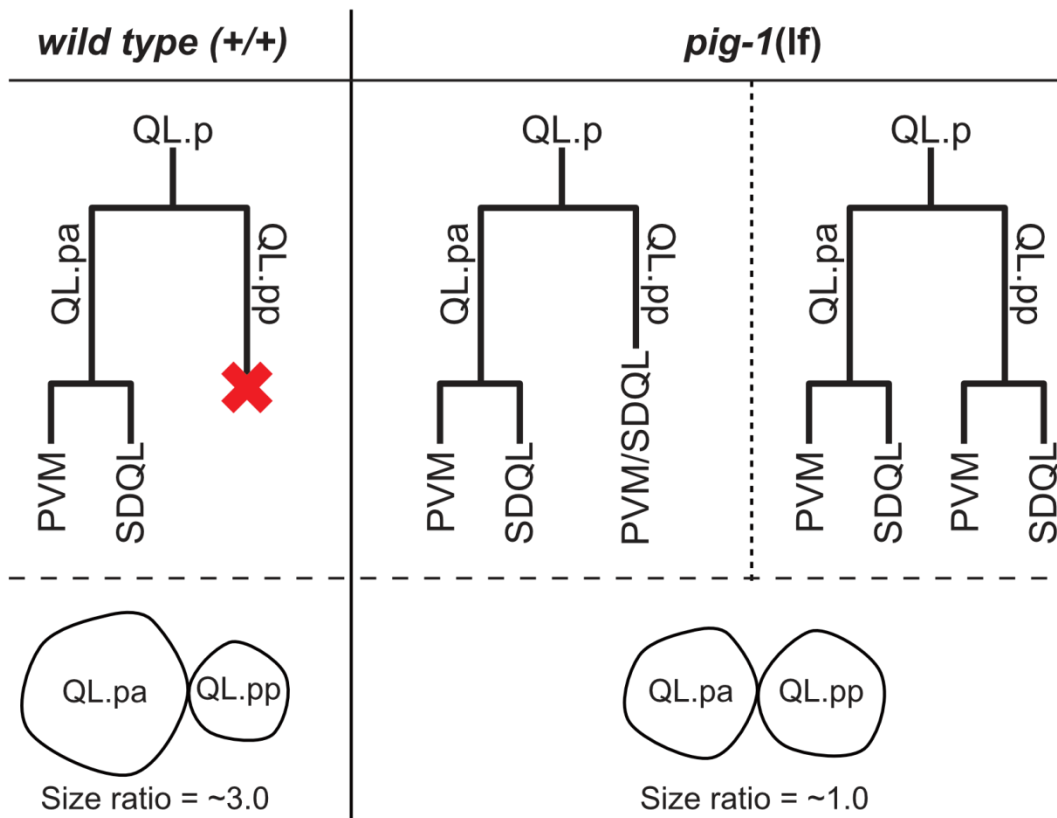


Figure 3.1: *pig-1* regulates size- and fate-asymmetries during QL.p division

Representation of the postembryonic QL.p lineage in wild type and *pig-1* loss-of-function (lf) mutants. In wild type animals, QL.p produces an anterior larger daughter cell, QL.pa, and a posterior smaller daughter, QL.pp. QL.pa is approximately three times as large as QL.pp (bottom-left) and divides to produce a pair of PVM and SDQL neurons, whereas QL.pp undergoes programmed cell death (as indicated by the red cross). In *pig-1*(lf), however, QL.pa and QL.pp are similar in size (bottom-right). In these animals, QL.pp survives and may either directly differentiate into a PVM/SDQL neuron or may divide, like QL.pa, to produce an extra pair of PVM and SDQL neurons.

divides to produce two neurons, a PVM neuron (**P**osterior **V**entral **M**echanosensory neuron) and an SDQL neuron, whereas QL.pp undergoes programmed cell death (Sulston and Horvitz 1977). In *pig-1* loss-of-function (lf) mutants, QL.p divides symmetrically, rather than asymmetrically, by both size and fate; i.e. in these animals, QL.pa and QL.pp are of similar size, and often QL.pp does not die (**Fig. 3.1**). Instead, it survives, and in many animals, divides, like QL.pa, to produce an extra set of a PVM and an SDQL neuron (Cordes *et al.* 2006; Chien *et al.* 2013). Therefore, *pig-1* is required to establish both size and fate asymmetries during QL.p division.

pig-1(gm344) animals have a 524 bp deletion in the *pig-1* coding sequence, which completely abolishes production of any functional PIG-1 protein (Chien *et al.* 2013). Therefore, *pig-1(gm344)* is likely a nullomorph. Using *bzIs190* (*P_{mec-4gfp}*), a GFP-reporter that labels all mechanosensory neurons, including the PVM neuron, I found that 30% of *pig-1(gm344)* animals produced an extra PVM neuron (**Fig. 3.2A and B**) (Mitani *et al.* 1993). Gian Garriga and co-workers have previously reported similar penetrances for the extra PVM neuron phenotype in these animals (Cordes *et al.* 2006; Chien *et al.* 2013). The extra PVM neurons in *pig-1*(lf) animals mainly arise from division of the ‘undead’ QL.pps (**Fig. 3.1**).

In wild-type animals, QL.pp dies through apoptosis, as evident from a failure of QL.pp death in animals defective for apoptosis, such as those lacking *egl-1* (*egg-laying defective*), *ced-4* (*cell death defective*) or *ced-3* function (**Fig. 3.6B**) (Ellis and Horvitz 1986). In these animals, however, as per previous reports, the undead QL.pp does not divide (Ellis and Horvitz 1986). As a result, these animals rarely produce an extra PVM neuron. This shows that QL.pp survival is not a sufficient condition for QL.pp to divide like its sister, QL.pa.

I found that, although a partial loss of *ced-3* function (*ced-3(n2427)*) did not lead to the presence of extra PVM neurons, it led to an enhancement of the penetrance with which extra PVM neurons were observed in *pig-1(gm344)* animals from 30% to 70% (**Fig. 3.2B**). In addition, the loss of *ced-1* function (*ced-1(e1735)*), an engulfment gene that has been previously shown to promote apoptosis in several cell lineages, also enhanced the penetrance of the *pig-1(gm344)*-extra PVM neuron phenotype from 30% to 58% (**Fig. 3.2B**) (Hoeppner *et al.* 2001; Reddien *et al.* 2001). Finally, 96% of *ced-1(e1735); pig-1(gm344) ced-3(n2427)* triple mutants showed the presence of an extra PVM neuron (**Fig. 3.2B**).

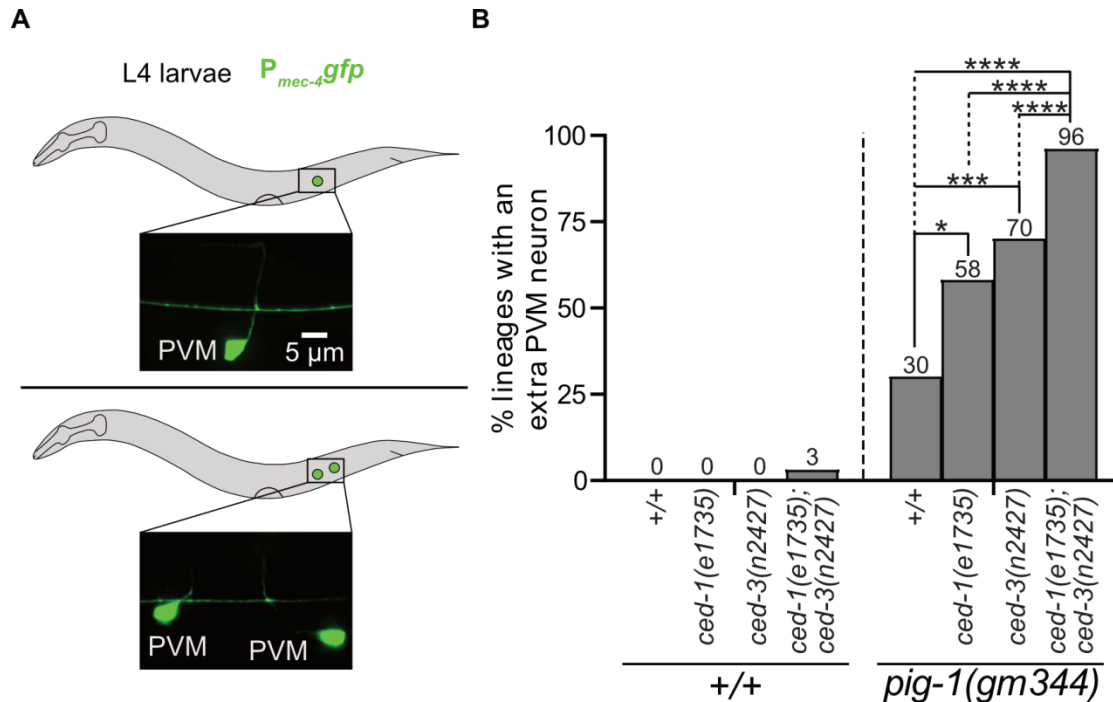


Figure 3.2: Lack of *ced-1* and *ced-3* lead to the generation of extra PVM neurons

(A) Diagrammatic representation and a representative image each of L4 larvae with one (top) or two (bottom) PVM neurons. PVM neurons were visualized with the help of a transgenic reporter - *bzIs190* ($P_{mec-4}::gfp$). (B) Bar graph showing percentage lineages (or animals, since each animal has only one QL.p lineage) that produce an extra PVM neuron. Statistical test: Fischer's Exact Test with Benjamini and Hochberg multiple comparisons correction. *: $p < 0.05$, ***: $p < 0.001$, ****: $p < 0.0001$, and $n > 50$ animals.

An extra PVM neuron is a result of a defect in one or more processes during QL.p lineage development. For instance, in the following cases, animals may produce extra PVM neurons:

1. QL.p divides symmetrically by size, thus producing two similar-sized cells, each of which produces a PVM neuron either by differentiation or by division.
2. QL.pp survives and differentiates into a PVM neuron
3. QL.pp mitotic fate transformation; i.e. QL.pp not only survives but also undergoes division, like QL.pa, to produce an extra set of a PVM neuron and an SDQL neuron.

I was interested in understanding which of the above processes were affected in *ced-1(e1735)* and *ced-3(n2427)* animals, as a result of which extra PVM neurons were produced. Therefore, I systematically examined the effects of the loss of *ced-1* or *ced-3* on QL.p division asymmetry, QL.pp death and the ability of the undead QL.pp to divide.

3.2 QL.p division asymmetry

3.2.1 *ced-3* promotes size-asymmetry in QL.p division

I first asked if the loss of *ced-1* or *ced-3* causes QL.p to divide symmetrically rather than asymmetrically. In order to visualize QL.p, I generated a transgenic multicopy reporter, *bcIs133* ($P_{toe-2}gfp$), which produces soluble GFP in all cells of the QL and QR lineages. Using this reporter, I generated time-lapse recordings of QL.p division at a rate of three minutes per time point. The first time point after the completion of QL.p cytokinesis was used to estimate QL.p daughter cell sizes (**Fig. 3.3A**). Cells of the QL.p lineage are relatively

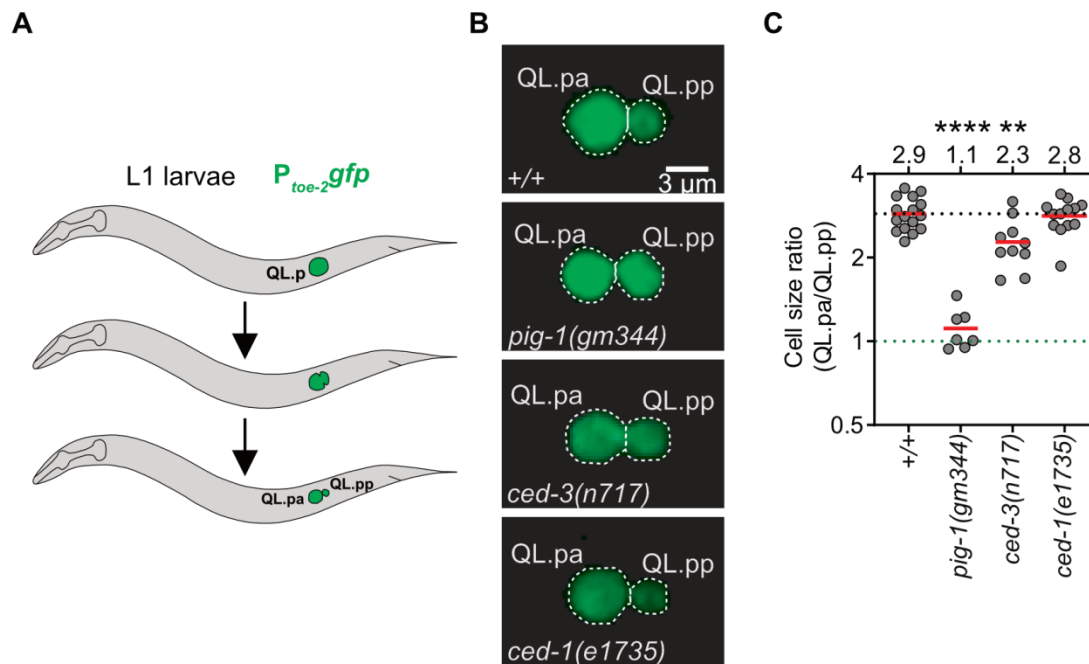


Figure 3.3: *ced-3* promotes size-asymmetry in QL.p division

(A) Diagrammatic representation of the assay used to assess QL.p division asymmetry. L1 larvae expressing *bcIs133* ($P_{toe-2}gfp$) were imaged every three minutes until QL.p division was complete. Upon completion of QL.p cytokinesis, QL.pa and QL.pp areas were measured. (B) Representative images showing QL.p daughter cells within three minutes upon completion of QL.p cytokinesis. (C) Dot plot showing cell size ratios (QL.pa/QL.pp) in the indicated genotypes. The black dotted line indicates the mean ratio in wild type, and the green dotted line indicates a ratio of 1.0. The mean ratio for each genotype is mentioned above the data points for the respective genotype. Statistical test: One-way ANOVA with Benjamini and Hochberg multiple comparisons correction. **: $p < 0.01$, ****: $p < 0.0001$, and $n \geq 7$ QL.p divisions.

flat cells (Cordes *et al.* 2006; Singhvi *et al.* 2011; Chien *et al.* 2013; Gurling *et al.* 2014; Teuliere *et al.* 2014). Therefore, single-plane or maximum-intensity projection measurements of cell area serve as an accurate indicator of cell volume. I measured QL.pa and QL.pp areas by circumscribing the respective cell boundaries in maximum intensity projection images. In wild-type animals, QL.pa was found to be 2.9 times as large as QL.pp on average (**Fig. 3.3B and C**). In *pig-1(gm344)* animals, on the other hand, consistent with previous reports, I found that this ratio was reduced to an average of 1.1 (**Fig. 3.3B and C**).

A similar analysis with *ced-1(e1735)* showed that, upon the loss of *ced-1* function, QL.pa was 2.8 times as large as QL.pp, suggesting that *ced-1* may not play a role in regulating size asymmetry in QL.p division (**Fig. 3.3B and C**). Further, QL.p division asymmetry also remained unaffected in *ced-3(n2427)* animals (average QL.pa/QL.pp size ratio = 2.8), which only partially lack *ced-3* function (**Fig. 3.10A and B**). However, animals completely lacking *ced-3* function, such as *ced-3(n717)* animals, showed a reduction in the size ratio of the QL.p daughters. In these animals, QL.pa was only 2.3 times as large as QL.pp on average (**Fig. 3.3B and C**). This shows that *ced-3* promotes size asymmetry during QL.p division.

3.2.2 Protease function of CED-3 is required for the regulation of size-asymmetry in QL.p division

ced-3 encodes a protease, which, when produced, is only partially catalytically active. This form of CED-3 is referred to as pro-CED-3 (Xue *et al.* 1996). In order for CED-3 to cleave its targets, it needs to autoactivate with assistance from CED-4, whose activation depends on EGL-1 (Yuan and Horvitz 1992; Conradt and Horvitz 1998). Therefore, although animals lacking *egl-1* or *ced-4* produce CED-3, most of the CED-3 remains only partially active. The analysis of QL.p daughter cell sizes in such animals can, thus, provide insights into the requirement for the CED-3 protease function in the regulation of QL.p division asymmetry. I examined a complete loss-of-function mutant for both *egl-1 (egl-1(n3330))* and *ced-4 (ced-4(n1162))* and found that animals lacking *egl-1* or *ced-4* exhibited a QL.pa to QL.pp size ratio of 2.2 or 2.0, respectively (**Fig. 3.4A and B**). In addition, I also analyzed QL.p division asymmetry in *ced-3(n2433)* animals, which harbor a disabling mutation in the CED-3 protease active site. In these animals, QL.pa was found to be 2.4 times as large as QL.pp on

average (**Fig. 3.4A and B**). These results demonstrate that *ced-3* promotes size asymmetry in QL.p division in a manner that is dependent on its protease function.

3.2.3 *ced-3* is required for posterior positioning of the cleavage furrow during QL.p division

QL.p daughter cell areas were determined using maximum intensity projection images based on previous observations that these are flat cells (see materials and methods). However, it is possible that in the apoptotic mutants QL.pa and QL.pp shapes are altered, and their morphologies are more rounded or spherical rather than flat. In such a scenario, cell area measurements obtained using maximum intensity projection images would be inaccurate indicators of cell volume. Therefore, in order to ascertain that the reduction in the QL.pa/QL.pp size ratio observed in the apoptotic mutants was not a result of altered cell morphology, I assessed the position of the QL.p cleavage furrow in these animals. Cleavage furrow positions were determined as shown in **Figure 3.5A** using the same movies that were used for daughter cell size estimations.

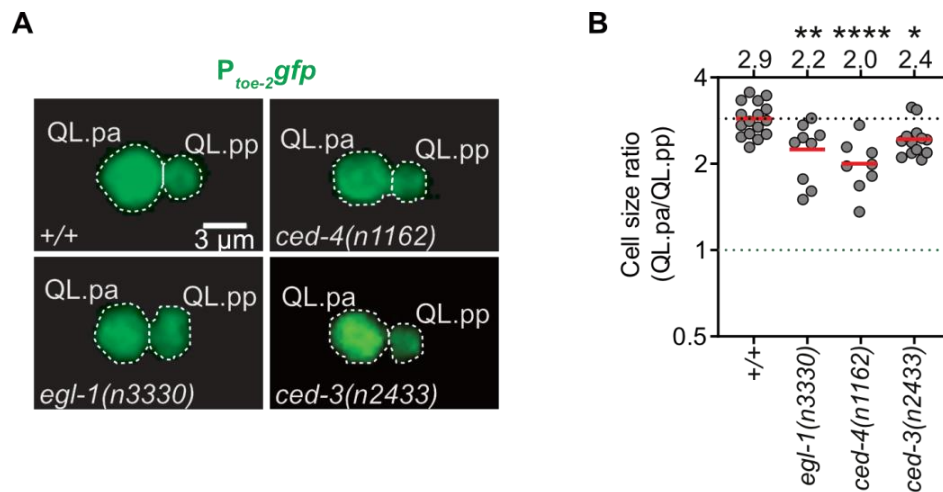


Figure 3.4: Protease function of CED-3 is required for the regulation of size asymmetry in QL.p division

(A) Representative images showing QL.p daughter cells within three minutes upon completion of QL.p cytokinesis in the indicated genotypes. (B) Dot plot showing cell size ratios (QL.pa/QL.pp) in the indicated genotypes. The black dotted line indicates the mean ratio in wild type, and the green dotted line indicates a ratio of 1.0. The mean ratio for each genotype is mentioned above the data points for the respective genotype. Statistical test: One-way ANOVA with Benjamini and Hochberg multiple comparisons correction. *: $p < 0.05$, **: $p < 0.01$, ****: $p < 0.0001$, and $n \geq 8$ QL.p divisions.

I found that, in wild-type animals, the QL.p cleavage furrow was positioned at 62.4% of QL.p length away from its anterior pole (**Fig. 3.5B**). In *pig-1(gm344)* animals, on the other hand, the cleavage furrow was positioned at 51.7% QL.p length (**Fig. 3.5B**). Therefore, a shift of 10.7% in the position of the cleavage furrow was sufficient to generate two daughters of similar sizes (*pig-1(gm344)* QL.pa/QL.pp size ratio = 1.1) rather than of significantly unequal sizes (wild-type QL.pa/QL.pp size ratio = 2.9) (**Fig. 3.3B and C, and Fig. 3.5B**). This suggests that small changes in QL.p daughter cell size ratio could potentially arise from statistically insignificant shifts in the cleavage furrow position.

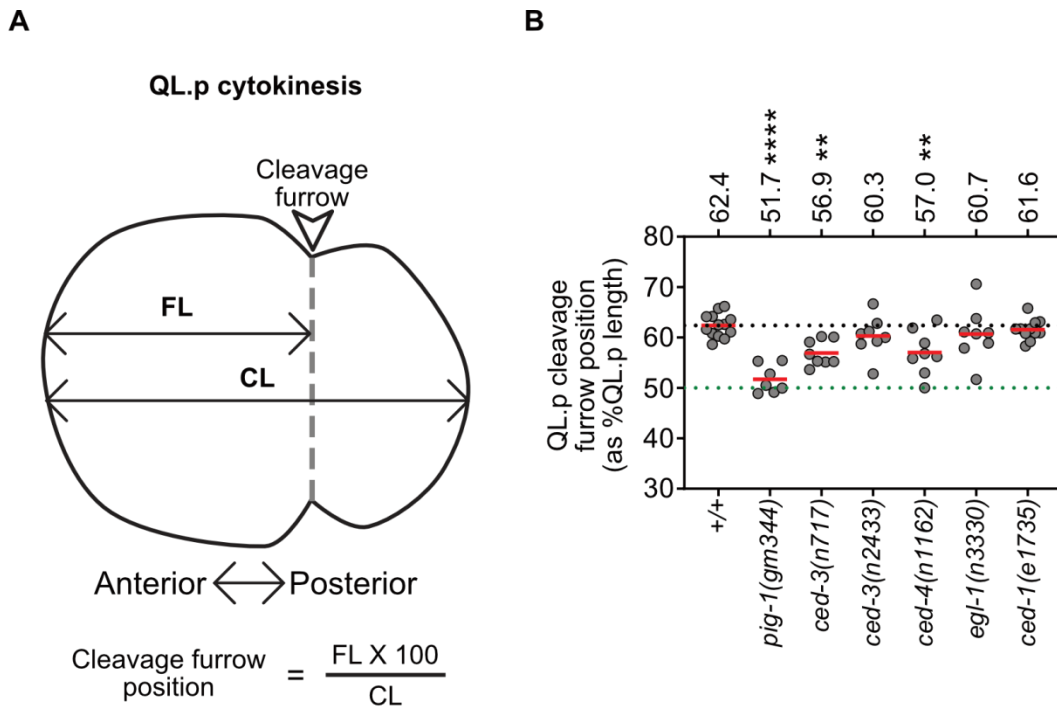


Figure 3.5: *ced-3* is required for posterior positioning of the QL.p cleavage furrow

(A) Representation of the methodology for the quantification of the cleavage furrow position during QL.p division. The ratio of distances between the cleavage furrow and the anterior pole (FL) and between the anterior and posterior poles (CL) was used to determine the position of the cleavage furrow. (B) Dot plot showing position of the QL.p cleavage furrow in the indicated genotypes. The black dotted line indicates the mean position in wild type, and the green dotted line indicates a position corresponding to 50% QL.p length. The mean position for each genotype is mentioned above the data points for the respective genotype. Statistical test: One-way ANOVA with Benjamini and Hochberg multiple comparisons correction. **: $p < 0.01$, ****: $p < 0.0001$, and $n \geq 8$ QL.p divisions.

I found that, in *ced-3(n717)* and *ced-4(n1162)* animals, the QL.p cleavage furrow was significantly shifted toward the anterior pole and was placed at 56.9% QL.p length and 57% QL.p length, respectively (**Fig. 3.5B**). This demonstrates that *ced-3*, and likely the protease function of CED-3, is required for posterior positioning of the QL.p cleavage furrow. QL.p cleavage furrow was also shifted toward the anterior pole in *egl-1(n3330)* (60.7% QL.p length) and *ced-3(n2433)* (60.3% QL.p length) animals, but these shifts were not found to be statistically significant (**Fig. 3.5B**). As discussed earlier, small shifts in the cleavage furrow position can result in significant changes in daughter cell size asymmetry. Therefore, I postulate that the statistically ‘not significant’ shifts in the QL.p cleavage furrow position observed in *egl-1(n3330)* and *ced-3(n2433)* may account for the significant reduction in QL.p daughter cell size asymmetry in these mutants. Consistent with the above observations and as a result of the anterior shift in the cleavage furrow position, I found that, in the apoptotic mutants, QL.pa was indeed slightly smaller than in wild-type (Mean QL.p areas in μm^2 : wild-type – 13.4, *pig-1(gm344)* – 9.9, *ced-3(n717)* – 13.1, *ced-4(n1162)* – 12.7, *egl-1(n3330)* – 11.7 and *ced-3(n2433)* – 12.9), whereas QL.pp was slightly larger than in wild-type (Mean areas in μm^2 : wild-type – 4.7, *pig-1(gm344)* – 9.1, *ced-3(n717)* – 5.9, *ced-4(n1162)* – 6.5, *egl-1(n3330)* – 5.3 and *ced-3(n2433)* – 5.3). In *ced-1(e1735)* animals, however, the QL.p cleavage furrow was positioned similar to that in wild-type (61.6% QL.p length) (**Fig. 3.5B**).

3.3 QL.pp death

3.3.1 The engulfment gene *ced-1* promotes QL.pp death

An extra PVM neuron could arise simply due to increased failure of QL.pp death and, therefore, the availability of a larger pool of undead QL.pps which can divide. Three studies have previously shown that *ced-1* and other engulfment genes promote apoptotic cell death in different cell lineages (Hoepfner *et al.* 2001; Reddien *et al.* 2001; Chakraborty *et al.* 2015). I, thus, examined if the loss of *ced-1* leads to increased failure of QL.pp death. Again, I used *bcIs133* in order to visualize cells of the QL.p lineage. Upon completion of the QL.p lineage development, in wild-type animals expressing *bcIs133*, only two GFP-positive cells are

normally present – PVM and SDQL (**Fig. 3.6A**). However, in animals, such as *ced-3(lf)*, *ced-4(lf)* or *egl-1(lf)*, where QL.pp fails to undergo apoptosis, a third GFP-positive cell is present (**Fig. 3.6A**). Indeed, using this assay, I found that *ced-3(n717)*, *ced-4(n1162)* and *egl-1(n3330)* animals, all of which are strong lf mutants for the respective genes, show a near complete failure of QL.pp death. Specifically, 94% of *ced-3(n717)*, 100% of *ced-4(n1162)* and 90% of *egl-1(n3330)* animals showed a third GFP-positive cell (**Fig. 3.6B**). In these animals, QL.pp failed to undergo apoptosis. In addition, in 85% of the caspase-dead *ced-3(n2433)* animals, QL.pps inappropriately survived, which reinforces the idea that CED-3 caspase activity is required for QL.pp death (**Fig. 3.6B**). On the other hand, 0% of *ced-1(e1735)* animals showed inappropriate QL.pp survival (**Fig. 3.6B**). Nevertheless, *ced-1(e1735)* enhanced inappropriate QL.pp survival observed in *ced-3(n2427)* animals from 37% to 58% (**Fig. 3.6B**). Similarly, mutations in two other engulfment genes – *ced-2(n1994)* and *ced-6(n1813)* – also enhanced QL.pp survival in *ced-3(n2427)* animals from 37% to 58% and 60%, respectively (**Fig. 3.6B**). These data establish that, as has been previously shown for other cell lineages, engulfment genes, including *ced-1*, promote apoptotic death of QL.pp.

3.3.2 *ced-1* acts in parallel to *pig-1* to promote QL.pp death

pig-1(gm344) animals exhibit a 45% QL.pp survival phenotype; i.e. QL.pp survives in 45% of these animals (**Fig. 3.6B**). Therefore, *pig-1*, like *ced-1*, is required for the specification and/or execution of the QL.pp apoptotic fate. I wondered, therefore, if *ced-1* and *pig-1* act in the same genetic pathway to promote QL.pp death. Since both *ced-1(e1735)* and *pig-1(gm344)* are complete loss-of-function mutants, relationship between the two genes can be reliably deciphered by examining *ced-1(e1735); pig-1(gm344)* double mutants. I found that in 86% of the double mutant animals, QL.pp inappropriately survived as compared to 45% of *pig-1(gm344)* single mutant animals (**Fig. 3.6B**). This enhancement of QL.pp survival observed in *pig-1(gm344)* animals by *ced-1(e1735)* suggests that *ced-1* and *pig-1* act in independent genetic pathways to promote QL.pp death. Similarly, partial loss of *ced-3* (*ced-3(n2427)*) also enhanced QL.pp survival in *pig-1(gm344)* from 45% to 94% (**Fig. 3.6B**). Finally, in 100% of *ced-1(e1735); pig-1(gm344) ced-3(n2427)* triple mutants, QL.pp failed to die (**Fig. 3.6B**). Therefore, lack of both *ced-1* and/or *ced-3* in *pig-1(gm344)* animals indeed results in the presence of a larger pool of undead QL.pps that can divide to produce extra PVM neurons.

3.3.3 CED-1 is in asymmetric contact with QL.p and promotes QL.pp death cell non-autonomously

While the mechanism through which *ced-3* causes cell death is well understood, so far, we have only a limited understanding of how *ced-1* promotes cell death. Therefore, in order to understand how *ced-1* promotes QL.pp death, I first examined the localization pattern of CED-1 with respect to the QL.p lineage. Using the transgenic reporters *enIs1* ($P_{ced-1}ced-1\Delta C::gfp$) to visualize CED-1 localization and *rdvIs1* ($P_{egl-17}mCherry::TEV-S::his-24$, $P_{egl-17}myristoylated\ mCherry$, $P_{egl-17}mig-10::yfp$) to visualize the QL.p lineage cells, I found that CED-1 $\Delta C::GFP$ localized to the entire plasma membrane of what seemed to be the hyp7 syncytium (**Fig. 3.7**). In addition, hyp7, and as a result, CED-1 $\Delta C::GFP$, was found to be in asymmetric contact with QL.p (**Fig. 3.7**). More specifically, while hyp7 was in near complete contact with the entire lateral surface of QL.p, it only formed visible contact with the posterior (but not the anterior) part of QL.p on the medial side (**Fig. 3.7**). Importantly, it is the posterior part of QL.p which later produces the smaller apoptotic daughter cell, QL.pp. These observations were further strengthened by images of transmission electron microscopy sections made publicly available on Wormatlas by Prof. David Hall (<http://www.wormatlas.org/>). Therefore, CED-1 localizes asymmetrically around QL.p, such that its posterior part, which later produces the apoptotic daughter cell, is apposed to a much larger amount of CED-1 as compared to its anterior part.

Further, no *ced-1* $\Delta C::gfp$ expression was detected in QL.p, suggesting that *ced-1* may act cell non-autonomously to promote QL.pp death (**Fig. 3.7**). To test this idea, I generated transgenes which express *ced-1* specifically in the QL.p lineage cells (*bcEx1334* ($P_{10e-2}ced-1::mKate2$)) or in hyp7 (*bcEx1277* ($P_{hyp7}ced-1::gfp$)). I asked if specific expression of *ced-1* in either QL.p or hyp7 could suppress the failure of QL.pp death observed in *ced-1(e1735); ced-3(n2427)* animals. Indeed, I found that *ced-1* expression in hyp7 alone suppressed inappropriate QL.pp survival in *ced-1(e1735); ced-3(n2427)* double mutants from 58% to 39% (**Fig. 3.6B**). Considering that *ced-3(n2427)* animals exhibit 37% QL.pp survival, this means that *ced-1* expression in hyp7 alone is sufficient to almost completely compensate for

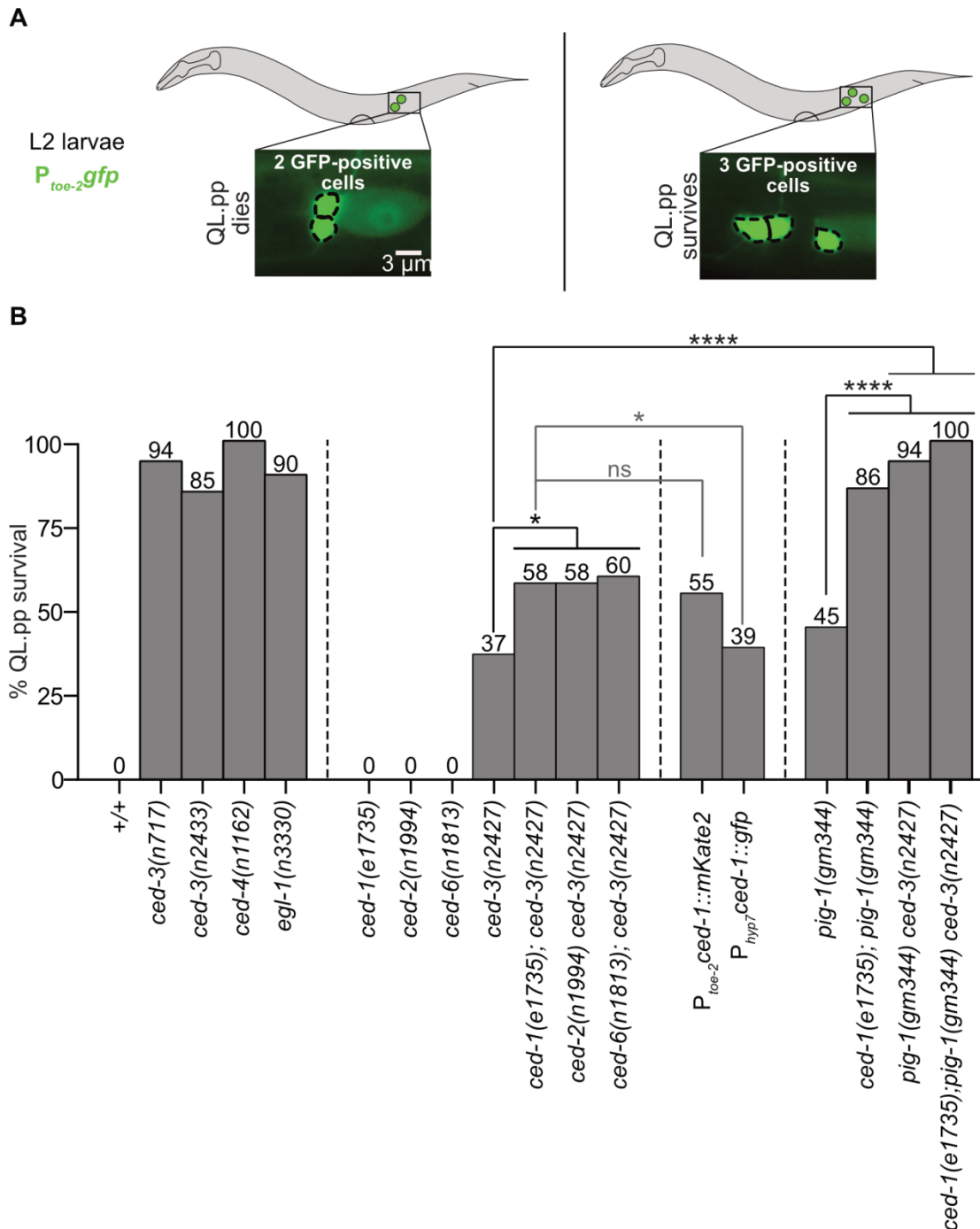


Figure 3.6: *ced-1* cell non-autonomously promotes QL.pp death by acting in parallel to *pig-1*.

(A) Representation of the assay. Cells were visualized using the *bcls133* transgene. In animals, where QL.pp successfully dies, two GFP-positive cells are present. On the other hand, at least three such cells are present in animals in which QL.pp does not die. (B) Bar graph showing percentage QL.p lineages in which QL.pp failed to undergo apoptosis. Statistical test: Fischer's Exact Test with Benjamini and Hochberg multiple comparisons correction. *: $p < 0.05$, ****: $p < 0.0001$, and $n \geq 50$ animals.

the lack of *ced-1* for QL.pp death. On the other hand, expression of *ced-1* specifically in the QL.p lineage cells did not alter QL.pp survival observed in *ced-1(e1735); ced-3(n2427)* animals (**Fig. 3.6B**). Therefore, *ced-1* most likely promotes QL.pp death cell non-autonomously by acting in hyp7.

3.3.4 *ced-1* is required to establish/maintain a gradient of active CED-3 in QL.p

Previous work from our group has shown that, during NSM neuroblast division, which also produces an apoptotic daughter cell, CED-3 is catalytically active in the mother cell (Chakraborty et al. 2015). In addition, active CED-3 is organized as a gradient in a manner that is dependent on *ced-1* and the other engulfment genes (Chakraborty et al. 2015). This gradient presumably facilitates a disproportionate segregation of active CED-3 in the smaller daughter, NSMsc, which is programmed to undergo apoptosis. I investigated if a similar gradient of active CED-3 exists in QL.p.

TAC-1, a centrosomal protein, is a CED-3-substrate (Chakraborty *et al.* 2015). Upon cleavage by CED-3, TAC-1 dissociates from the centrosome, and therefore, the localization of TAC-1 to a centrosome can be used as readout to decipher the amount of active CED-3 in its vicinity. To visualize TAC-1 in the QL.p lineage, I generated a single-copy transgenic reporter strain *bcSi82* ($P_{toe-2}mKate2::tac-1$) and combined it with *bcIs133* ($P_{toe-2}gfp$). During QL.p metaphase, I then compared the amounts of TAC-1 associated with both the anterior and the posterior centrosomes. I found that, in wild-type animals, 1.25-fold more TAC-1 was associated with the anterior centrosome as compared to the posterior centrosome on average (**Fig. 3.8A and B**). This means that more active CED-3 is present in the posterior part of QL.p as compared to the anterior part and, like in the NSM neuroblast lineage, presumably leads to a greater segregation of active CED-3 in the posterior daughter, which is programmed to die (**Fig. 3.8B**). As expected, in *ced-3(n717)* animals, this TAC-1 asymmetry is lost (mean ratio anterior/posterior = 0.97), confirming that the TAC-1 asymmetry is indeed dependent on *ced-3* (**Fig. 3.8A and C**). Further, in *ced-1(e1735)* animals as well, TAC-1 asymmetry (and therefore, active CED-3 gradient) was abolished (mean ratio

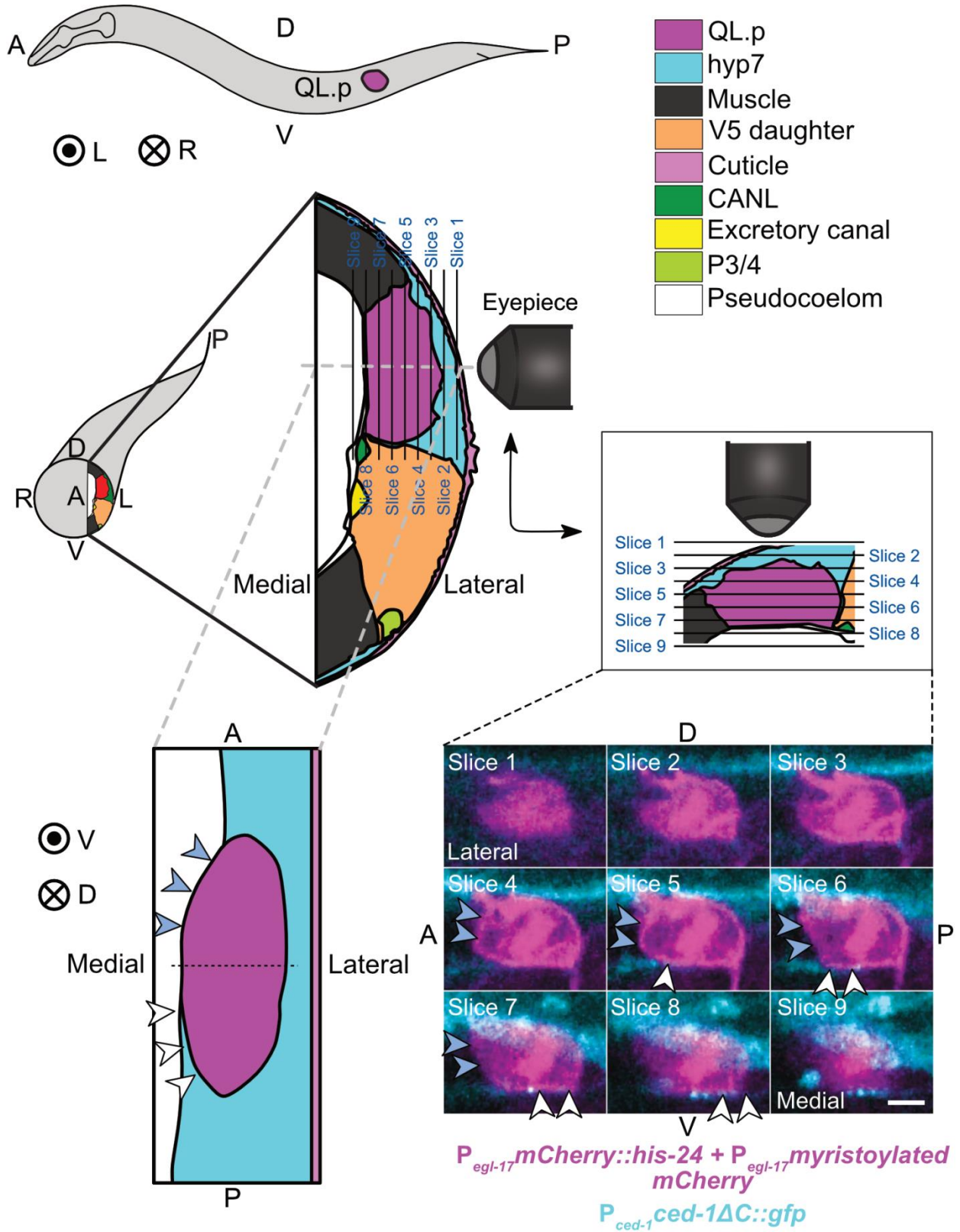


Figure 3.7: CED-1 is in asymmetric contact with QL.p

Figure 3.7: CED-1 is in asymmetric contact with QL.p

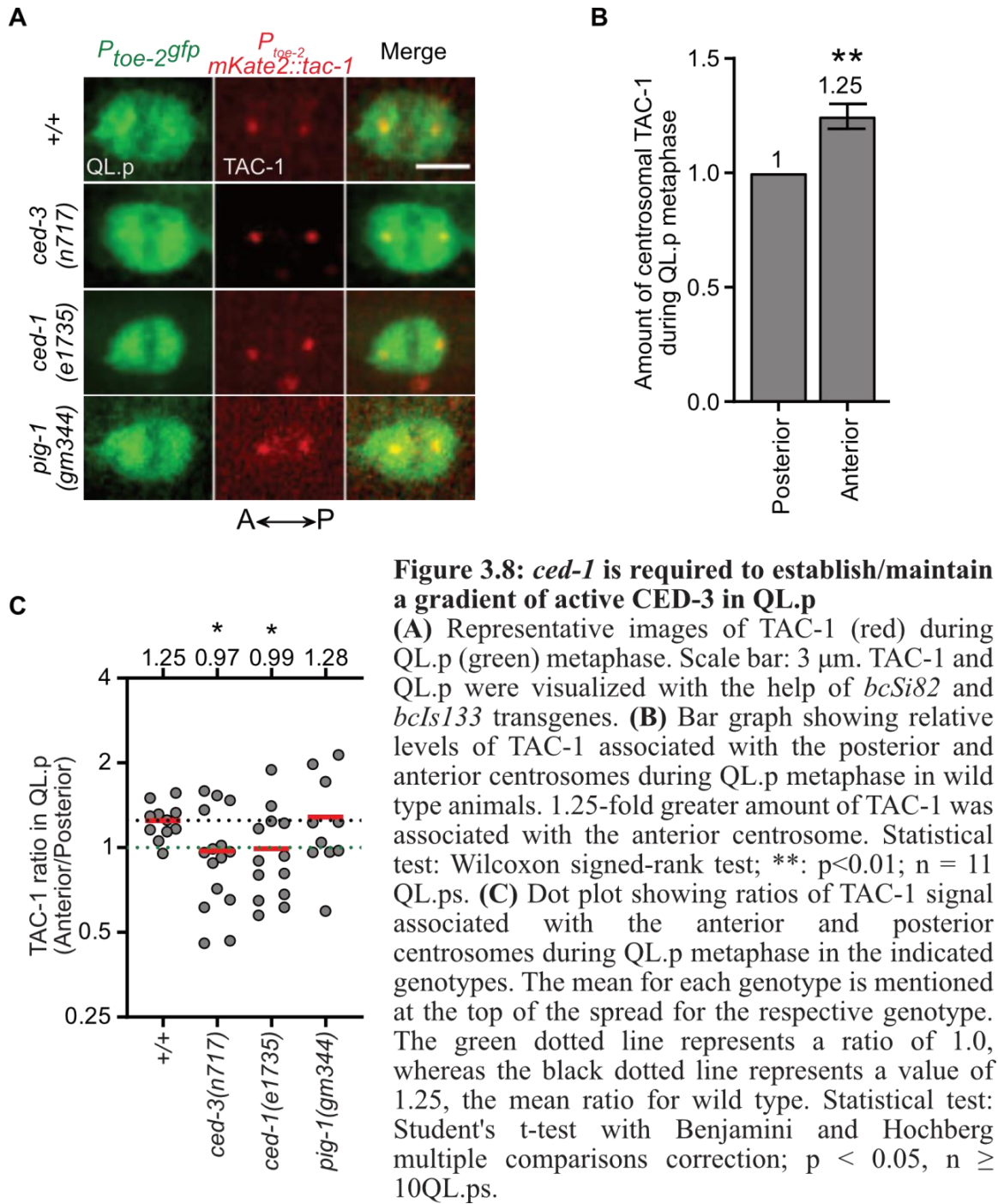
Schematic of the position of QL.p in an L1 larva (top-left); A: anterior, P: posterior, D: dorsal, V: ventral, L: left, and R: right. Concentric circles represent the direction projecting toward the reader, while the circle with a cross represents the direction projecting away from the reader. Schematics below the L1 larva (middle-left and middle-right) represent a transverse section through QL.p. This and the coronal section (bottom-left) were drawn based on fluorescence images and images of electron microscopy sections available on WormAtlas (<http://www.wormatlas.org/>). The key for cell colors is at the top-right. Larvae were imaged from the side, and individual image slices were acquired while gradually moving from the left to the middle of the worm. QL.p was labeled with the transgene $P_{egl-17}::mCherry::his-24$, $P_{egl-17}::myristoylated\ mCherry$, $P_{egl-17}::mig-10::yfp$ (*rdvIs1*) and *hyp7* with the transgene $P_{ced-1}::ced-1\Delta C::gfp$ (*enIs1*) (see Materials and Methods for details). The diagram in the middle-right represents the orientation of the image planes, images for which have been shown at the bottom-right. In these images, white arrowheads indicate a contact between CED-1 $\Delta C::GFP$ and QL.p, whereas blue arrowheads indicate the lack of contact. Bar, 2 μm . It can be seen in the images for slices 4–9 that CED-1 $\Delta C::GFP$ is in contact with the posterior half of QL.p but not with its anterior part. The coronal section (bottom-left) has been created based on the fluorescence images (slices shown at the bottom-right) and the images of the electron microscopy sections. It can be seen in this diagram that while *hyp7* almost entirely envelopes the posterior part of QL.p, it only forms contact with the lateral side of the anterior part.

anterior/posterior = 0.99) (**Fig. 3.8A and C**). Interestingly, however, the active CED-3 gradient remained intact in *pig-1(gm344)* animals (mean ratio anterior/posterior = 1.28), which has been previously suggested to be required for segregation of fate determinants during QL.p division (**Fig. 3.8A and C**) (Cordes *et al.* 2006; Chien *et al.* 2013). Hence, a *ced-1*-dependent, *pig-1*-independent, active CED-3 gradient is present in QL.p at metaphase. *ced-1*, therefore, likely promotes QL.pp death by promoting increased segregation of active CED-3 into QL.pp.

3.4 QL.pp division

3.4.1 *ced-3* prevents division of undead QL.pp

Extra PVM neurons are often generated when the undead QL.pps undergo a mitotic fate transformation; i.e. when QL.pps divide, like QL.pa, to produce an extra pair of a PVM and an SDQL neuron (**Fig. 3.1**). In principle, failure of QL.pp death (and therefore, an increase in the pool of undead QL.pps) upon the loss of *ced-3* or *ced-1* could be sufficient to increase the penetrance with which extra PVM neurons appear in a *pig-1(gm344)* background.



Nevertheless, I was wondering if *ced-3* and/or *ced-1* also influence the frequency with which undead QL.pps undergo a mitotic fate transformation. When QL.pp survives but does not divide, *bcIs133* animals show the presence of three QL.p-descendant cells (**Fig. 3.9A**). However, in animals where QL.pp divides, a fourth QL.p-descendant cell is visible (**Fig.**

3.9A). Using this assay, I determined the frequencies with which undead QL.pps divide in several genetic backgrounds.

In all wild-type animals, QL.pp successfully dies (**Fig. 3.6B**). Therefore, the above assay, which requires the presence of undead QL.pps, cannot be performed in wild-type animals. I examined *pig-1(gm344)* animals as positive control. In 56% of *pig-1(gm344)* animals, four QL.p-descendant cells were visible – in these animals, QL.pp had undergone a mitotic fate transformation (**Fig. 3.9B**). Interestingly, 11% of *ced-3* null mutants, *ced-3(n717)*, showed the presence of four QL.pp-descendant cells (**Fig. 3.9B**). Therefore, in a small fraction of *ced-3(n717)* animals, the undead QL.pp had indeed undergone a mitotic fate transformation. This shows that *ced-3* prevents QL.pp mitotic fate specification/execution.

3.4.2 Protease function of CED-3 is required to prevent the division of undead QL.pp

To understand if *ced-3* prevents QL.pp mitotic fate specification/execution in a manner that is dependent on the protease function of CED-3, I asked if undead QL.pps in *ced-4(n1162)* and *egl-1(n3330)* animals also underwent a mitotic fate transformation. *ced-4* and *egl-1* are required for CED-3 protease activity, and in animals lacking *ced-4* or *egl-1* function, most CED-3, therefore, remains only partially catalytically active. I found that 7% of *ced-4(1162)* and 2% of *egl-1(n3330)* animals observed had four QL.pp-descendant cells (**Fig. 3.9B**). In addition, *ced-3(n2433)* animals, which produce CED-3 that is incapable of performing its protease function, also showed a 4% frequency with which the undead QL.pp underwent a mitotic fate transformation (**Fig. 3.9B**). Put together, these data establish that *ced-3* prevents mitotic fate transformation of QL.pp in a manner that is dependent on the protease activity of CED-3.

3.4.3 *ced-3* prevents QL.pp division independently of QL.pp size

Since null mutations in *ced-3*, *ced-4* and *egl-1* only produced mild phenotypes of QL.pp division, I wondered if the phenotypes would be more pronounced in a sensitized genetic background, such as *pig-1(gm344)*. In an otherwise wild-type background, *ced-3(n2427)* animals, which only partially lack *ced-3* function, did not exhibit a QL.pp mitotic fate

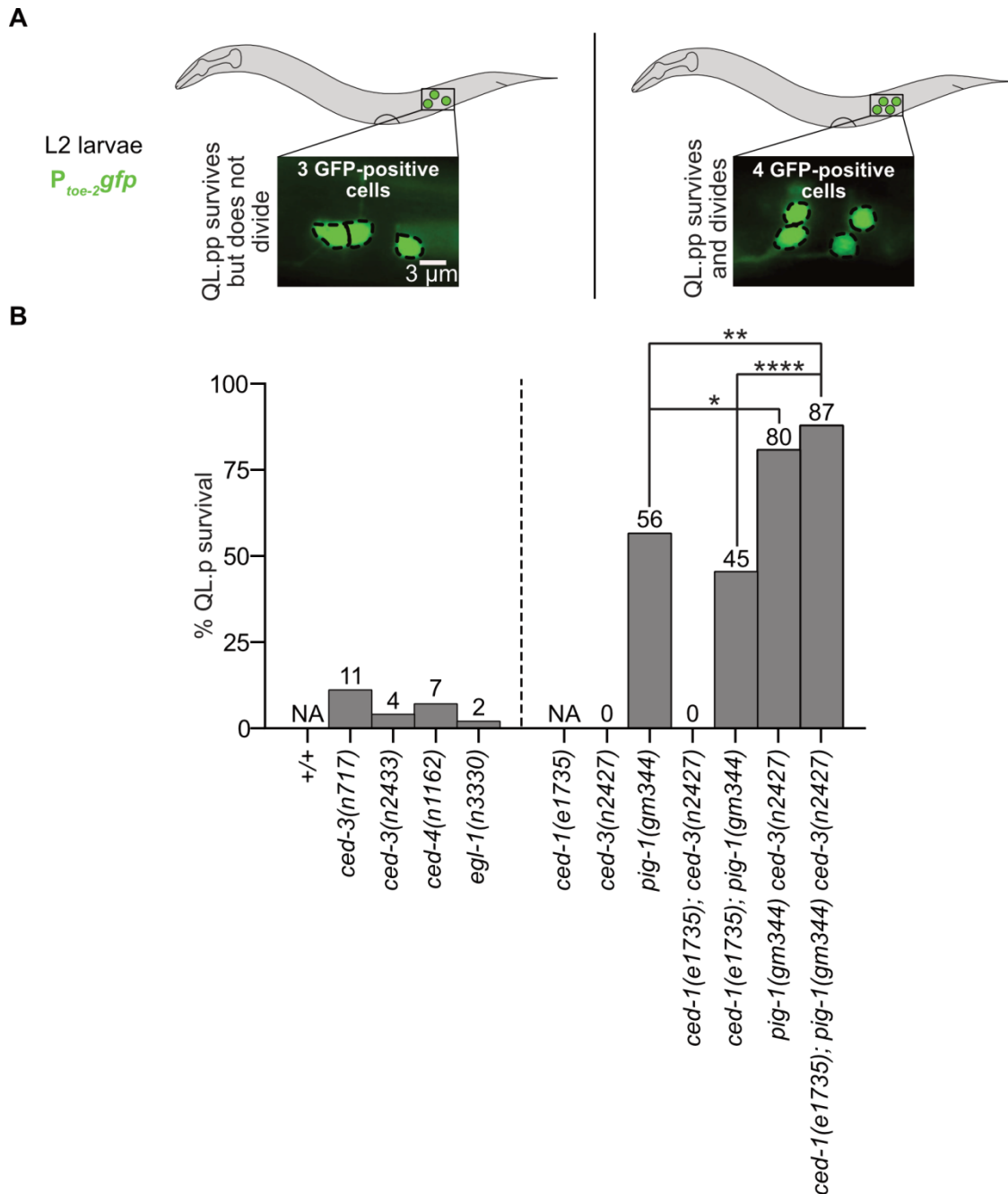


Figure 3.9: *ced-3*, but not *ced-1*, prevents division of undead QL.p.p

(A) Representation of the assay. Cells were visualized using the *bclL133* transgene. Only those animals were considered for this assay in which QL.p.p had inappropriately survived. In such animals, when the undead QL.p.p does not divide, three GFP-positive cells can be seen. On the other hand, if the undead QL.p.p divides, four GFP-positive cells can be seen. (B) Bar graph showing percentage undead QL.p.p.s that divided. Statistical test: Fischer's Exact Test with Benjamini and Hochberg multiple comparisons correction. NA: Not Applicable (as there are no undead QL.p.p.s in these genotypes), *: p<0.05, **: p<0.01, ****: p<0.0001, and n \geq 50 animals.

transformation phenotype (**Fig. 3.9B**). However, *ced-3(n2427)* enhanced the penetrance with which undead QL.pps divided in a *pig-1(gm344)* mutant background from 56% to 80% (**Fig. 3.9B**). This, again, confirmed that *ced-3* influences mitotic fate determination of QL.pp.

pig-1 is required for QL.p division to occur asymmetrically by size as well as for the correct segregation of mitotic fate determinants during QL.p division. However, altered cell size asymmetry during the mother cell division alone can also be sufficient to modify daughter cell fate through a passive effect on the amount/concentration of fate determinants segregated into each daughter cell. In a previous section of this thesis, I described a novel role of *ced-3* in regulating size asymmetry during QL.p division. In *ced-3(lf)* animals, QL.pp is larger in size as compared to that in wild-type animals. Therefore, the next logical step was to investigate if the QL.pp mitotic fate transformation in *ced-3(lf)* animals was simply a passive effect of an increased QL.pp size. Since undead QL.pps in animals lacking both *pig-1* and *ced-3* (i.e. *pig-1(gm344) ced-3(n2427)*) had a greater potential to divide as compared to those lacking *pig-1* alone (i.e. *pig-1(gm344)*), I asked if the defect in QL.p division asymmetry was also greater in the double mutants. I reasoned that a greater defect in QL.p division asymmetry in *pig-1(gm344) ced-3(n2427)* animals could result in a more extreme missegregation of mitotic fate determinants and therefore, could cause a greater fraction of undead QL.pps to divide.

I acquired time lapse images of QL.p division in *pig-1(gm344) ced-3(n2427)* animals as described earlier and assessed QL.p division asymmetry by measuring QL.pa and QL.pp sizes within three minutes after the completion of cytokinesis. In *ced-3(n2427)* animals, QL.pa is 2.8 times in size as compared to QL.pp, whereas the corresponding ratio for *pig-1(gm344)* animals is 1.1 (**Fig. 3.10A and B**). *pig-1(gm344) ced-3(n2427)* double mutants did not exhibit a greater defect in QL.p division asymmetry as the QL.pa/QL.pp size ratio in these animals was 1.0, which was similar to that in *pig-1(gm344)* animals (**Fig. 3.10A and B**). Yet, the undead QL.pps in *pig-1(gm344) ced-3(n2427)* double mutants had a greater ability to divide despite being of a size comparable to that in *pig-1(gm344)* animals (**Fig. 3.9B**). This suggests that the effect of the loss of *ced-3* on QL.pp mitotic fate transformation is not a passive result of an increase in QL.pp size in these animals. In other words, *ced-3*

actively prevents the segregation of mitotic fate determinants into QL.pp and/or inhibits their activity in QL.pp.

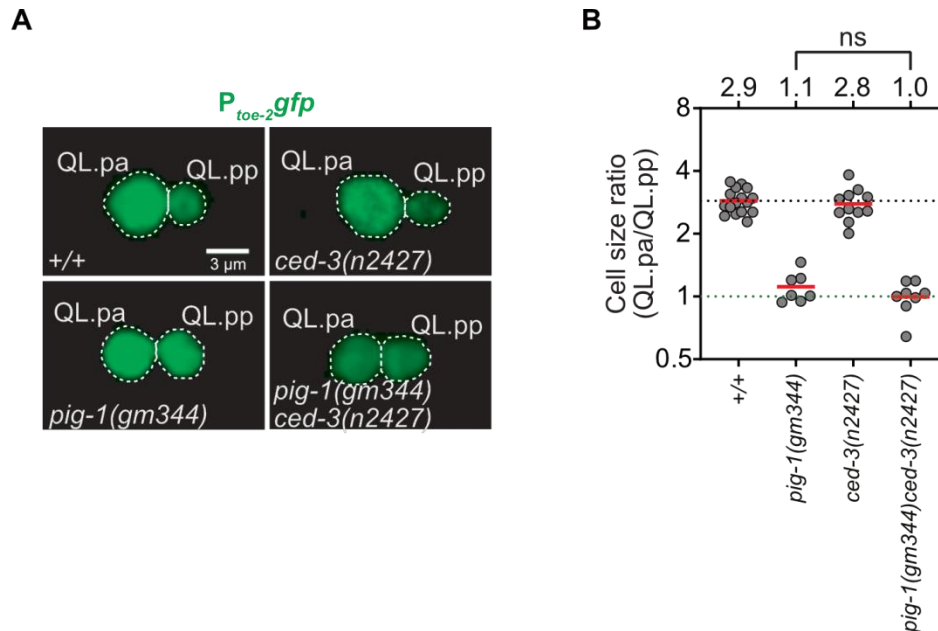


Figure 3.10: *ced-3* prevents QL.pp division independently of QL.pp size

(A) Representative images showing QL.p daughter cell sizes within three minutes upon completion of QL.p cytokinesis in the indicated genotypes (B) Dot plot showing cell size ratios (QL.pa/QL.pp) in the indicated genotypes. The black dotted line indicates the mean ratio in wild type, and the green dotted line indicates a ratio of 1.0. The mean ratio for each genotype is mentioned above the data points for the respective genotype. Statistical test: One-way ANOVA with Benjamini and Hochberg multiple comparisons correction. ns: not significant and $n \geq 7$ QL.p divisions.

3.4.4 *ced-1* may not be required to prevent QL.pp division

I then asked if, similar to that of *ced-3*, the loss of *ced-1* also causes a missegregation or ectopic activation of mitotic fate determinants in QL.pp, which may explain the appearance of extra PVM neurons upon the loss of *ced-1*. I determined the frequency with which QL.pp divided to result in the presence of four QL.p-descendant cells. In all *ced-1(e1735)* single mutants, like in wild-type, QL.pp successfully undergoes apoptosis (Fig. 3.6B). Thus, there are no undead QL.pps whose division can be assessed in these animals. Therefore, I asked if *ced-1(e1735)* could alter the penetrance of QL.pp mitotic fate transformation in *pig-*

I(gm344) or *ced-3(n2427)* animals. I found that *ced-1(e1735)* did not cause an increase in instances of mitotic fate transformation in either of these genotypes. *ced-1(e1735); pig-1(gm344)* animals showed a 45% penetrance of QL.pp mitotic fate transformation (v/s 56% in *pig-1(gm344)*), and *ced-1(e1735); ced-3(n2427)* animals showed a 0% penetrance (v/s 0% in *ced-3(n2427)*) (**Fig. 3.9B**). Further, loss of *ced-1* also did not enhance the frequency of QL.pp mitotic fate transformation in *pig-1(gm344); ced-3(n2427)* animals. In *ced-1(e1735); pig-1(gm344) ced-3(n2427)* triple mutants, 87% of the undead QL.pps divided as compared to 80% in *pig-1(gm344) ced-3(n2427)* double mutants (**Fig. 3.9B**). Therefore, the loss of *ced-1* does not alter the frequency with which QL.pp undergoes mitotic fate transformation in any of the genetic backgrounds examined. This suggests that *ced-1* does not play a role in preventing QL.pp division.

I have shown in an earlier section of this thesis that *ced-1* helps establish/maintain a gradient of catalytically active CED-3 in QL.p at metaphase. Therefore, an interesting implication of the data presented so far is that, while CED-3 activity is required to regulate both size- and fate-asymmetries during QL.p division, a gradient *per se* of active CED-3 is not necessary. In addition, these data show that, although both *ced-1* and *ced-3* prevent the generation of extra PVM neurons, they accomplish this in two different ways. *ced-1* promotes QL.pp death and therefore limits the pool of undead QL.pps that could divide to produce extra PVM neurons. On the other hand, *ced-3* regulates at least three different processes during the progression of the QL.p lineage. It promotes size asymmetry during QL.p division by helping to position the QL.p cleavage furrow posteriorly, promotes QL.pp death and thus limits the pool of undead QL.pps and finally, prevents QL.pp division by potentially regulating mitotic fate determinants segregation/activity in QL.pp. Appropriate execution of these three processes ensures that QL.pp is small in size (which may render it too small to divide) and that it inherits factors that promote an apoptotic fate and prevent a mitotic fate.

3.5 Role of *ced-3* in cell division in other cell lineages

3.5.1 *ced-3* promotes size-asymmetry during QL.a division

Upon having established that *ced-3* promotes asymmetry during QL.p division, I was interested in determining if *ced-3* performs a similar role during asymmetric divisions of other cells that produce an apoptotic daughter. QL.a, the sister cell of QL.p, also divides

asymmetrically and produces a smaller anterior daughter, QL.aa, and a larger posterior daughter, QL.ap (Sulston and Horvitz 1977). QL.aa undergoes apoptosis, whereas QL.ap differentiates into an oxygen- and minor CO₂-sensory neuron referred to as the PQR neuron (Sulston and Horvitz 1977).

I asked if *ced-3* plays a role in regulating asymmetry in QL.a division. To that end, I performed time lapse recordings similar to that for assessing QL.p division asymmetry. I found that, in wild-type animals, QL.ap is 2.7 times as large as QL.aa on average (**Fig. 3.11A and B**). However, in *ced-3(n717)* animals, this ratio was reduced to 2.1 (**Fig. 3.11A and B**). This shows that *ced-3* promotes size-asymmetry in cell division of more than one postembryonic lineage that produces an apoptotic cell.

3.5.2 *ced-3* promotes size-asymmetry in NSM neuroblast division

We then wondered if *ced-3* performs a similar function also during embryonic cell divisions that give rise to an apoptotic daughter cell. To address this, Hai Wei, a doctoral student in our group, examined asymmetry during the NSM neuroblast (NSMnb) division. In wild-type embryos, NSMnb divides asymmetrically by size to produce a larger ventral daughter cell, which differentiates into an NSM (**N**eu**S**ecretory **M**otorneuron) neuron, and a smaller dorsal daughter cell, NSMsc (NSM **s**ister **c**ell), which dies by apoptosis within 20-25 minutes of its birth (Sulston *et al.* 1983; Chakraborty *et al.* 2015). Using *lIs44* (*P_{pie-1}mCherry::ph^{plcδ}*) to visualize the plasma membrane of the NSM neuroblasts and their daughter cells, he assessed the effect of the loss of *ced-3* on NSMnb division asymmetry. Sizes of the cells were measured as described previously (Hatzold and Conradt 2008; Chakraborty *et al.* 2015; Wei *et al.* 2017).

In wild-type embryos, the NSM/NSMsc size ratio is 1.6 on average (**Fig. 3.11C and D**). This ratio is reduced to 1.0 in *pig-1(gm344)* embryos; i.e. in *pig-1(gm344)*, NSMnb divides symmetrically to produce two similar-sized daughter cells (**Fig. 3.11C and D**). However, while embryos lacking *ced-3* (*ced-3(n717)*) or *ced-4* (*ced-4(n1162)*) did not show a reduced asymmetry during NSMnb division in an otherwise wild-type background, they altered the asymmetry-defect observed in a *pig-1(gm344)* background (**Fig. 3.11C and D**). In a *pig-1(gm344)* background, both *ced-3(n717)* and *ced-4(n1162)* embryos exhibited an

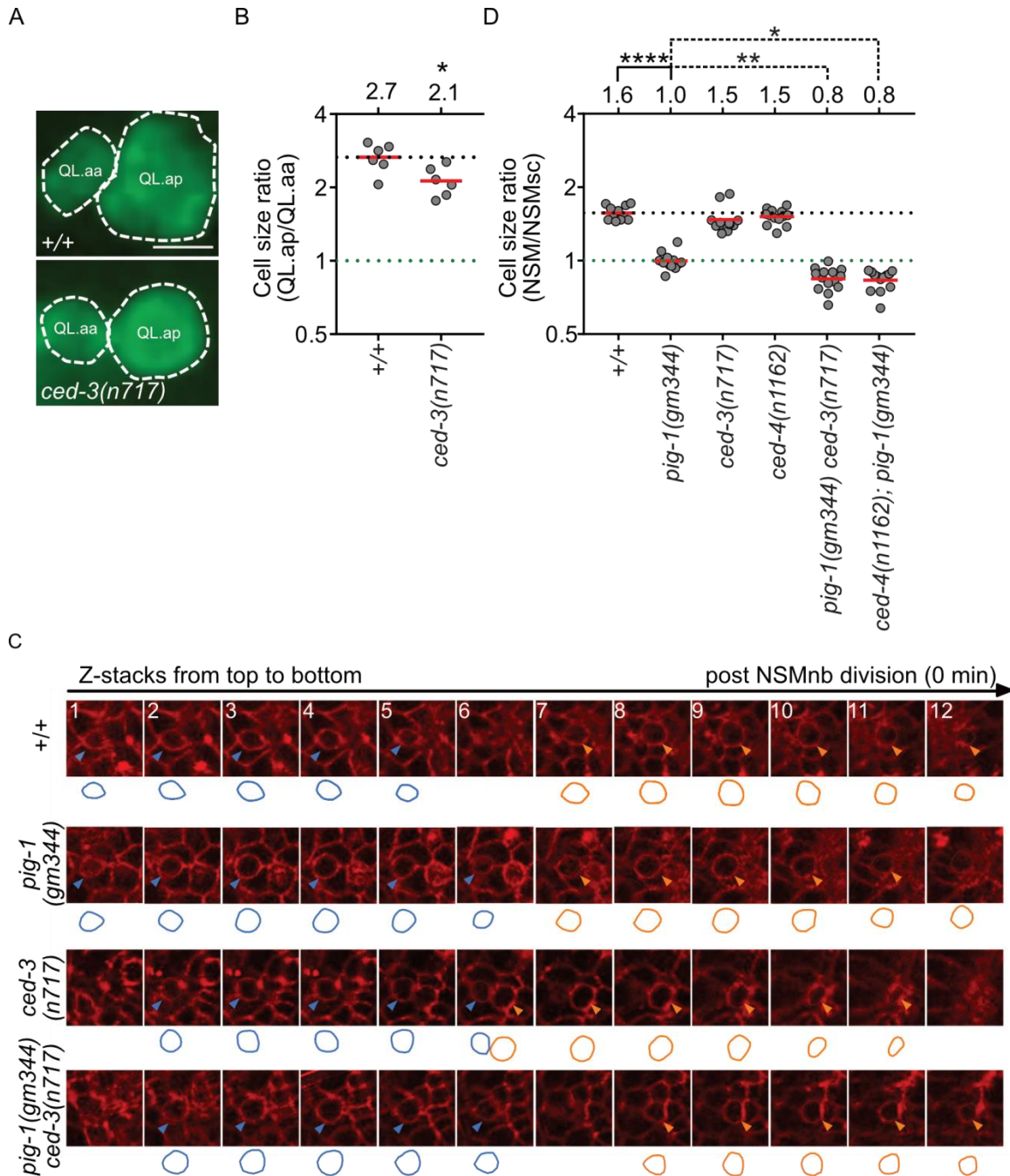


Figure 3.11: *ced-3* promotes asymmetry in QL.a and NSMnb divisions

(A) Representative images and (B) dot plot showing QL.a daughter cell size ratios in the indicated genotypes. Scale bar: 3 μ m. Statistical test: Mann-Whitney test; *: $p < 0.05$ and $n = 6$ QL.a divisions. (C) Representative images showing NSMnb daughter cells visualized with $P_{pie-1}mCherry::ph^{plc\delta}$. The circumferences of the daughter cells were traced to determine cell size and are shown below the images. (D) Dot plot showing NSM/NSMsc cell size ratios in the indicated genotypes. Statistical test: One-way ANOVA with Tukey's multiple comparisons test. *: $p < 0.05$, **: $p < 0.01$, ****: $p < 0.0001$ and $n \geq 11$ NSMnb divisions.

NSM/NSMsc ratio of 0.8 (**Fig. 3.11C and D**). Indeed, in these embryos, the ventral daughter cell (NSM) was smaller in size as compared to the dorsal daughter cell (NSMsc); i.e. the polarity of the NSMnb division was reversed (**Fig. 3.11C**). Since both *pig-1(gm344)* and *ced-3(n717)* are null mutants for the respective genes, these results suggest that *pig-1* and *ced-3* act in parallel genetic pathways to ensure that NSMnb divides asymmetrically. Further, the dependence of the NSMnb division asymmetry on *ced-4* suggests that, like in the QL.p lineage, the protease function of CED-3 is required for the asymmetric division of NSMnb. Furthermore, these data also establish that the role of *ced-3* in promoting asymmetry in cell divisions that produce apoptotic daughter cells is not restricted to postembryonic development.

3.5.3 *ced-3* may play an important role across cell lineages during *C. elegans* embryonic development

All data discussed so far suggest that *ced-3* may play a much broader role, such as the regulation of cell polarity, and therefore, have an impact on the size- and fate- asymmetries at least during cell divisions that produce an apoptotic daughter cell. If this is true, and if *ced-3* plays a similar role also in non-cell death lineages, then the loss of *ced-3* should have a strong adverse impact on development. To test this idea, I performed an embryonic lethality assay. Specifically, I asked what fraction of *ced-3(n717)* embryos failed to survive. I found that only 0.5% of *ced-3(n717)* embryos failed to survive, which was similar to the 0.2% embryonic lethality observed with wild-type (**Fig. 3.12**). However, *ced-3(n717)* enhanced embryonic lethality observed with *pig-1(gm344)* from 8.4% to 42.6% (**Fig. 3.12**). This suggests that *ced-3* likely plays much broader roles which may be critical to embryonic development. However, the impact of the lack of *ced-3* may only be detectable in a sensitized background, such as *pig-1(gm344)*. Further, it also asserts that while *ced-3* plays critical roles during development, it may still act redundantly with *pig-1*, which is a major regulator of cell polarity, asymmetric cell division and cell fate specification.

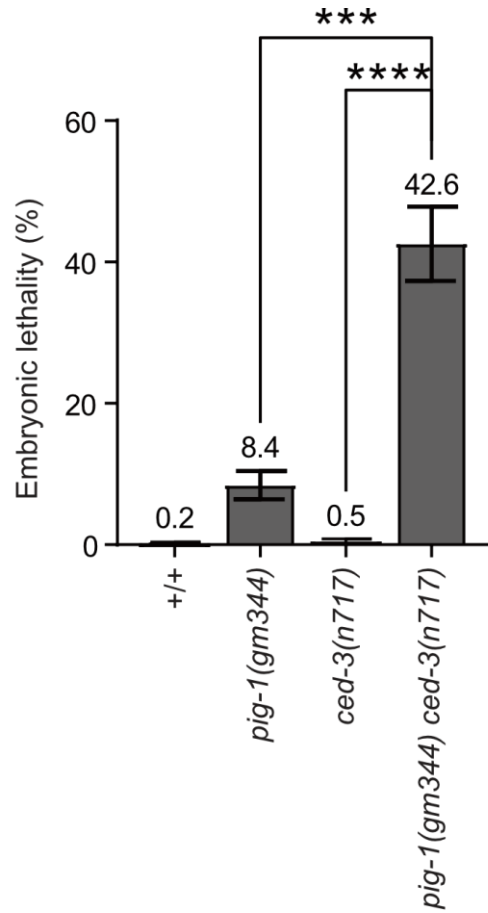


Figure 3.12: Loss of *ced-3* causes embryonic lethality

A bar graph showing percentage embryos examined in the indicated genotypes that failed to survive. Statistical test: One-way ANOVA with Tukey's multiple comparisons test. ***: $p < 0.001$, ****: $p < 0.0001$ and $n \geq 397$ embryos.

Part II: Mechanistic insights into the regulation of asymmetric cell division by ced-3 caspase

3.6 Spindle is symmetrically positioned during QL.p metaphase

The most important pre-requisite for understanding how *ced-3* promotes asymmetry during QL.p division is to understand the mechanism underlying QL.p division asymmetry. Asymmetric cell division is perhaps best understood in *C. elegans* one-cell embryos. The one-cell embryo divides asymmetrically to produce a larger anterior daughter, AB, and a smaller posterior daughter, P1 (Sulston *et al.* 1983). The mechanism through which this division occurs asymmetrically has been widely studied. Several studies have attributed the generation of unequal-sized daughters to an asymmetric positioning of the spindle (and of the metaphase plate) (Albertson 1984; Kemphues *et al.* 1988). Specifically, it has been shown that the spindle in these cells is shifted toward the posterior during metaphase. This shift in the spindle directs a posterior positioning of the cleavage furrow, which splits the one-cell embryo into two daughter cells (Albertson 1984). Indeed, in *C. elegans* one-cell embryos lacking factors that promote asymmetric spindle positioning, such as the G α proteins *goa-1* (**G** protein, **O**, **A**lpha subunit) or *gpa-16* (**G** **P**rotein, **A**lpha subunit), the spindle is positioned symmetrically, and such embryos also divide symmetrically by size to produce two daughters of similar sizes (Gotta and Ahringer 2001).

It has been previously reported that QL.p implements a similar mechanism in order to divide asymmetrically. Ou *et al* showed that, during QL.p metaphase, the spindle is asymmetric and is shifted toward the posterior pole (Ou *et al.* 2010). I began by attempting to verify their observation. To that end, I generated time lapse images of QL.p division using animals expressing the *rdvIs1* (*P_{egl-17}myristoylated-mCherry*, *P_{egl-17}mCherry::TEV-S::his-24*) transgene. In the QL.p lineage in these animals, the plasma membrane and the chromosomes are fluorescently labeled with mCherry (**Fig. 3.13A**). I assessed the position of the metaphase plate along the anterior-posterior axis of QL.p using the last image acquired during metaphase. Since the images were acquired with a temporal resolution of 15 seconds, the analyzed time points represent the near end of metaphase (<15 seconds before anaphase onset). I found that, at this time point, the metaphase plate was positioned at 52.23% of QL.p length away from its anterior pole on average (**Fig. 3.13A, B and E**). Further, I performed a similar analysis with time lapse images acquired using animals expressing the *bclIs133* transgene. In these animals, the QL.p lineage cells are labeled with cytoplasmic GFP (**Fig.**

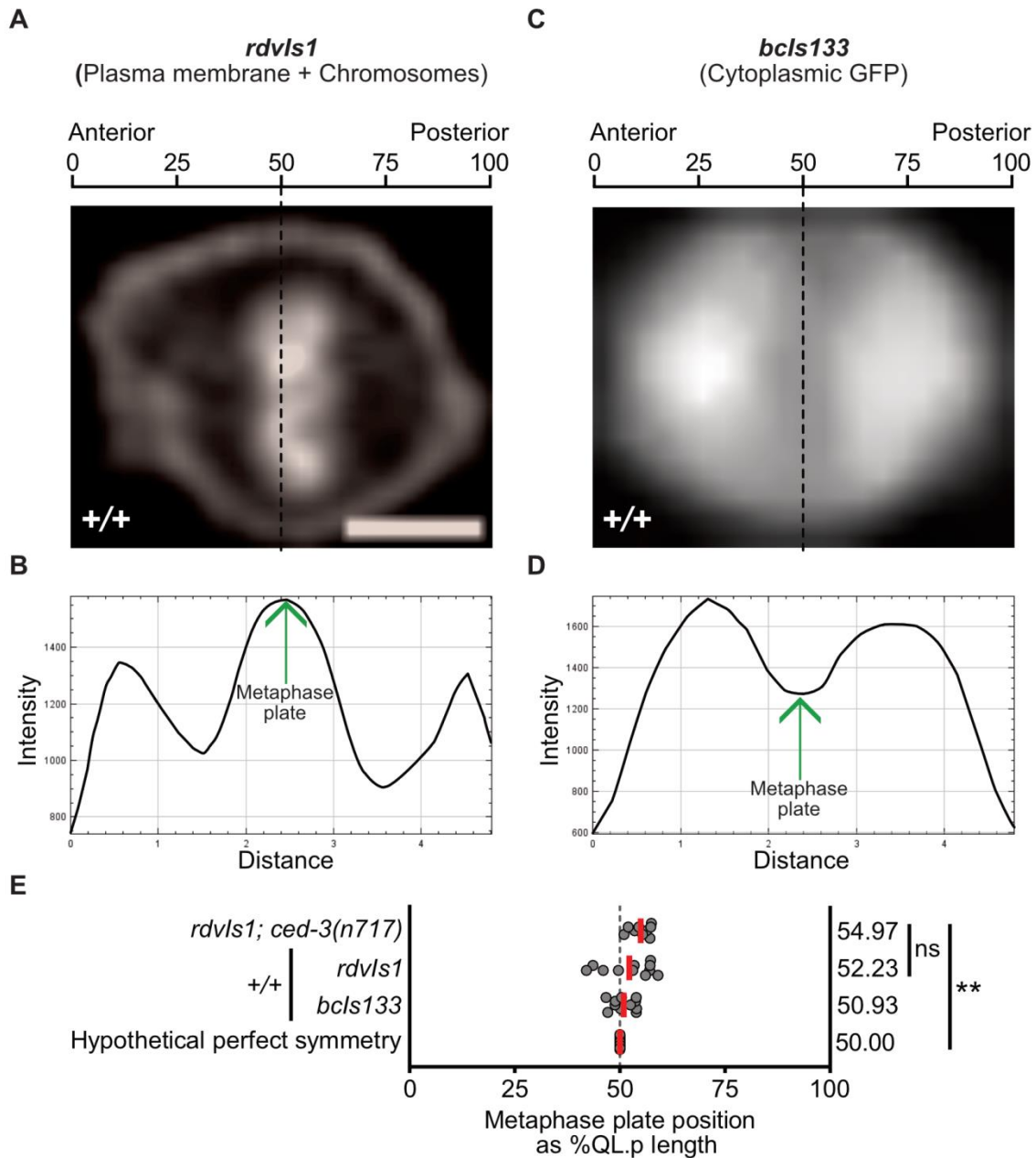


Figure 3.13: *ced-3* is not required to correctly position the QL.p metaphase plate
(A) Representative image and **(B)** the corresponding anterior-posterior fluorescence intensity profile of QL.p at metaphase in a wild type animal expressing the *rdvls1* transgene. The peak in the centre of the intensity profile indicates the position of the metaphase plate, and the peaks flanking the central peak indicate the positions of the plasma membrane on either side. **(C)** Representative image and **(D)** the corresponding anterior-posterior fluorescence intensity profile of QL.p at metaphase in a wild type animal expressing the *bcls133* transgene. The exclusion of cytoplasmic GFP from the central part of the cell is represented in the intensity profile as a depression. This position was interpreted to be that of the metaphase plate. **(E)** A dot plot showing the position of the metaphase plate in the indicated backgrounds. Statistical test: One-sample Wilcoxon test for comparisons with hypothetical perfect symmetry and Welch's t test for comparison between *rdvls1* and *rdvls1; ced-3(n717)*. **: $p < 0.01$, $n \geq 8$ QL.ps, Scale bar = 2 μm .

3.13C). These movies were generated with a temporal resolution of five minutes, and the position of the QL.p metaphase plate in these animals was deduced indirectly based on the exclusion of the cytoplasmic GFP. Consistent with the observations made using the *rdvIs1* transgene, I found that, in these animals, the metaphase plate was positioned at 50.93% of QL.p length away from its anterior pole (**Fig. 3.13C-E**). Statistical comparison with a hypothetical perfect symmetry scenario (i.e. position 50% of QL.p length) established that the observed distributions could not be classified as being asymmetric (**Fig. 3.13E**). Therefore, using two independent reporter transgenes, I found that the metaphase plate is, in fact, not asymmetrically positioned during QL.p division.

3.7 *ced-3* may not be required for spindle positioning during QL.p metaphase

A similar analysis with *ced-3(n717)* animals (expressing the *rdvIs1* transgene) showed that the metaphase plate position in these animals (54.97% of QL.p length) was statistically similar to that in wild-type (52.23% of QL.p length) (**Fig. 3.13E**). Interestingly, however, the distribution in *ced-3(n717)* significantly differed from a hypothetical perfect symmetry scenario and was shifted toward the posterior pole (**Fig. 3.13E**). This is a statistical paradox. On one hand, an observation similar to that in wild-type, in which the metaphase plate is symmetrically positioned, suggests that, in *ced-3(n717)* animals, the metaphase plate position should be considered symmetric. However, on the other hand, a statistically significant difference between *ced-3(n717)* and the hypothetical perfect symmetry scenario directs that the metaphase plate position in *ced-3(n717)* be regarded as being asymmetric. Nevertheless, these observations establish that the loss of *ced-3* does not significantly alter spindle (metaphase plate) position during QL.p division, and that it may not be required to position the QL.p metaphase spindle.

3.8 Chromosomes migrate unequally during QL.p anaphase

During cytokinesis, the cleavage furrow is positioned such that it bisects the gap between the two sets of chromosomes present at opposite poles of the cell at the end of telophase

(Albertson 1984; Kemphues *et al.* 1988). Therefore, symmetric division of cells can be achieved through equidistant positioning of the two sets of chromosomes with respect to the poles. This can be achieved through equal migration of the chromosomes toward opposite poles from their central starting position at the end of metaphase. On the other hand, if the chromosomes migrate unequally, the position of the cleavage furrow would be shifted to one side. For instance, during anaphase in the *C. elegans* one-cell embryo, the chromosomes that migrate toward the anterior pole migrate a shorter distance as compared to the ones that migrate toward the posterior pole (Albertson 1984; Grill *et al.* 2001). As a result of this, the ‘geometric’ centre of the hypothetical segment connecting the positions of the two sets of chromosomes is shifted toward the posterior pole. This means that the cleavage furrow is then positioned posteriorly, due to which a larger anterior daughter cell and a smaller posterior daughter cell are produced. Considering that the QL.p metaphase plate is symmetrically positioned in wild-type animals, I was wondering if the asymmetry in QL.p division could arise from unequal migration of the two sets of chromosomes during anaphase, and therefore, a shift in the position of the cleavage furrow away from the cell centre.

To test this idea, I generated movies of QL.p division with a temporal resolution of 15 seconds using *rdvIs1* as the reporter to label the chromosomes and the plasma membrane of QL.p and its daughters. I then generated kymographs to track the chromosomes during anaphase (**Fig. 3.14A and B**). The positions of the chromosomes when the cleavage furrow began to constrict was used to determine how far they had migrated from the position of the metaphase plate (**Fig. 3.14B**).

I found that, during QL.p anaphase in wild-type animals, the anterior set of chromosomes migrated a distance of 0.77 μm on average (**Fig. 3.14B and C**). On the other hand, the posterior set of chromosomes migrated an average distance of 1.11 μm (**Fig. 3.14B and C**). Similar distances have also been reported by the Gian Garriga’s lab (Teuliere and Garriga 2018). This means that the two sets of chromosomes indeed migrate unequally such that the cleavage furrow would be positioned posteriorly, similar to that in the *C. elegans* one-cell embryo. Therefore, the first sign of QL.p spindle asymmetry is only apparent during anaphase.

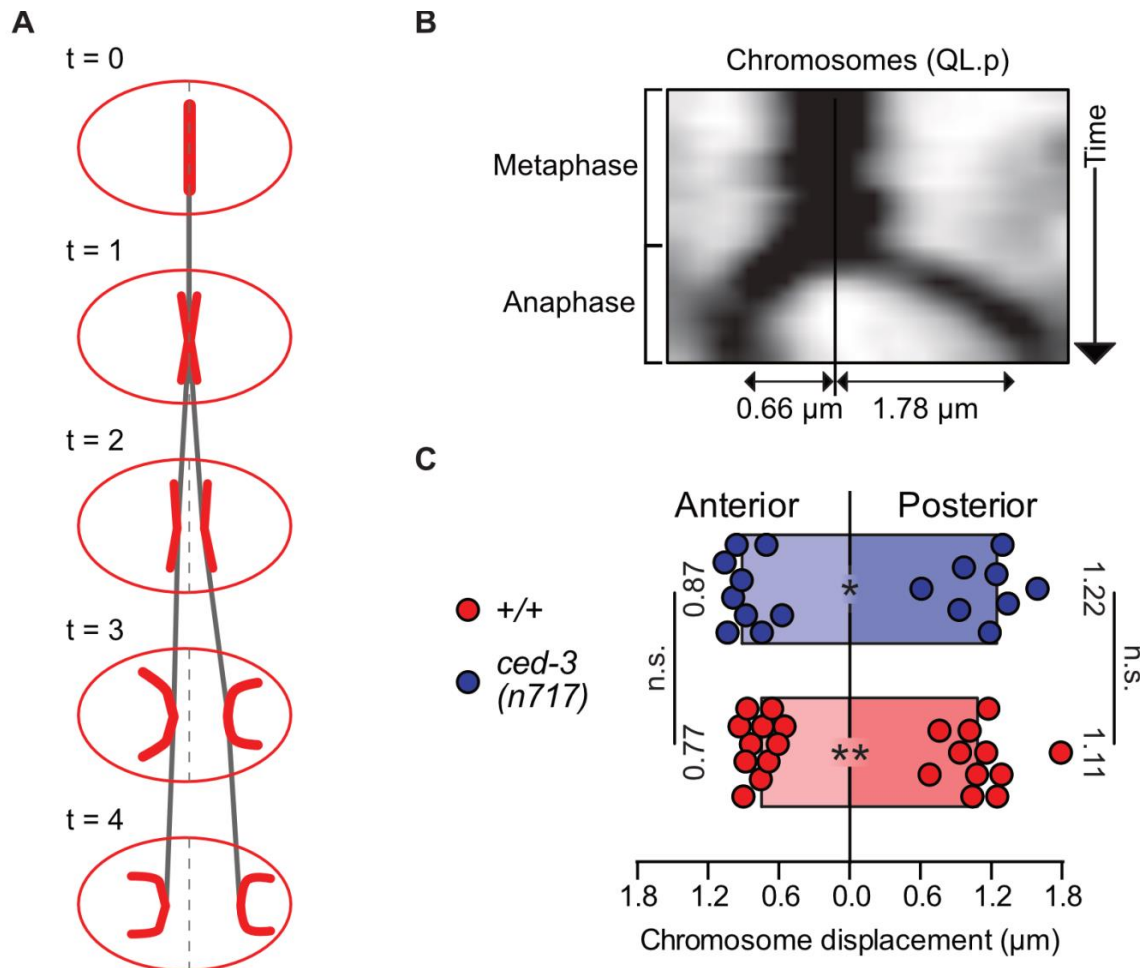


Figure 3.14: *ced-3* does not control chromosome migration during QL.p anaphase
(A) Representation of the method used for assessing chromosome migration during anaphase. Movies of QL.p division were generated using animals expressing the *rdvIs1* transgene. When QL.p is at metaphase, the chromosomes are aligned in the centre ($t = 0$). Upon anaphase onset ($t = 1$), chromosomes begin to segregate ($t = 1-4$). The position of the chromosomes are followed during this period through generation of kymographs (black lines). The final positions of the chromosomes before the beginning of cytokinesis is then used to determine the distance the chromosomes have migrated from their starting position at $t = 0$. **(B)** An actual kymograph generated using a movie acquired as described (see methods). In the kymograph, the anterior and the posterior are to the left and the right, respectively. The vertical line marks the start position of the chromosomes (metaphase plate). In this particular example, for instance, the anterior chromosomes have migrated $0.66 \mu\text{m}$ from their position at $t = 0$, whereas the posterior chromosomes have migrated a distance of $1.78 \mu\text{m}$. **(C)** Graph representing the mean distances migrated by the anterior and the posterior chromosomes during QL.p anaphase in the indicated genotypes. The numbers besides the bars indicate the mean values in μm . Individual data points, where each dot represents the observation from one animal, have also been shown. Statistical test: Multiple t test with Benjamini, Krieger and Yekutieli correction. *: $p < 0.05$, **: $p < 0.01$ and $n \geq 9$ QL.ps.

3.9 *ced-3* may not be required to regulate chromosome migration during QL.p anaphase

It is plausible that the reduced asymmetry in QL.p division in *ced-3(lf)* arises due to a reduced inequality between migration distances of the anterior and posterior sets of chromosomes during QL.p anaphase. A reduced inequality would mean that the chromosomes migrate similar distances away from the cell's geometric centre. As a result, the cleavage furrow would also be positioned less asymmetrically. To test this hypothesis, I analyzed chromosome migration during QL.p anaphase in *ced-3(n717)* animals. I observed that the anterior and the posterior sets of chromosomes migrated average distances of 0.87 μm and 1.22 μm , respectively from their starting position (i.e. the position of the metaphase plate) (**Fig. 3.14C**). These distances were comparable to those observed in wild-type. In addition, the total distances (mean \pm SD) migrated by both sets of chromosomes combined during anaphase in *ced-3(n717)* ($1.5 \pm 0.39 \mu\text{m}$) was also statistically similar to that in wild-type ($1.23 \pm 0.33 \mu\text{m}$). Therefore, *ced-3* may not be required for unequal chromosome migration during QL.p anaphase.

3.10 NMY-2 localizes anisotropically during QL.p metaphase

While spindle asymmetry is thought to be the most common means of introducing asymmetry during cell divisions, recent studies have described a novel mechanism to attain a similar result. During neuroblast divisions in *Drosophila*, the metaphase spindle is symmetric (Cabernard *et al.* 2010). Yet, these neuroblasts divide asymmetrically to produce a larger apical and a smaller basal daughter cell. In these neuroblasts, during metaphase, myosin II is anisotropic (Connell *et al.* 2011; Roubinet *et al.* 2017; Tsankova *et al.* 2017). Myosin II is enriched at the apical cortex and is released from the apical cortex upon anaphase onset. The release of myosin II from the apical cortex triggers an expansion of the apical cortex as the cleavage furrow constricts during cytokinesis and produces a larger apical and a smaller basal daughter cell. This myosin II anisotropy and the spatiotemporally regulated myosin II release are determinative to asymmetry in the neuroblast division (Tsankova *et al.* 2017).

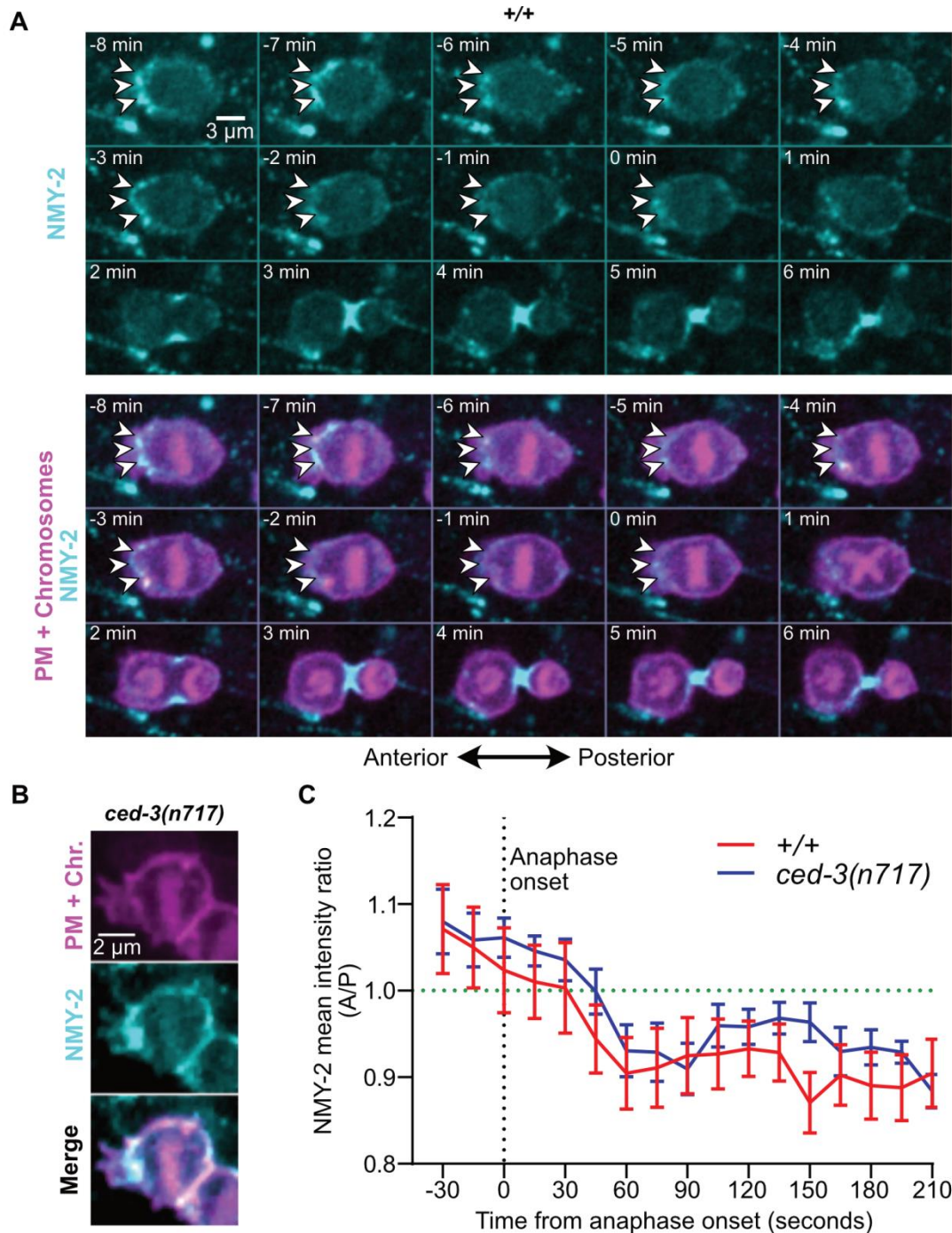


Figure 3.15: *ced-3* does not control NMY-2 dynamics

(A) Representative images showing NMY-2::GFP localization during QL.p division. NMY-2 and QL.p were visualized using the *zuls45* and *rdvIs1* transgenes, respectively (see methods). Timings with respect to anaphase onset are mentioned at the top-left of each image. Anterior is to the left, and posterior is to the right. The anterior cortex of QL.p has a greater NMY-2 signal during metaphase (arrowheads). This anisotropy was lost upon anaphase onset. (B) A representative montage showing metaphase NMY-2 anisotropy in *ced-3(n717)*. (C) A graph showing the NMY-2 mean intensity ratio (A/P) as a function of time during QL.p division in wild type and *ced-3(n717)*. $n \geq 9$ QL.ps.

I wondered if a similar mechanism may be responsible for establishing the QL.p division asymmetry. Therefore, I first examined the subcellular localization pattern and dynamics of NMY-2, the *C. elegans* ortholog of myosin heavy chain, during QL.p division. Myosin heavy chain is a subunit of myosin II and is often used as proxy to learn about the localization of myosin II. I imaged QL.p division in animals expressing the *zuls45* transgene ($P_{nmy-2}::gfp$). QL.p in these animals was visualized with the help of the *rdvIs1* transgene. Movies were generated with a temporal resolution of 15 seconds beginning at QL.p metaphase. I found that, during QL.p metaphase, NMY-2 localization was indeed anisotropic. Consistent with the observations made in *Drosophila* neuroblasts, more NMY-2 was present at the anterior cortex – i.e. at the cortex that later produces the larger daughter cell (**Fig. 3.15A**). Further, NMY-2 was released from the anterior cortex upon anaphase onset (0 minute in **Fig. 3.15A**). In fact, upon anaphase onset, the NMY-2 anisotropy was reversed (**Fig. 3.15A and C**). Therefore, NMY-2 localizes dynamically during QL.p division, such that more NMY-2 is present at the anterior cortex during metaphase, which is released upon anaphase onset.

3.11 Size asymmetry during QL.p division arises during anaphase

When myosin II is released from the apical cortex in dividing *Drosophila* neuroblasts, the apical cortex begins to expand, which gives rise to the asymmetry in daughter cell sizes (Cabernard *et al.* 2010; Connell *et al.* 2011). Since I found a similarity between NMY-2 and myosin II dynamics in the *C. elegans* QL.p neuroblast and *Drosophila* neuroblasts, respectively, I investigated if this NMY-2 dynamics is responsible for QL.p division asymmetry. Therefore, I asked when the size asymmetry first becomes apparent during QL.p division. To that end, I measured sizes of the anterior and the posterior parts of QL.p starting at late metaphase as QL.p divided. For this purpose, I used movies generated with *rdvIs1*, which labels both the plasma membrane and the chromosomes in QL.p (**Fig. 3.16A**). Chromosomes were used to define the boundary between the anterior and the posterior parts of QL.p until the cleavage furrow was formed (**Fig. 3.16A**). Once the cleavage furrow was apparent, it was used to define the boundary between the anterior and the posterior parts rather than the chromosomes (**Fig. 3.16A**).

I found that, toward the end of metaphase (i.e. 30 seconds before anaphase onset), the anterior and the posterior parts of QL.p were of a similar size (**Fig. 3.16A**). Specifically, the anterior part was $12.81 \mu\text{m}^2$ in size, whereas the posterior part was $10.96 \mu\text{m}^2$ in size (**Fig. 3.16B**). On average, the anterior part was 1.23 times as large as the posterior part of QL.p toward the end of metaphase (**Fig. 3.16C**). Interestingly, upon anaphase onset, the anterior part began to expand, whereas the posterior part began to contract. As a result, the average ratio of the areas of the anterior and the posterior parts nearly doubled from 1.23 (30 seconds before anaphase onset) to 2.28 at 210 seconds after anaphase onset (**Fig. 3.16A-C**). Therefore size-asymmetry during QL.p division first becomes apparent upon anaphase onset.

3.12 Release of NMY-2 from the anterior cortex may cause its expansion

Since the increase in the area ratio coincided with the switch in the NMY-2 anisotropy during QL.p division, I asked if the two were correlated. Indeed, I found that there was a strong correlation between the NMY-2 release and the expansion of the anterior part of QL.p (Pearson $r = 0.796$, $p = 6.469\text{e-}009$). Further, there was also a strong correlation between the release of NMY-2 and the contraction of the posterior part of QL.p (Pearson $r = 0.861$, $p = 1.698\text{e-}011$). Finally, as a result, I also found that the anterior/posterior NMY-2 ratio was negatively correlated with the anterior/posterior area of QL.p – i.e. the greater the excess of NMY-2 at the posterior cortex, the larger was the anterior part of QL.p as compared to the posterior part (Pearson $r = 0.801$, $p = 4.606\text{e-}009$) (**Fig. 3.16C**). Although these results do not establish a causal relationship between the release of NMY-2 from the anterior cortex and the establishment of asymmetry during QL.p division, they, nevertheless, support the idea that the release of NMY-2 from the anterior cortex is responsible for the asymmetry.

3.13 *ced-3* may not control NMY-2 dynamics

The obvious next question to ask was whether *ced-3* regulates NMY-2 dynamics during QL.p division. Therefore, I performed a similar analysis with *ced-3(n717)* animals. I found that NMY-2 localization also appeared anisotropic in *ced-3(n717)* during QL.p metaphase,

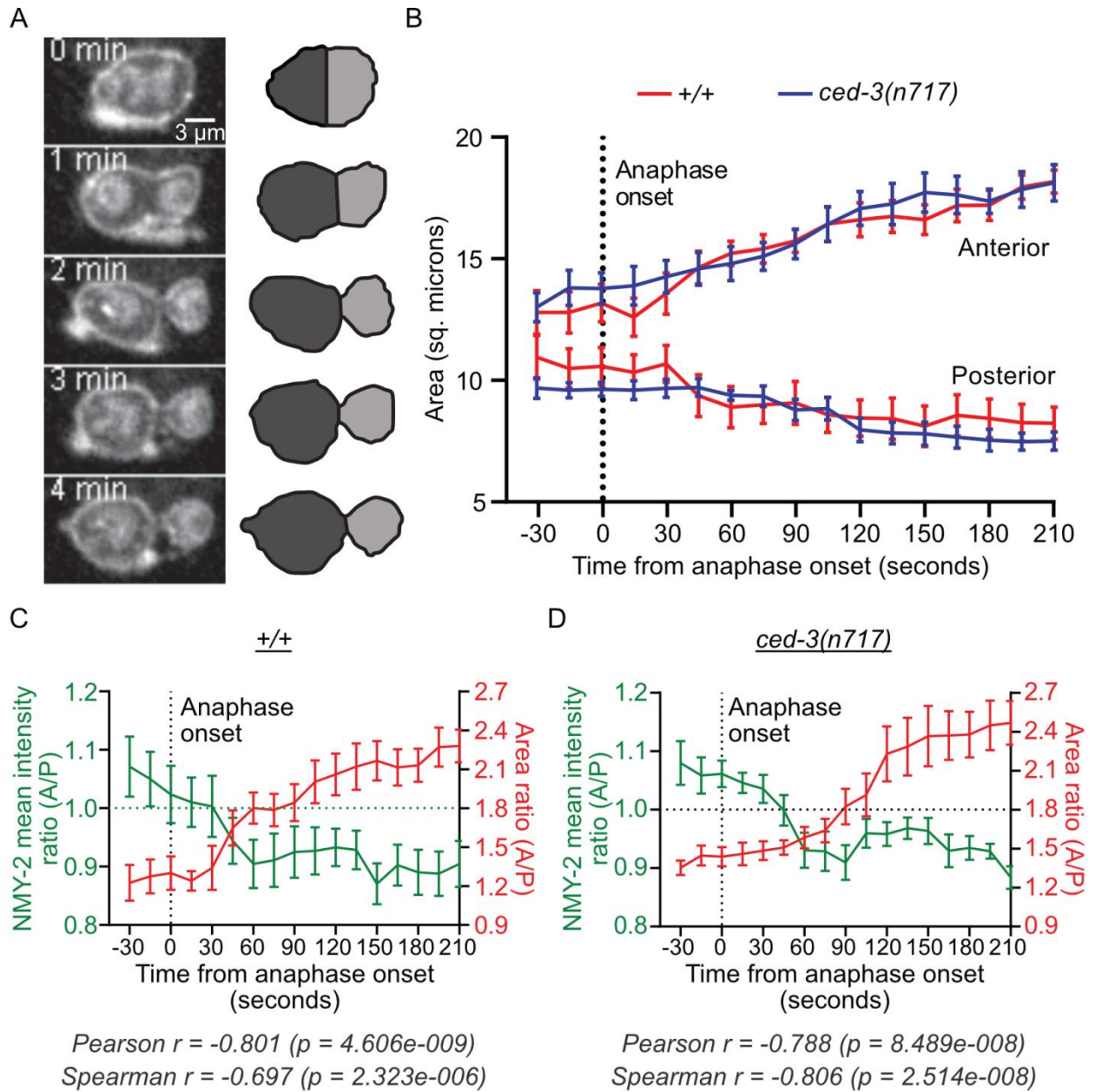


Figure 3.16: Generation of asymmetry during QL.p division correlates with NMY-2 release

(A) Representative images from a movie (left) and traced cell outlines (right) demonstrating the gradual changes in the sizes of the anterior and the posterior parts of QL.p starting at anaphase onset. QL.p was visualized using the *rdvIs1* transgene. (B) A graph showing the changes in the sizes of the anterior and the posterior parts of QL.p in wild type and *ced-3(n717)* (measured as shown in A). (C) and (D) Graphs showing the changes in the NMY-2 ratio and the cell size ratio in wild type and *ced-3(n717)* as a function of time. Co-efficients of the correlation between the NMY-2 ratio and cell size ratio and the corresponding p values are mentioned below the graphs. $n \geq 9$ QL.ps for NMY-2 ratio and $n \geq 8$ QL.ps for cell size ratio.

similar to that in wild-type (**Fig. 3.15B**). Further, the anisotropy was also reversed upon anaphase onset (**Fig. 3.15C**). Overall, the NMY-2 dynamics observed in *ced-3(n717)* was indistinguishable from that in wild-type. Therefore, it is likely that *ced-3* does not regulate NMY-2 dynamics.

In addition, similar to that in wild-type, the anterior and the posterior parts of QL.p began to expand and contract upon anaphase onset, respectively (**Fig. 3.16B**). Further, the NMY-2 dynamics in *ced-3(n717)* also correlated with the expansion of the anterior part of QL.p, the contraction of the posterior part of QL.p and the ratio of the areas of these parts (**Fig. 3.16D**). Furthermore, the rates of changes in areas of the anterior and the posterior parts were also similar to those in wild-type (**Fig. 3.16B**).

One surprising result obtained from this experiment was the lack of difference between the QL.p daughter cell size ratios in wild-type and *ced-3(n717)*. In ‘Results Part I’, I showed that the daughter cell size ratio was reduced in *ced-3(n717)*, as determined using a soluble GFP reporter (*bcIs133*), whereas no such reduction was observed when a reporter that labels the plasma membrane (*rdvIs1*) was used instead to determine the daughter cell sizes. This disparity can be attributed to the nature of the fluorescent reporter. For instance, using *bcIs133*, lamellipodia-like structures are often not visible unlike when using *rdvIs1* (**Fig. 3.17**). This inability of soluble GFP to label the ‘entire’ cell may stem from its inability to, perhaps, enter lamellipodia. This means that the difference between size asymmetries in wild-type and *ced-3(n717)* animals could also be a result of an altered organization of lamellipodia in *ced-3(n717)* animals.

3.14 NMY-2 anisotropy may dictate spindle positioning

Finally, I wondered if the two mechanisms – spindle asymmetry and NMY-2 anisotropy – cooperate to ensure asymmetric QL.p division. Therefore, I asked if the two were correlated. Indeed, I observed a strong correlation between NMY-2 anisotropy and metaphase spindle position (Pearson $r = 0.920$, $p = 4.34e-004$) (**Fig. 3.18A**). Specifically, I found that the greater the net excess of NMY-2 at the anterior cortex during metaphase, the larger was the shift of the metaphase plate away from the anterior pole (**Fig. 3.18A**). In addition, in the two

cases where the posterior cortex instead had a greater amount of NMY-2, the metaphase plate was positioned anteriorly – i.e. away from the posterior pole (**Fig. 3.18A**). Finally, in the two cases where NMY-2 localization was nearly isotropic, the metaphase plate was also positioned more symmetrically – i.e. approximately at the geometric centre of QL.p (**Fig. 3.18A**). This supports the idea that a potential cause-and-effect relationship may exist between NMY-2 anisotropy and spindle positioning. Therefore, it seems likely that both NMY-2 anisotropy and spindle asymmetry function in a coordinated manner to ensure the asymmetry in QL.p division.

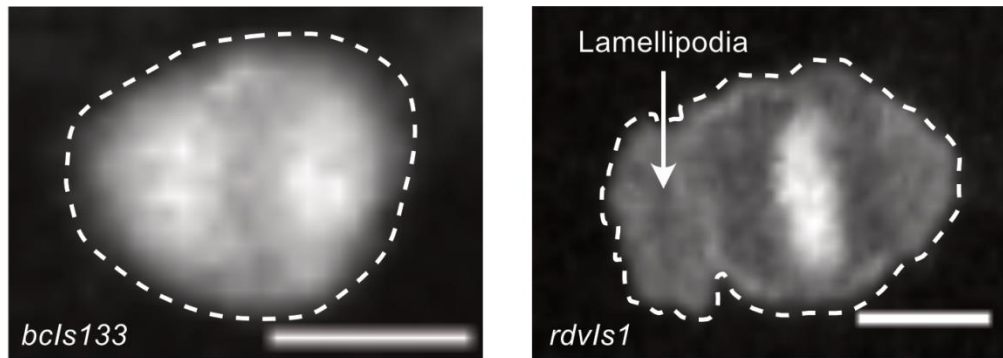


Figure 3.17: QL.p architecture looks different when visualized using two different fluorescent reporter transgenes.

QL.p at metaphase visualized using the *bcIs133* (*Ptoe-2gfp*) (left) or the *rdvIs1* (*Pegl-17myri-mCherry* + *Pegl-17mCherry::TEV-S::his24*) (right) transgene. *bcIs133* expresses soluble (cytoplasmic) GFP, whereas *rdvIs1* labels the plasma membrane and the chromosomes. However, the presence of lamellipodial structures can only be detected when QL.p is visualized using the *rdvIs1* transgene as reporter. This disparity could arise due to the inability of soluble GFP to 'enter' the lamellipodial compartment of the cell. Scale bar: 3 μ m

3.15 *ced-3* may link NMY-2 anisotropy with spindle positioning during QL.p division

Neither spindle positioning nor NMY-2 dynamics was found to be affected during QL.p division in *ced-3(n717)* animals. However, I was interested in understanding if the loss of *ced-3* would have an impact on the coordination between the two. Therefore, I performed a

similar analysis with *ced-3(n717)* animals. I found that, in *ced-3(n717)*, the correlation between NMY-2 anisotropy and spindle asymmetry was lost (Pearson $r = -0.307$, $p = 0.46$) (**Fig. 3.18B**). In these animals, the metaphase plate was positioned in the posterior half of QL.p irrespective of the NMY-2 polarity. Therefore, although *ced-3* is not necessary for the regulation of NMY-2 dynamics or spindle positioning individually, it, nevertheless, links the two to each other. In *ced-3(n717)*, this link is severed, and their coordination is lost.

Further, in wild-type animals, QL.p daughter cell size ratio (QL.pa/QL.pp) only weakly correlated with NMY-2 anisotropy during metaphase, metaphase plate position and chromosome migration asymmetry during anaphase (Pearson $r = -0.276$, 0.289 and -0.473 , respectively, and Spearman $r = -0.033$, 0.245 and -0.409 , respectively) (**Fig. 3.18C and E**). These observations raise the possibility that QL.p division asymmetry is ensured through a combination of all three processes. Therefore, affecting only one of these processes may not be sufficient to result in a statistically significant change in the daughter cell size ratio. However, interestingly, in *ced-3(n717)* animals, while the correlation of QL.p daughter cell size ratio with NMY-2 anisotropy remains weak (Pearson $r = -0.146$ and Spearman $r = -0.357$), its correlation with both metaphase plate position and chromosome migration asymmetry was greater (Pearson $r = 0.834$ and -0.610 , respectively, and Spearman $r = 0.786$ and -0.762 , respectively) (**Fig. 3.18D and F**). This suggests that, upon the loss of *ced-3*, spindle asymmetry (metaphase plate positioning and anaphase chromosome migration) likely plays a much more pronounced role to ensure the asymmetry in QL.p division. Furthermore, while NMY-2 dynamics remains unaffected in *ced-3(n717)* animals, it is possible that some other property of NMY-2, such as activity or contractility, is affected. In such a scenario, although NMY-2 may be recruited at and derecruited from the cortex in a manner that is similar to that in wild-type, it may, however, be incapable of performing its appropriate function to determine the QL.p daughter cell sizes. A reduction in contribution from NMY-2 may, therefore, necessitate that spindle asymmetry plays a greater and a more decisive role in determining QL.p daughter cell size. It is, thus, likely that *ced-3* either regulates NMY-2 function or that it mediates the coordination between NMY-2 and spindle positioning to ensure QL.p division asymmetry.

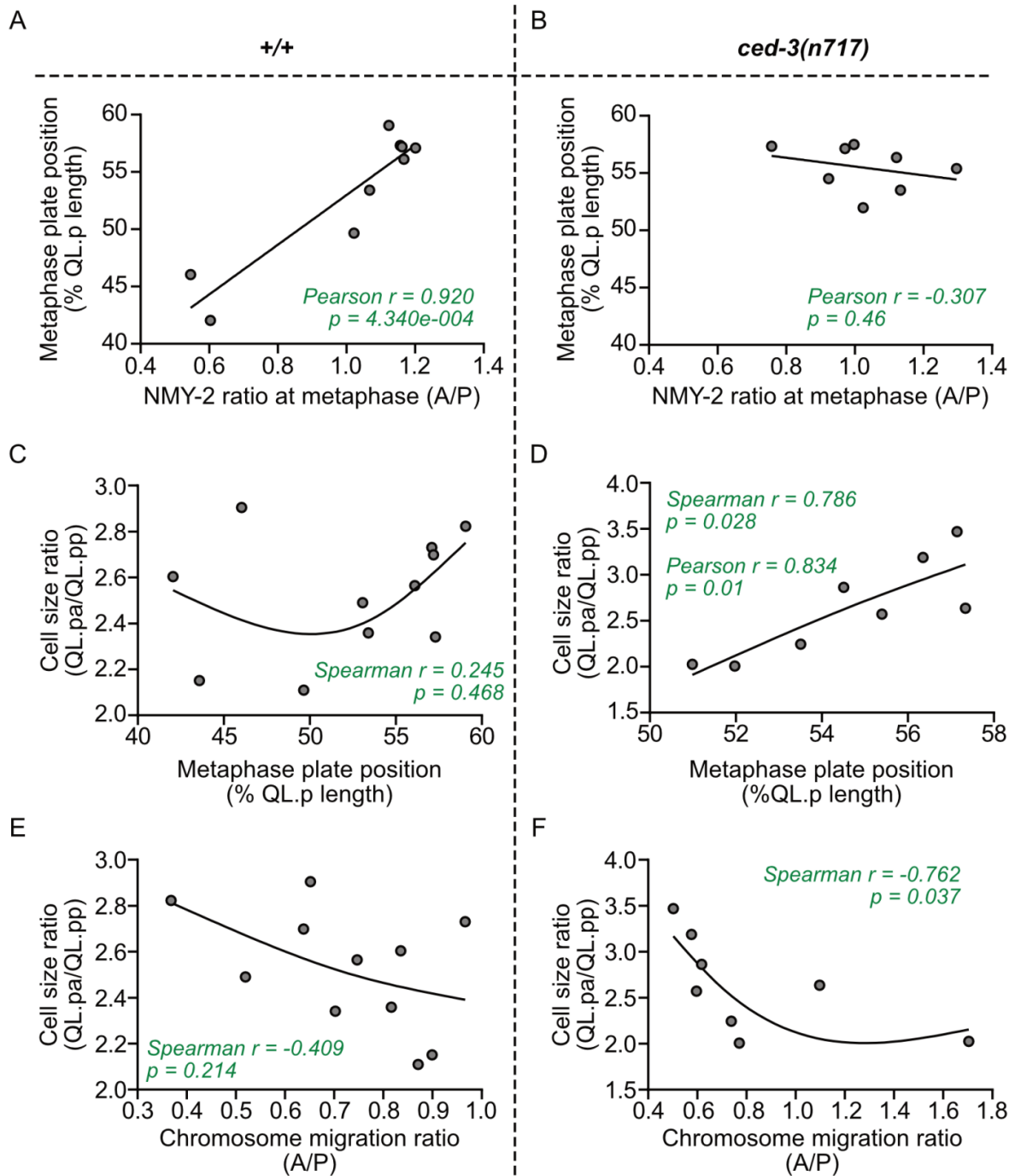


Figure 3.18: Loss of *ced-3* may alter the mechanism of asymmetric QL.p division
(A) and **(B)** Scatter plot showing the correlations between metaphase NMY-2 ratio (A/P) and the position of the metaphase plate (as % QL.p length) in wild type and *ced-3(n717)*. **(C)** and **(D)** Scatter plot showing the correlations between metaphase plate position and QL.p daughter cell size ratio in wild type and *ced-3(n717)*. **(E)** and **(F)** Scatter plot showing the correlations between the ratio (A/P) of anaphase chromosome migration and the QL.p daughter cell size ratio in wild type and *ced-3(n717)*. The co-efficients of correlation and the corresponding p values are indicated on the respective graphs. $n \geq 8$ QL.ps for all.

3.16 CED-3 physically interacts with ECT-2, a regulator of NMY-2 contractility

So far, I have discussed results, some of which indicate that NMY-2 functionality may be affected in *ced-3(lf)* and that *ced-3* may regulate NMY-2 activity. Interestingly, we identified ECT-2, a positive regulator of NMY-2 contractility, as an interactor of CED-3 in a yeast two-hybrid screen (Motegi and Sugimoto 2006; Zhong and Sternberg 2006) (**Fig. 3.19**). This screen was performed by me and Hai Wei (a doctoral student in the lab) in collaboration with Next Interactions Inc. The screen employed two forms of CED-3 as baits – wild-type pro-CED-3 and mutant pro-CED-3. The mutant pro-CED-3 bait harbors a missense mutation (C358S) in its active site which renders it incapable of performing its protease function. CED-3 cleaves itself and autoactivates. Therefore, the wild-type pro-CED-3 bait could help identify interactors of active CED-3. On the other hand, the mutant pro-CED-3, which cannot

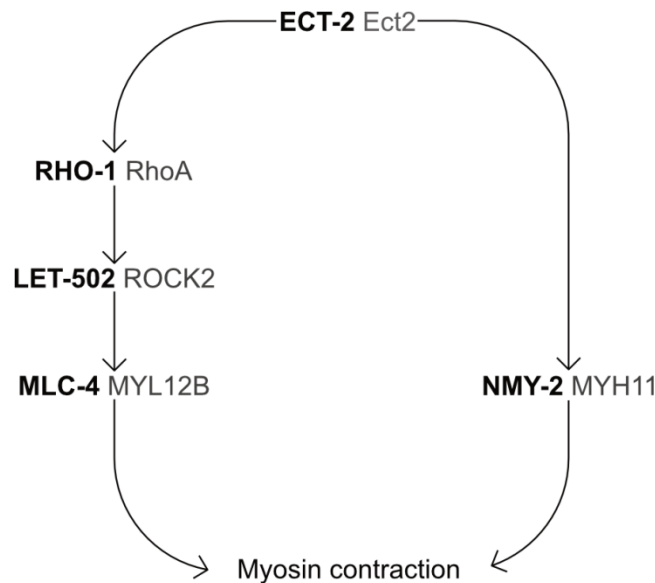


Figure 3.19: ECT-2 promotes myosin contractility

ECT-2 (**E**pithelial **C**ell **T**ransforming), a Rho-GEF, activates RHO-1 (**R**as **H**omolog family member). RHO-1 then binds to and increases the activity of LET-502 (**L**ETHal). Once active, LET-502 phosphorylates and activates MLC-4 (**M**Yosin **L**ight **C**hain). ECT-2 also activates NMY-2 (**N**on-Muscle **M**Yosin heavy chain) by acting in another pathway. NMY-2 and MLC-4 are subunits of non-muscle myosin, which combine to generate contractility when crosslinked with actin filaments. To the right of each protein, its mammalian ortholog has been indicated.

autoactivate, can be used as bait to identify interactors of full-length CED-3 (i.e. pro-CED-3). These baits were tested for interaction against a cDNA library generated from transcripts isolated from eight different developmental stages (three embryonic and five postembryonic) of *C. elegans*. All stages were equally represented in the library, which included approximately 13000 genes. Through the yeast two-hybrid screen, 71 proteins were found to interact with the wild-type CED-3 bait, whereas 163 proteins were found to interact with the mutant CED-3 bait. 31 proteins were found to interact with both wild-type and mutant CED-3 baits. ECT-2 was one of the proteins that were found to strongly interact with the mutant CED-3 bait but not with the wild-type CED-3 bait. This bait-prey interaction was more than 16-fold stronger as compared to the two negative controls used for the screen (empty bait-vector control and the cDNA control). This suggests that ECT-2 may interact with pro-CED-3 rather than active CED-3. It seems likely that CED-3 may act through ECT-2 to control NMY-2 activity/contractility and, thus, influence the asymmetry in QL.p division and in potentially other cell divisions.

Chapter IV: DISCUSSION

4.1 Novel non-apoptotic roles of the *C. elegans ced-3* caspase

Caspases and their orthologs have previously been shown to perform a variety of non-apoptotic functions. During *Drosophila* larval development, for instance, active caspases have been shown to act on a kinase, Shaggy (Sgg), and control cell fate specification (Kanuka *et al.* 2005). One particular isoform, Sgg46 is cleaved in a manner dependent on caspases; the cleaved Sgg46 functions as an active kinase and negatively regulates Wnt signaling, thereby regulating sensory organ precursor specification (Kanuka *et al.* 2005). Dronc, one of the initiator caspases in *Drosophila*, is also required for border cell migration (Oshima *et al.* 2006). In mammals, Caspase-3 has been shown to cleave Rho-associated protein kinase (ROCK) and control macrophage polarity (Liu *et al.* 2016). In *C. elegans*, *ced-3* promotes regeneration of damaged neuronal processes (Pinan-Lucarre *et al.* 2012). In addition, *ced-3* also has been shown to inhibit *lin-28*, which encodes a pluripotency factor, in the seam cells (Weaver *et al.* 2017). This inhibition of *lin-28* by *ced-3* is crucial to ensuring proper temporal cell fate patterning. Furthermore, *ced-3* and the central apoptotic pathway also assist in the sensing of mitochondrial ROS and protect nematodes against stress (Yee *et al.* 2014). My thesis has uncovered two novel non-apoptotic functions of *ced-3*: the regulation of size-asymmetry and the regulation of fate-asymmetry in cell divisions that give rise to cells programmed to die.

4.1.1 The regulation of size-asymmetry in cell divisions by *ced-3*

This study identified *ced-3* as a positive regulator of daughter cell size asymmetry in at least three different asymmetric cell divisions that occur during *C. elegans* embryonic and postembryonic development. While in the postembryonic QL.a and QL.p lineages, the loss of *ced-3* was sufficient to significantly reduce daughter cell size asymmetry, in the embryonic NSM lineage, the effects of the loss of *ced-3* on daughter cell size asymmetry could only be seen in a *pig-1(lf)* background. This disparity between the effects of the loss of *ced-3* in the embryonic and postembryonic lineages can be explained in two ways, which may not be mutually exclusive. First, it is clear that in all three cell divisions, other molecules, such as *pig-1*, are the major determinants of daughter cell size through asymmetric cell division as the loss of *pig-1* alone is sufficient to render all divisions nearly perfectly symmetric by size. On the other hand, the loss of *ced-3* only has a weak impact on cell division asymmetry, which suggests that it plays a role that is secondary to that played by *pig-1*. Yet, in QL.a and

QL.p divisions, *ced-3* may play a greater role as compared to that in NSMnb division, which may explain the disparity. Second, considering that, in wild-type, the daughter cell size asymmetry is much greater for QL.a and QL.p divisions (2.7 and 2.9, respectively) as compared to that for NSMnb division (1.6), it is possible that small changes in NSMnb daughter cell size asymmetry were not detected due to the narrow phenotypic landscape. Nevertheless, size-asymmetry phenotypes observed in three different cell divisions in the embryo and the larva clearly establish that *ced-3* promotes asymmetry in at least those cell divisions that produce an apoptotic daughter cell. Furthermore, this regulation of size asymmetry is dependent on the protease activity of CED-3.

4.1.2 The regulation of fate-asymmetry in cell divisions by *ced-3*

In addition to cell size, *ced-3* was also found to govern daughter cell fate. More specifically, the loss of *ced-3* resulted in an increased penetrance with which the undead QL.pp adopted a mitotic fate. Previously, it has been proposed that the mitotic fate of QL.pa is specified through selective inheritance of mitotic fate promoters by QL.pa during QL.p division (Cordes et al. 2006). In mutants, such as *pig-1(lf)* animals, this process is severely compromised, thus resulting in a mitotic fate transformation of the undead QL.pp in 56% of the population. I observed a similar mitotic fate transformation phenotype, albeit much weaker than in *pig-1(lf)*, in animals lacking *ced-3* (**Fig. 4.1**). Further, this acquired ability of the undead QL.pp to divide in the absence of *ced-3* is at least partially independent of its size as undead QL.pps in *pig-1(gm344) ced-3(n2427)* double mutants undergo mitotic fate transformation with a higher penetrance as compared to those in *pig-1(gm344)* single mutants despite being of a similar size in both genotypes. Overall, I propose that a *ced-3*-dependent gradient of mitotic fate determinants is present in QL.p at the time of its division. This gradient may enable a disproportionate segregation of the mitotic factors in QL.pa, which normally divides (**Fig. 4.1A**). In the absence of *ced-3*, the gradient may be abolished, thus resulting in the missegregation of those factors into QL.pp (**Fig. 4.1B**). Furthermore, similar to the regulation of size-asymmetry, the regulation of cell fate-asymmetry is also dependent on the protease activity of CED-3.

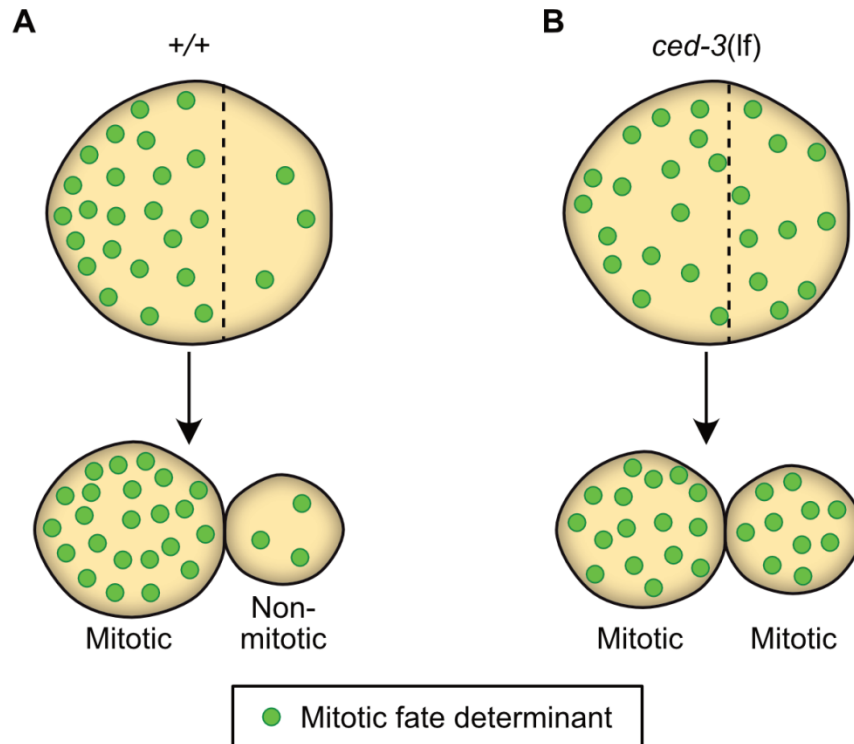


Figure 4.1: *ced-3* promotes the segregation of mitotic fate determinants during QL.p division

(A) In QL.p, factors promoting mitotic cell fate, whose identity is, as yet, unknown, may be organized as a gradient. This gradient would likely favor a disproportionate segregation of the mitotic fate determinants into the anterior daughter cell, QL.pa, which is programmed to divide. Due to lack of mitotic factors, QL.pp would fail to divide. Instead, it undergoes apoptosis. (B) In *ced-3(lf)* animals, the gradient of mitotic fate determinants is likely abolished. This, combined with the reduced size-asymmetry in QL.p division, may result in both QL.p daughters inheriting similar concentrations of the mitotic fate determinant, thus causing QL.pp division.

In summary, I found that *ced-3* regulates a process as fundamental as asymmetric cell division. Although my thesis describes the roles of *ced-3* specifically in those cell divisions that produce apoptotic daughters, I also observed that the lack of *ced-3* in a *pig-1(lf)* background led to an increased lethality during embryonic development as compared to *pig-1(lf)* single mutants. This supports the idea that *ced-3* plays similar key roles in other cell divisions, including those that do not produce apoptotic daughter cells. The regulation of asymmetric cell divisions by *ced-3* may, therefore, serve as a redundant mechanism to ensure the robustness with which the invariance of the *C. elegans* somatic cell lineage is maintained,

at least in the case of apoptotic cell lineages. By promoting asymmetric cell division and the segregation of cell fate determinants during the mother cell division, *ced-3*, thus, predisposes the future apoptotic daughter to adopting an apoptotic fate. It also shows that, while asymmetric cell division governs apoptotic fate specification and execution, *ced-3* and the apoptotic pathway also, in turn, influence asymmetric cell division. This study, thus, provides the first evidence for the role of caspases (here, CED-3) in asymmetric cell division and adds to an already growing list of non-apoptotic functions of caspases and their orthologs.

4.2 NMY-2 (Myosin) as a regulator of cell behaviors

Myosin and its orthologs have been established as key players in the regulation of cell shape and division. It is a motor protein that tracks on actin filaments. A single myosin motor, when cross-linked to actin filaments in an anti-parallel fashion/orientation, forms a bipolar filament which is contractile in nature (Tan 1992; Howard and Clark 2002). Perhaps its most well-studied function in cells is that of a tension/force generator. In addition to being present freely within the cytoplasm (cytoplasmic pool), it also associates with the cell cortex (cortical pool), which lies underneath the plasma membrane. Myosin contraction, when coupled to the plasma membrane, leads to stabilization of the plasma membrane deformation and thereby constricts the interfaces to which it localizes (**Fig. 4.2A-C**). However, like other motor proteins, myosin also has a limited processivity, which is determined by its structure. Also, specific kinases and phosphatases regulate the contractility of myosin by regulating its phosphorylation and de-phosphorylation states/cycle within the cells (Howard and Clark 2002). This means that, after a short duration of pulling two junctions closer to each other, and therefore shortening the interface between the junctions, myosin disengages from the actin filaments or gets inactivated due to de-phosphorylation (GTP/GDP binding cycles). At this time, the tension on the plasma membrane is released, and the plasma membrane reverts back to its original shape/size (unless the deformation is stabilized via-cell-cell adhesion) (**Fig. 4.2A**). This leads to cycles of shortening and relaxation phases of the plasma membrane, each of which is referred to as a pulse (a pulsatile behavior of the interface), and by extension, of the cell (**Fig. 4.2A**). Such a behavior is observed, for instance, during the *C. elegans* one-cell stage division and in the cells of the amnioserosa during the initial phase of

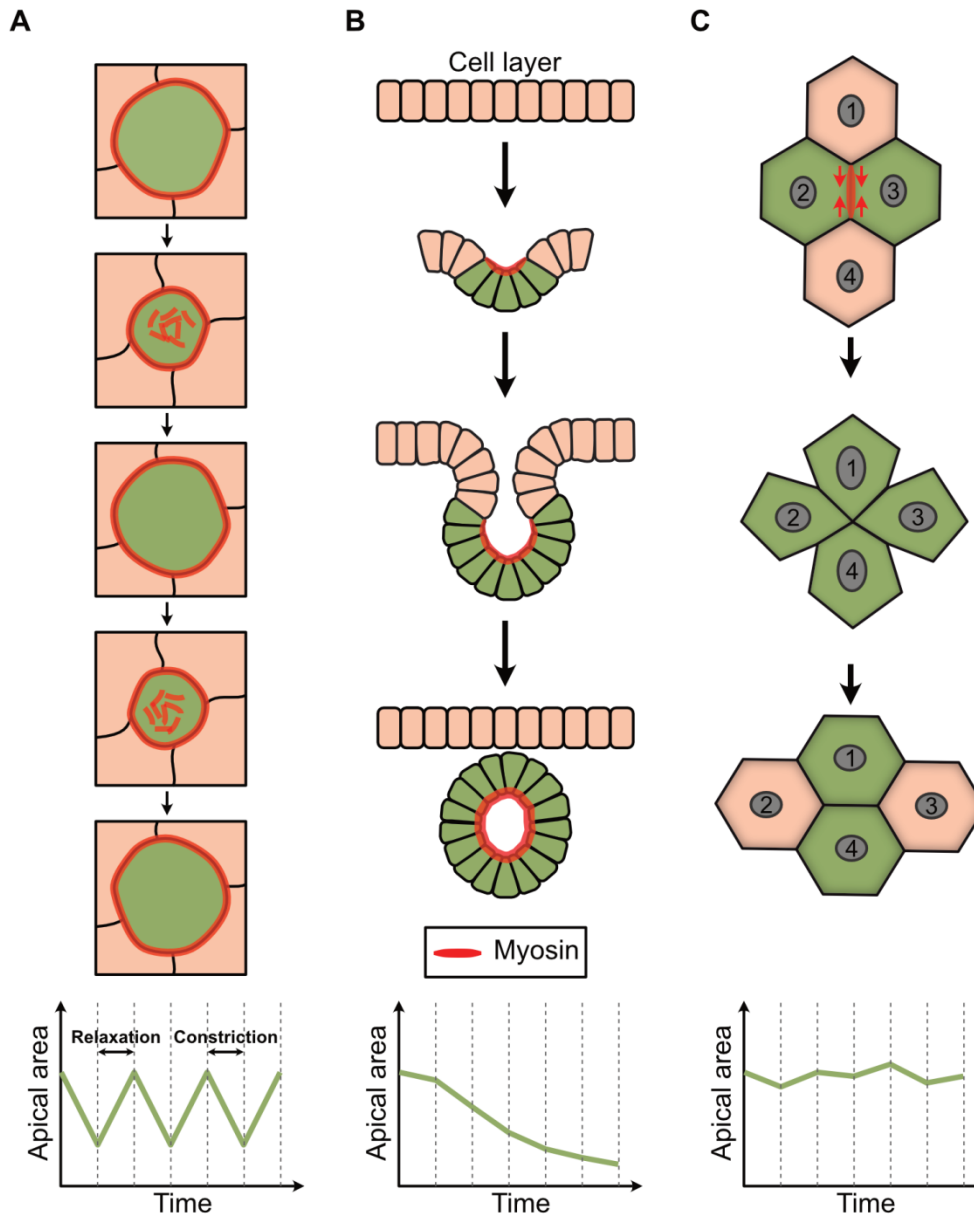


Figure 4.2: Myosin contractility in cell behaviors and in morphogenesis

(A) Representation of the pulsatile behavior of a cell. Myosin localizes to the cell cortex and constricts it. However, when myosin is released from the cortex or is inactivated by phosphatases, the plasma membrane returns to its original size. This is also represented in the graph shown below. (B) Diagram showing tube formation (example: neural tube). The apical areas of some cells in a sheet decrease over time (also see the graph below), which leads to the invagination of the sheet and the formation of a tube. (C) Representation of cell intercalation. Through the contractile action of myosin on selected cell-cell interfaces, those interfaces are eliminated, and new ones are formed, leading to change of cell neighbors. In the example shown, cells 2 and 3 are neighbors in the initial stage, whereas at the end, cells 1 and 4 are neighbors. Cell intercalation is often not associated with a change in the apical cell area (graph below).

dorsal closure in *D. melanogaster* (Franke et al. 2005; Blanchard et al. 2010). Pulsatile behavior of cells can lead to cytoplasmic streaming and is also often associated with segregation of cell fate determinants.

On the other hand, upon the disengagement of myosin from the actin filaments, in many cases, the interfaces do not revert back to their original sizes. This happens when other force generators, such as cadherins, reinforce the ‘new’ contracted interface as the myosin motor disengages. In such a scenario, the interface remains shortened. This is referred to as a contractile behavior of myosin (the interface and the plasma membrane contract). Contractility is required to alter the shape of a cell and that of the tissue; for example, selective contraction of cell-cell interfaces along one axis often leads to an expansion of the interfaces along an axis that is orthogonal to it (**Fig. 4.2C**). This enables cell behaviors, such as intercalation (Irvine and Wieschaus 1994; Bertet et al. 2004; Blankenship et al. 2006; Gorfinkiel and Blanchard 2011). Myosin-based contractility also regulates other cell behaviors, for instance apical constriction, which is essential in processes such as tissue folding and tube formation during animal development (Martin *et al.* 2009) (**Fig. 4.2B**).

During cell division, specifically, myosin accumulates at the cleavage furrow and leads to the constriction of the cleavage furrow, which pinches off the two daughter cells to mark the end of cytokinesis. However, from this study and other recent studies, it is now becoming increasingly clear that myosin not only separates two daughter cells during cell division but also governs their sizes by establishing division asymmetry at least in some *C. elegans* and *D. melanogaster* neuroblasts.

4.3 NMY-2 may play an important role in the asymmetric division of the QL.p neuroblast.

It has been shown previously that QL.p divides asymmetrically through a mechanism that is dependent on asymmetric spindle positioning, whereas its sister, QL.a, divides asymmetrically in a spindle-independent manner (Ou et al. 2010). On the other hand, the motor protein myosin has been suggested to be responsible for the asymmetric division of QL.a but not for that of QL.p (Ou et al. 2010). Ou et al showed that the *C. elegans* ortholog

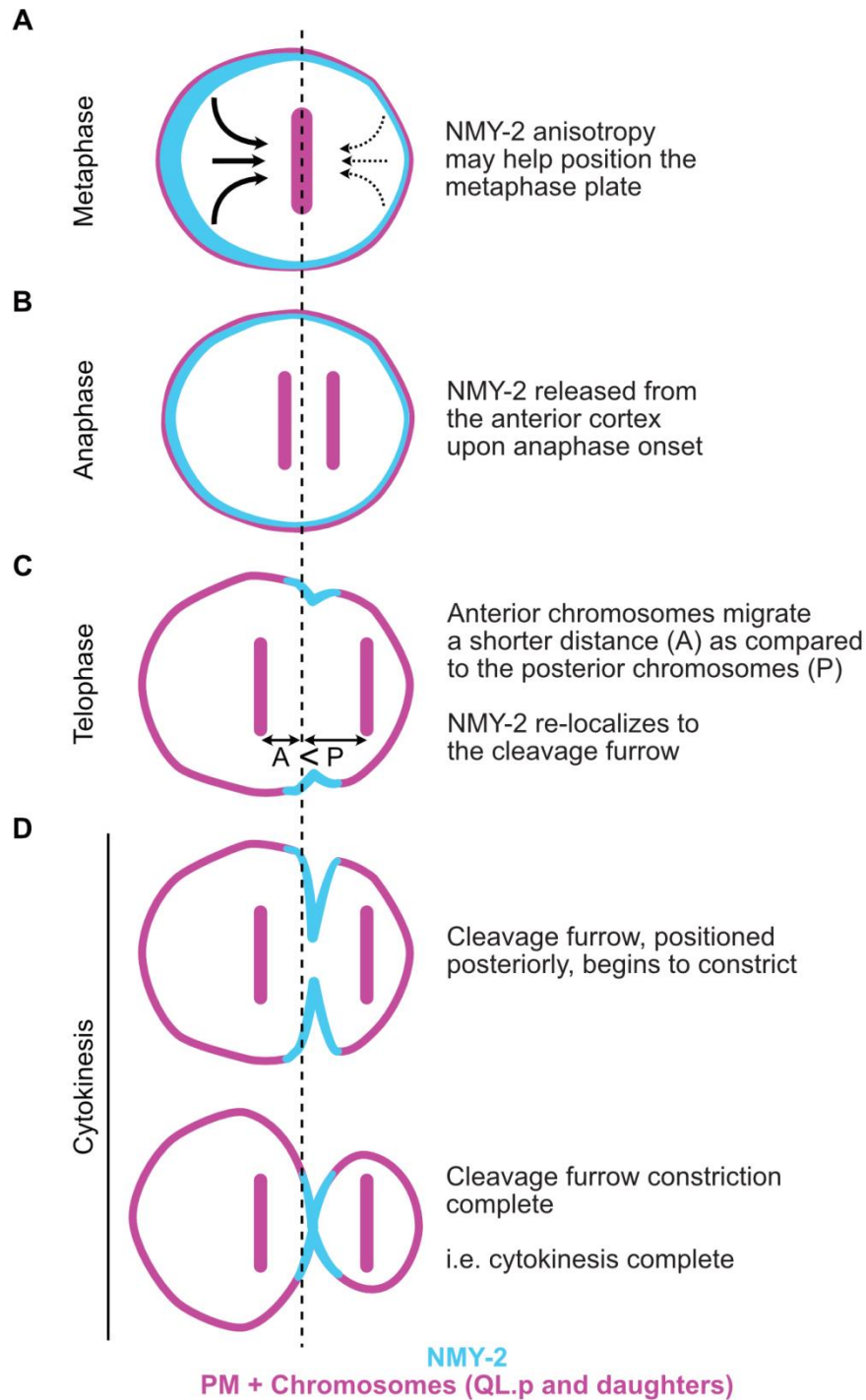


Figure 4.3: Mechanism for asymmetric QL.p division

(A) During QL.p metaphase, more NMY-2 localizes to the anterior cortex as compared to the posterior cortex. This likely helps to position the metaphase plate posteriorly. (B) Upon anaphase onset, NMY-2 from the anterior cortex is released, and (C) begins to localize at the cleavage furrow. The chromosomes move apart, such that the anterior chromosomes move a longer distance, causing a shift in the position of the cleavage furrow toward the posterior pole. (D) Cleavage furrow constricts to complete an asymmetric QL.p division.

of non-muscle myosin heavy chain, NMY-2, asymmetrically localizes to the cortex of QL.a undergoing cytokinesis and that this asymmetry is determinative to the asymmetric division of QL.a. On the contrary, no such asymmetry was detected during QL.p cytokinesis. In *Drosophila* neuroblasts that divide asymmetrically, it has been shown that the apical cortex of neuroblasts that produce a larger apical daughter cell have a greater amount of myosin II as compared to the basal cortex when the neuroblast is at metaphase (Connell et al. 2011; Roubinet et al. 2017; Tsankova et al. 2017). Upon anaphase onset, this myosin II is released, which results in the release of tension at and the expansion of the apical cortex and leads to the generation of a larger apical daughter cell (Tsankova et al. 2017). In those neuroblasts, however, the spindle is positioned symmetrically (Cabernard et al. 2010). Interestingly, I find that QL.p employs a combination of both asymmetric spindle and anisotropic myosin to divide asymmetrically. My results show that, while QL.p positions the spindle symmetrically during metaphase, it shows unequal chromosome migration during anaphase, as has been reported for the *C. elegans* one-cell embryo (**Fig. 4.3A-C**). This inequality in the distances migrated by each set of chromosomes leads to a shift in the position of the cleavage furrow toward the posterior (**Fig. 4.3C**). In addition, similar to *Drosophila* neuroblasts, NMY-2 is anisotropic during QL.p metaphase – more NMY-2 is present at the anterior cortex, which later produces the larger daughter, QL.pa (**Fig. 4.3A**). Upon anaphase onset, NMY-2 from the anterior cortex is released, presumably leading to the release of contractile forces, which prevent the expansion of the anterior cortex (**Fig. 4.3B**). This release coincides with a gradual expansion of the anterior cortex, indicating that the expansion of the anterior cortex may, in fact, be a result of the release of NMY-2 from the anterior cortex (**Fig. 4.3B-D**).

4.4 Several mechanisms may act partially redundantly of each other to regulate asymmetry in cell divisions.

Through a yeast two-hybrid screen, we identified the Rho-GEF ECT-2 as an interactor of CED-3. Preliminary biochemical analysis by Aditya Sethi, a doctoral candidate in the lab, suggests that ECT-2 may be a target of CED-3 (**Fig. 4.4A**). ECT-2 functions as a positive regulator of NMY-2 activity, which, in the QL.p lineage, seems to play a role in asymmetric cell division (**Figs. 4.3 and 4.4A**). Therefore, it is plausible that, in animals lacking *ced-3*,

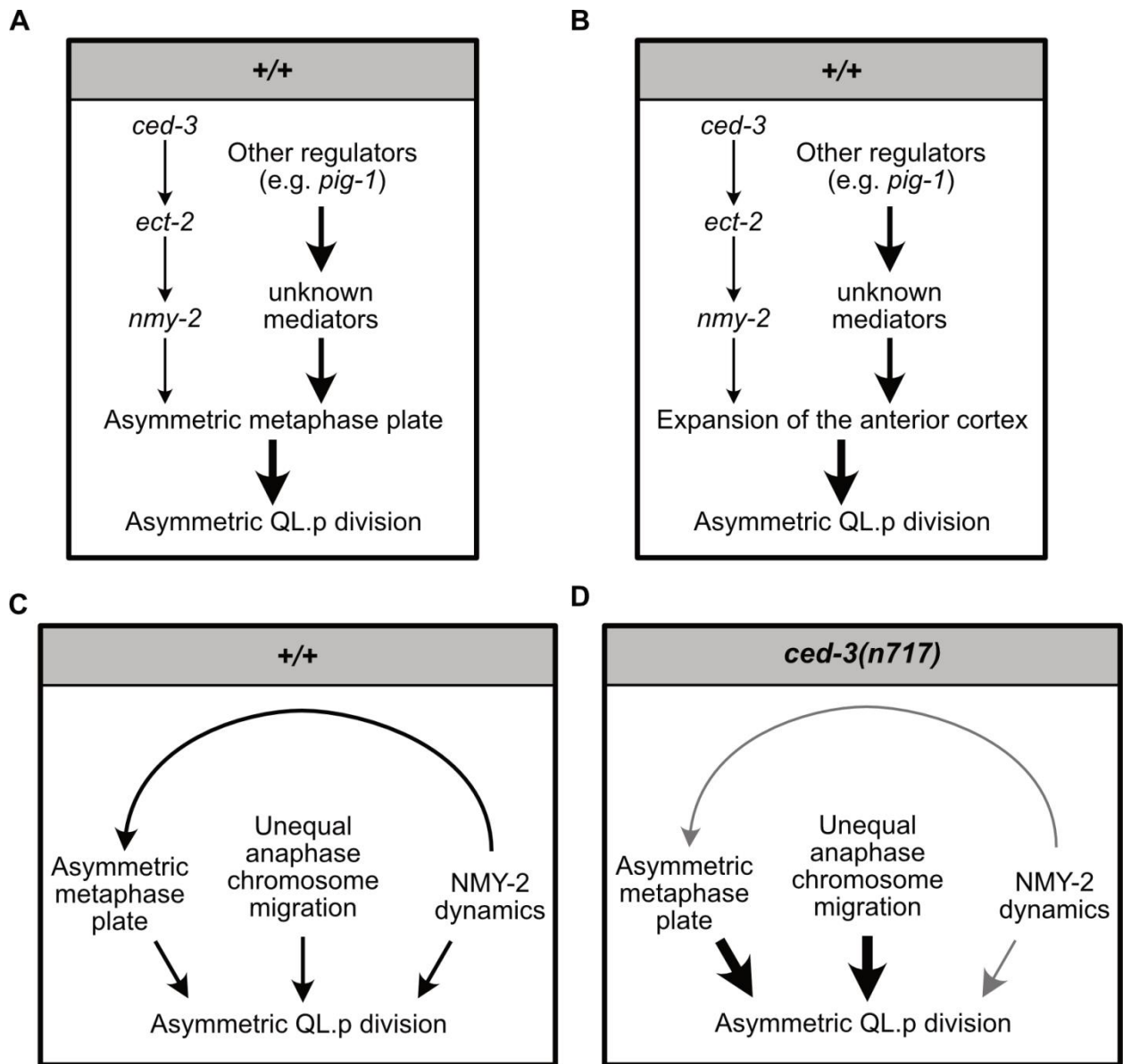


Figure 4.4: Working model for the regulation of asymmetric QL.p division by *ced-3*

(A) *ced-3* may promote NMY-2 activity through *ect-2* and govern the positioning of the QL.p metaphase plate and (B) the expansion of the anterior cortex during QL.p anaphase. Other genes, such as *pig-1*, however, may function as the major regulator. (C) Asymmetric metaphase plate, unequal anaphase chromosome migration and NMY-2 anisotropy and dynamics may together establish asymmetry in QL.p division in wild type. (D) In animals lacking *ced-3*, NMY-2 may be inactive (grey arrows), which may necessitate a larger contribution (thick black arrows) from asymmetric metaphase plate and unequal chromosome migration in determining daughter cell size.

NMY-2 activity may be reduced. This may result in a reduction in the QL.p division asymmetry (**Fig. 4.4B**).

Additional observations suggest that the NMY-2 activity may be reduced in *ced-3(lf)* animals. Specifically, I found that, in wild-type animals, the QL.p daughter cell size asymmetry does not correlate with spindle asymmetry during metaphase or anaphase or with the NMY-2 asymmetry during metaphase. This could mean that none of the three factors play a dominant or a stand-alone role in determining the daughter cell size asymmetry (**Fig. 4.4C**). On the other hand, interestingly, in animals lacking *ced-3*, the QL.p daughter cell size asymmetry directly and strongly correlates with spindle asymmetry both during metaphase and anaphase but not with the metaphase NMY-2 asymmetry (**Fig. 4.4D**). These observations hint toward a possibility where the NMY-2 activity may be reduced in *ced-3(lf)*, thus necessitating a larger role of spindle asymmetry in establishing the QL.p division asymmetry. Based on the observations presented in this thesis, I, thus, propose a model where spindle and NMY-2 asymmetries coordinate to ensure that QL.p divides asymmetrically.

4.5 The organization of an active CED-3 gradient by engulfment genes is a general phenomenon.

Upon apoptotic death, cells in *C. elegans* form a corpse, which is engulfed and degraded by one of the cells around it. The first step of this process, corpse engulfment, depends on two partially redundant parallel genetic pathways - the *ced-1* pathway, which comprises of three other genes, *ced-6*, *ced-7* and *dyn-1*, and the *ced-2* pathway, which comprises of three other genes, *ced-5*, *ced-10* and *ced-12* (Hedgecock *et al.* 1983; Ellis *et al.* 1991a; Gumienny *et al.* 2001; Zhou *et al.* 2001a; Yu *et al.* 2008). Originally it was believed that these genes are only required for the clearance of cell corpses. However, two studies in 2001 showed that they, in fact, are also required for the actual killing of the cells (Hoepfner *et al.* 2001; Reddien *et al.* 2001). For more than a decade, how the engulfment genes promote apoptosis remained an enigma. The answer to the question was provided by a study from our lab (Chakraborty *et al.* 2015). The authors showed that, in the *C. elegans* embryo, during the NSM neuroblast

division, a gradient of catalytically active CED-3 is present at metaphase. This gradient is organized in a manner that presumably favors a disproportionate segregation of the active CED-3 in the dorsal daughter cell – NSMsc, which undergoes apoptosis at approximately 21 minutes after its birth. The establishment/maintenance of this gradient was found to be dependent on both engulfment pathways. This means that, in the absence of the engulfment genes, the active CED-3 gradient was abolished, and the asymmetric segregation of active CED-3 was also presumably disrupted. Therefore, the authors proposed that the engulfment genes promote apoptosis by promoting the asymmetric segregation of active CED-3 during the NSM neuroblast division.

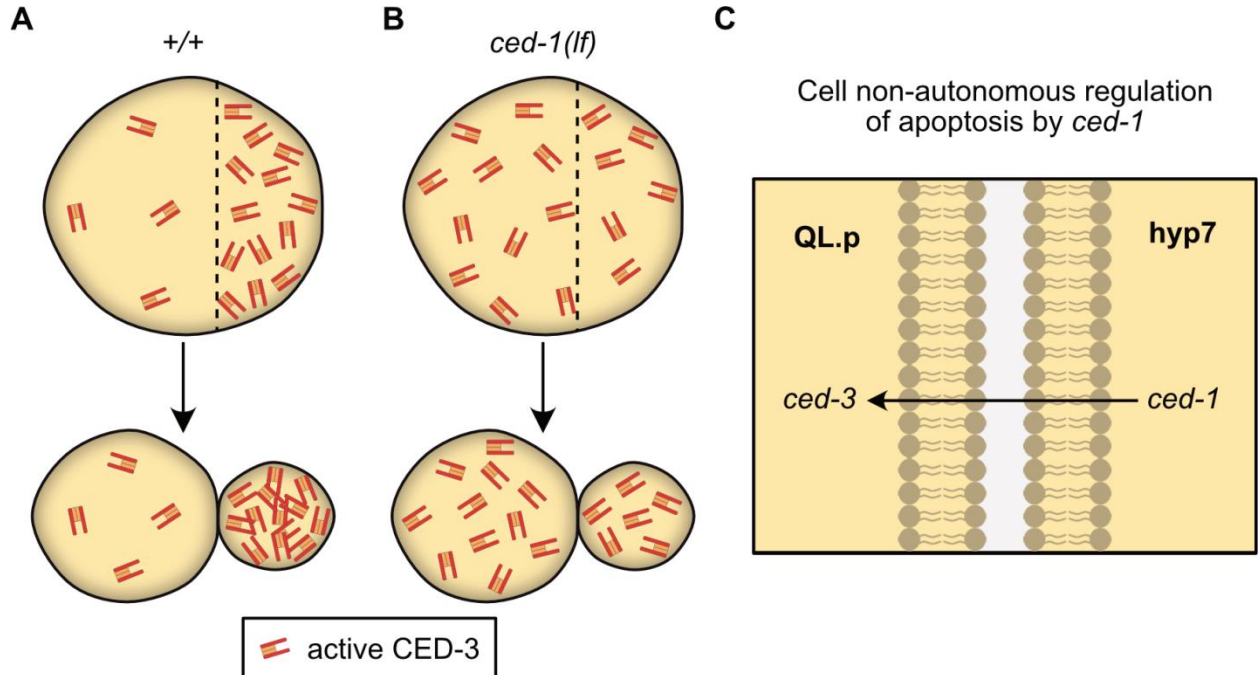


Figure 4.5: The engulfment gene *ced-1* promotes QL.pp death through cell non-autonomous regulation of active CED-3

(A) In QL.p during metaphase, active CED-3 is organized as a gradient along the anterior-posterior axis, with a higher concentration in the posterior part of QL.p. This gradient presumably favors a disproportionate segregation of active CED-3 in the posterior daughter cell, QL.pp, which is programmed to die. (B) In *ced-1(lf)* animals, the gradient of active CED-3 is abolished. This may result in both QL.p daughters inheriting similar concentrations of active CED-3. (C) *ced-1* likely functions in the engulfing cell, hyp7, to promote QL.pp death through the regulation of the active CED-3 gradient.

So far, we did not know if such a gradient is only established in the NSM neuroblast lineage or if it is a general characteristic of all lineages that produce an apoptotic daughter cell. My thesis partially addresses this question. I have shown that active CED-3 is organized as a gradient in the mother cell in at least one more cell lineage – the postembryonic QL.p lineage (**Fig. 4.5A**). I first confirmed that the engulfment genes also promote QL.pp death and discovered that they likely act in the neighboring hyp7 syncytium, which also functions as the engulfing cell, in order to do so (**Fig. 4.5C**). Specifically, CED-1 was found to be asymmetrically localized around QL.p, such that more CED-1 apposed its posterior part. Interestingly, it was the posterior part of QL.p that showed a higher concentration of active CED-3 at metaphase as compared to its anterior part (**Fig. 4.5A**). In other words, in QL.p, during metaphase, active CED-3 is organized as a gradient along the anterior-posterior axis, which would favor a higher segregation of active CED-3 in the posterior daughter, QL.pp, which dies. This gradient, similar to that in the NSM lineage, is dependent on *ced-1* (**Fig. 4.5B**). This shows that engulfment gene-dependent establishment of the active CED-3 gradient may be a general feature of cell divisions that produce an apoptotic daughter cell.

REFERENCES

- Albertson D. G., 1984 Formation of the first cleavage spindle in nematode embryos. *Dev. Biol.* [https://doi.org/10.1016/0012-1606\(84\)90117-9](https://doi.org/10.1016/0012-1606(84)90117-9)
- Anglade P., 1997 Apoptosis and autophagy in nigral neurons of patients with Parkinson's disease. *Histol. Histopathol.*
- Audhya A., F. Hyndman, I. X. McLeod, A. S. Maddox, J. R. Yates, *et al.*, 2005 A complex containing the Sm protein CAR-1 and the RNA helicase CGH-1 is required for embryonic cytokinesis in *Caenorhabditis elegans*. *J. Cell Biol.* <https://doi.org/10.1083/jcb.200506124>
- Bao Q., and Y. Shi, 2007 Apoptosome: A platform for the activation of initiator caspases. *Cell Death Differ.* <https://doi.org/10.1038/sj.cdd.4402028>
- Benjamini Y., and Y. Hochberg, 1995 Controlling the False Discovery Rate: A Practical and Powerful Approach to Multiple Testing. *J. R. Stat. Soc. Ser. B.* <https://doi.org/10.1111/j.2517-6161.1995.tb02031.x>
- Bertet C., L. Sulak, and T. Lecuit, 2004 Myosin-dependent junction remodelling controls planar cell intercalation and axis elongation. *Nature.* <https://doi.org/10.1038/nature02590>
- Blanchard G. B., S. Murugesu, R. J. Adams, A. Martinez-Arias, and N. Gorfinkiel, 2010 Cytoskeletal dynamics and supracellular organisation of cell shape fluctuations during dorsal closure. *J. Cell Sci.* <https://doi.org/10.1242/jcs.078279>
- Blankenship J. T., S. T. Backovic, J. S. S. P. Sanny, O. Weitz, and J. A. Zallen, 2006 Multicellular Rosette Formation Links Planar Cell Polarity to Tissue Morphogenesis. *Dev. Cell.* <https://doi.org/10.1016/j.devcel.2006.09.007>
- Brenner S., 1974 The genetics of *Caenorhabditis elegans*. *Genetics* 77: 71–94. [https://doi.org/10.1016/S0047-2484\(78\)80101-8](https://doi.org/10.1016/S0047-2484(78)80101-8)
- Cabernard C., K. E. Prehoda, and C. Q. Doe, 2010 A spindle-independent cleavage furrow positioning pathway. *Nature.* <https://doi.org/10.1038/nature09334>
- Chakraborty S., E. J. Lambie, S. Bindu, T. Mikeladze-Dvali, and B. Conradt, 2015 Engulfment pathways promote programmed cell death by enhancing the unequal segregation of

- apoptotic potential. *Nat. Commun.* 6: 1–9. <https://doi.org/10.1038/ncomms10126>
- Chen Y. Z., J. Mapes, E. S. Lee, R. Robert Skeen-Gaar, and D. Xue, 2013 Caspase-mediated activation of *Caenorhabditis elegans* CED-8 promotes apoptosis and phosphatidylserine externalization. *Nat. Commun.* <https://doi.org/10.1038/ncomms3726>
- Chien S. C., E. M. Brinkmann, J. Teuliere, and G. Garriga, 2013 *Caenorhabditis elegans* PIG-1/MELK acts in a conserved PAR-4/LKB1 polarity pathway to promote asymmetric neuroblast divisions. *Genetics* 193: 897–909. <https://doi.org/10.1534/genetics.112.148106>
- Chinnaiyan A. M., K. O'Rourke, B. R. Lane, and V. M. Dixit, 1997 Interaction of CED-4 with CED-3 and CED-9: A molecular framework for cell death. *Science* (80-.). <https://doi.org/10.1126/science.275.5303.1122>
- Clarke P. G. H., and S. Clarke, 1995 Historic apoptosis. *Nature.* <https://doi.org/10.1038/378230c0>
- Clarke P. G. H., and S. Clarke, 1996 Nineteenth century research on naturally occurring cell death and related phenomena. *Anat. Embryol. (Berl.)*. <https://doi.org/10.1007/BF00214700>
- Connell M., C. Cabernard, D. Ricketson, C. Q. Doe, and K. E. Prehoda, 2011 Asymmetric cortical extension shifts cleavage furrow position in *Drosophila* neuroblasts. *Mol. Biol. Cell.* <https://doi.org/10.1091/mbc.e11-02-0173>
- Conradt B., and H. R. Horvitz, 1998 The *C. elegans* Protein EGL-1 Is Required for Programmed Cell Death and Interacts with the Bcl-2-like Protein CED-9. *Cell* 93: 519–529. [https://doi.org/10.1016/S0092-8674\(00\)81182-4](https://doi.org/10.1016/S0092-8674(00)81182-4)
- Cordes S., C. A. Frank, and G. Garriga, 2006 The *C. elegans* MELK ortholog PIG-1 regulates cell size asymmetry and daughter cell fate in asymmetric neuroblast divisions. *Development* 133: 2747 LP – 2756. <https://doi.org/10.1242/dev.02447>
- D'Agostino R., and E. S. Pearson, 1973 Tests for departure from normality. Empirical results for the distributions of B and \sqrt{b} . *Biometrika.* <https://doi.org/10.1093/biomet/60.3.613>
- Ellis H. M., and H. R. Horvitz, 1986 Genetic control of programmed cell death in the nematode

- C. elegans. Cell. [https://doi.org/10.1016/0092-8674\(86\)90004-8](https://doi.org/10.1016/0092-8674(86)90004-8)
- Ellis R. E., D. M. Jacobson, and H. R. Horvitz, 1991a Genes required for the engulfment of cell corpses during programmed cell death in *Caenorhabditis elegans*. Genetics.
- Ellis R., J. Yuan, and R. Horvitz, 1991b Mechanisms And Functions Of Cell Death. Annu. Rev. Cell Dev. Biol. 7: 663–698. <https://doi.org/10.1146/annurev.cellbio.7.1.663>
- Fadok V. A., J. S. Savill, C. Haslett, D. L. Bratton, D. E. Doherty, *et al.*, 1992a Different populations of macrophages use either the vitronectin receptor or the phosphatidylserine receptor to recognize and remove apoptotic cells. J. Immunol.
- Fadok V. A., D. R. Voelker, P. A. Campbell, J. J. Cohen, D. L. Bratton, *et al.*, 1992b Exposure of phosphatidylserine on the surface of apoptotic lymphocytes triggers specific recognition and removal by macrophages. J. Immunol.
- Fisher R. A., 1921 On the “probable error” of coefficient of correlations deduced from a small sample. Metron. <https://doi.org/10.2307/1928524>
- Flemming W., 1885 Ueber die Bildung von Richtungsfiguren in Saugethiereiern beim Untergang Graaf’scher Follikel. Arch Anat Physiol 221–244.
- Franke J. D., R. A. Montague, and D. P. Kiehart, 2005 Nonmuscle myosin II generates forces that transmit tension and drive contraction in multiple tissues during dorsal closure. Curr. Biol. <https://doi.org/10.1016/j.cub.2005.11.064>
- Frøkjær-Jensen C., M. W. Davis, M. Sarov, J. Taylor, S. Flibotte, *et al.*, 2014 Random and targeted transgene insertion in *Caenorhabditis elegans* using a modified Mos1 transposon. Nat. Methods. <https://doi.org/10.1038/nmeth.2889>
- Gibson D. G., L. Young, R.-Y. Chuang, J. C. Venter, C. A. Hutchison, *et al.*, 2009 Enzymatic assembly of DNA molecules up to several hundred kilobases. Nat. Methods. <https://doi.org/10.1038/nmeth.1318>
- Gorfinkiel N., G. B. Blanchard, R. J. Adams, and A. Martinez Arias, 2009 Mechanical control of global cell behaviour during dorsal closure in *Drosophila*. Development.

<https://doi.org/10.1242/dev.030866>

Gorfinkiel N., and G. B. Blanchard, 2011 Dynamics of actomyosin contractile activity during epithelial morphogenesis. *Curr. Opin. Cell Biol.*

Gotta M., and J. Ahringer, 2001 Distinct roles for G α and G $\beta\gamma$ in regulating spindle position and orientation in *Caenorhabditis elegans* embryos. *Nat. Cell Biol.*
<https://doi.org/10.1038/35060092>

Grill S. W., P. Gönczy, E. H. K. Stelzer, and A. A. Hyman, 2001 Polarity controls forces governing asymmetric spindle positioning in the *caenorhabditis elegans* embryo. *Nature.*
<https://doi.org/10.1038/35054572>

Gumienny T. L., E. Brugnera, A. C. Tosello-Tramont, J. M. Kinchen, L. B. Haney, *et al.*, 2001 CED-12/ELMO, a novel member of the CrkII/Dock180/Rac pathway, is required for phagocytosis and cell migration. *Cell* 107: 27–41. [https://doi.org/10.1016/S0092-8674\(01\)00520-7](https://doi.org/10.1016/S0092-8674(01)00520-7)

Gurling M., K. Talavera, and G. Garriga, 2014 The DEP domain-containing protein TOE-2 promotes apoptosis in the Q lineage of *C. elegans* through two distinct mechanisms. *Development* 141: 2724–2734. <https://doi.org/10.1242/dev.110486>

Hartmann A., P. P. Michel, J. D. Troadec, A. Mouatt-Prigent, B. A. Faucheux, *et al.*, 2001 Is bax a mitochondrial mediator in apoptotic death of dopaminergic neurons in Parkinson's disease? *J. Neurochem.* <https://doi.org/10.1046/j.1471-4159.2001.00160.x>

Hatzold J., and B. Conradt, 2008 Control of apoptosis by asymmetric cell division. *PLoS Biol.* 6: 771–784. <https://doi.org/10.1371/journal.pbio.0060084>

Hedgecock E. M., J. E. Sulston, and J. N. Thomson, 1983 Mutations affecting programmed cell deaths in the nematode *Caenorhabditis elegans*. *Science* (80-.).
<https://doi.org/10.1126/science.6857247>

Hengartner M. O., R. Ellis, and H. R. Horvitz, 1992 *Caenorhabditis elegans* gene *ced-9* protects cells from programmed cell death. *Nature.* <https://doi.org/10.1038/356494a0>

- Hengartner M. O., and H. R. Horvitz, 1994 *C. elegans* cell survival gene *ced-9* encodes a functional homolog of the mammalian proto-oncogene *bcl-2*. *Cell*. [https://doi.org/10.1016/0092-8674\(94\)90506-1](https://doi.org/10.1016/0092-8674(94)90506-1)
- Hernández-Martínez R., and L. Covarrubias, 2011 Interdigital cell death function and regulation: New insights on an old programmed cell death model. *Dev. Growth Differ.*
- Hoepfner D. J., M. O. Hengartner, and R. Schnabel, 2001 Engulfment genes cooperate with *ced-3* to promote cell death in *Caenorhabditis elegans*. *Nature* 412: 202–206. <https://doi.org/10.1038/35084103>
- Howard J., and R. Clark, 2002 Mechanics of Motor Proteins and the Cytoskeleton. *Appl. Mech. Rev.* <https://doi.org/10.1115/1.1451234>
- Hunt-Newbury R., R. Viveiros, R. Johnsen, A. Mah, D. Anastas, *et al.*, 2007 High-throughput in vivo analysis of gene expression in *Caenorhabditis elegans*. *PLoS Biol.* 5: 1981–1997. <https://doi.org/10.1371/journal.pbio.0050237>
- Irvine K. D., and E. Wieschaus, 1994 Cell intercalation during *Drosophila* germband extension and its regulation by pair-rule segmentation genes. *Development*.
- Kanuka H., E. Kuranaga, K. Takemoto, T. Hiratou, H. Okano, *et al.*, 2005 *Drosophila* caspase transduces Shaggy/GSK-3 β kinase activity in neural precursor development. *EMBO J.* <https://doi.org/10.1038/sj.emboj.7600822>
- Kemphues K. J., J. R. Priess, D. G. Morton, and N. Cheng, 1988 Identification of genes required for cytoplasmic localization in early *C. elegans* embryos. *Cell*. [https://doi.org/10.1016/S0092-8674\(88\)80024-2](https://doi.org/10.1016/S0092-8674(88)80024-2)
- Kerr J. F. R., A. H. Wyllie, and A. R. Currie, 1972 Apoptosis: A basic biological phenomenon with wide-ranging implications in tissue kinetics. *Br. J. Cancer*. <https://doi.org/10.1038/bjc.1972.33>
- Liu Y., L. J. Minze, L. Mumma, X. C. Li, R. M. Ghobrial, *et al.*, 2016 Mouse macrophage polarity and ROCK1 activity depend on RhoA and non-apoptotic Caspase 3. *Exp. Cell Res.* <https://doi.org/10.1016/j.yexcr.2016.02.004>

- Maduro M., and D. Pilgrim, 1995 Identification and cloning of *unc-119*, a gene expressed in the *Caenorhabditis elegans* nervous system. *Genetics*.
- Mann H. B., and D. R. Whitney, 1947 On a Test of Whether one of Two Random Variables is Stochastically Larger than the Other. *Ann. Math. Stat.*
<https://doi.org/10.1214/aoms/1177730491>
- Martin A. C., M. Kaschube, and E. F. Wieschaus, 2009 Pulsed contractions of an actin-myosin network drive apical constriction. *Nature*. <https://doi.org/10.1038/nature07522>
- Mitani S., H. Du, D. H. Hall, M. Driscoll, and M. Chalfie, 1993 Combinatorial control of touch receptor neuron expression in *Caenorhabditis elegans*. *Development* 119: 773–83.
- Motegi F., and A. Sugimoto, 2006 Sequential functioning of the ECT-2 RhoGEF, RHO-1 and CDC-42 establishes cell polarity in *Caenorhabditis elegans* embryos. *Nat. Cell Biol.*
<https://doi.org/10.1038/ncb1459>
- Nance J., 2003 *C. elegans* PAR-3 and PAR-6 are required for apicobasal asymmetries associated with cell adhesion and gastrulation. *Development*. <https://doi.org/10.1242/dev.00735>
- Oshima K., M. Takeda, E. Kuranaga, R. Ueda, T. Aigaki, *et al.*, 2006 IKK ϵ Regulates F Actin Assembly and Interacts with *Drosophila* IAP1 in Cellular Morphogenesis. *Curr. Biol.*
<https://doi.org/10.1016/j.cub.2006.06.032>
- Ou G., N. Stuurman, M. D'Ambrosio, and R. D. Vale, 2010 Polarized myosin produces unequal-size daughters during asymmetric cell division. *Science* (80-.). 330: 677–680.
<https://doi.org/10.1126/science.1196112>
- Pearson K., 2006 Note on Regression and Inheritance in the Case of Two Parents. *Proc. R. Soc. London*. <https://doi.org/10.1098/rsp1.1895.0041>
- Peso L. Del, V. M. González, and G. Núñez, 1998 *Caenorhabditis elegans* EGL-1 disrupts the interaction of CED-9 with CED-4 and promotes CED-3 activation. *J. Biol. Chem.*
<https://doi.org/10.1074/jbc.273.50.33495>
- Pinan-Lucarre B., C. V. Gabel, C. P. Reina, S. E. Hulme, S. S. Shevkoplyas, *et al.*, 2012 The

- core apoptotic executioner proteins CED-3 and CED-4 promote initiation of neuronal regeneration in *Caenorhabditis elegans*. *PLoS Biol.* <https://doi.org/10.1371/journal.pbio.1001331>
- Radman I., S. Greiss, and J. W. Chin, 2013 Efficient and Rapid *C. elegans* Transgenesis by Bombardment and Hygromycin B Selection. *PLoS One.* <https://doi.org/10.1371/journal.pone.0076019>
- Reddien P. W., S. Cameron, and H. R. Horvitz, 2001 Phagocytosis promotes programmed cell death in *C. elegans*. *Nature.* <https://doi.org/10.1038/35084096>
- Rosenblatt J., M. C. Raff, and L. P. Cramer, 2001 An epithelial cell destined for apoptosis signals its neighbors to extrude it by an actin- and myosin-dependent mechanism. *Curr. Biol.* [https://doi.org/10.1016/S0960-9822\(01\)00587-5](https://doi.org/10.1016/S0960-9822(01)00587-5)
- Roubinet C., A. Tsankova, T. T. Pham, A. Monnard, E. Caussinus, *et al.*, 2017 Spatio-temporally separated cortical flows and spindle geometry establish physical asymmetry in fly neural stem cells. *Nat. Commun.* 8: 1–15. <https://doi.org/10.1038/s41467-017-01391-w>
- Saunders J. W., 1966 Death in embryonic systems. *Science* (80-). <https://doi.org/10.1126/science.154.3749.604>
- Schindelin J., I. Arganda-Carreras, E. Frise, V. Kaynig, M. Longair, *et al.*, 2012 Fiji: an open-source platform for biological-image analysis. *Nat. Methods.* <https://doi.org/10.1038/nmeth.2019>
- Shaham S., P. W. Reddien, B. Davies, and H. Robert Horvitz, 1999 Mutational analysis of the *Caenorhabditis elegans* cell-death gene *ced-3*. *Genetics.*
- Sherrard R., S. Luehr, H. Holzkamp, K. McJunkin, N. Memar, *et al.*, 2017 Mirnas cooperate in apoptosis regulation during *C. Elegans* development. *Genes Dev.* <https://doi.org/10.1101/gad.288555.116>
- Singhvi A., J. Teuliere, K. Talavera, S. Cordes, G. Ou, *et al.*, 2011 The arf GAP CNT-2 regulates the apoptotic fate in *C. elegans* asymmetric neuroblast divisions. *Curr. Biol.* 21: 948–954. <https://doi.org/10.1016/j.cub.2011.04.025>

- Soengas M. S., R. M. Alarcón, H. Yoshida, A. J. Giaccia, R. Hakem, *et al.*, 1999 Apaf-1 and caspase-9 in p53-dependent apoptosis and tumor inhibition. *Science* (80-.). <https://doi.org/10.1126/science.284.5411.156>
- Spearman C., 1904 The Proof and Measurement of Association between Two Things: The American Journal of Psychology. *Am. J. Psychol.* <https://doi.org/10.1037/h0065390>
- Spector M. S., S. Desnoyers, D. J. Hoepfner, and M. O. Hengartner, 1997 Interaction between the *C. elegans* cell-death regulators CED-9 and CED-4. *Nature*. <https://doi.org/10.1038/385653a0>
- Student, 1908 The Probable Error of a Mean. *Biometrika*. <https://doi.org/10.2307/2331554>
- Sulston J. E., and H. R. Horvitz, 1977 Post-embryonic cell lineages of the nematode, *Caenorhabditis elegans*. *Dev. Biol.* 56: 110–156. [https://doi.org/10.1016/0012-1606\(77\)90158-0](https://doi.org/10.1016/0012-1606(77)90158-0)
- Sulston J. E., E. Schierenberg, J. G. White, and J. N. Thomson, 1983 The embryonic cell lineage of the nematode *Caenorhabditis elegans*. *Dev. Biol.* 100: 64–119. [https://doi.org/10.1016/0012-1606\(83\)90201-4](https://doi.org/10.1016/0012-1606(83)90201-4)
- Tan J., 1992 Control of Nonmuscle Myosins by Phosphorylation. *Annu. Rev. Biochem.* <https://doi.org/10.1146/annurev.biochem.61.1.721>
- Tatton N. A., A. Maclean-Fraser, W. G. Tatton, D. P. Perl, and C. O. Warren, 1998 A fluorescent double-labeling method to detect and confirm apoptotic nuclei in parkinson's disease. *Ann. Neurol.* <https://doi.org/10.1002/ana.410440721>
- Teuliere J., S. Cordes, A. Singhvi, K. Talavera, and G. Garriga, 2014 Asymmetric neuroblast divisions producing apoptotic cells require the cytohesin GRP-1 in *caenorhabditis elegans*. *Genetics* 198: 229–247. <https://doi.org/10.1534/genetics.114.167189>
- Teuliere J., and G. Garriga, 2018 The *Caenorhabditis elegans* HAM-1 protein modifies G protein signaling and membrane extension to reverse the polarity of asymmetric cell division. *bioRxiv*. <https://doi.org/https://doi.org/10.1101/504787>

- Tompkins M. M., E. J. Basgall, W. D. Hill, and E. Zamrini, 1997 Apoptotic-like changes in Lewy-body-associated disorders and normal aging in substantia nigral neurons. *Am. J. Pathol.*
- Toyama Y., X. G. Peralta, A. R. Wells, D. P. Kiehart, and G. S. Edwards, 2008 Apoptotic force and tissue dynamics during *Drosophila* embryogenesis. *Science* (80-.). <https://doi.org/10.1126/science.1157052>
- Tsankova A., T. T. Pham, D. S. Garcia, F. Otte, and C. Cabernard, 2017 Cell Polarity Regulates Biased Myosin Activity and Dynamics during Asymmetric Cell Division via *Drosophila* Rho Kinase and Protein Kinase N. *Dev. Cell* 42: 143-155.e5. <https://doi.org/10.1016/j.devcel.2017.06.012>
- Tukey J. W., and Anonymous, 1949 Comparing Individual Means in the Analysis of Variance. *Biometrics*.
- Turek M., I. Lewandrowski, and H. Bringmann, 2013 An AP2 transcription factor is required for a sleep-active neuron to induce sleep-like quiescence in *C. elegans*. *Curr. Biol.* <https://doi.org/10.1016/j.cub.2013.09.028>
- Vogt C., 1842 Untersuchungen tiber die Entwicklungsgeschichte der Geburtshelferkroete (*Alytes obstetricans*). Jent und Gassmann, Solothurn.
- Wagener G., 1879 Bemerkungen ueber den Eierstock und den gelben Koerper. *Arch Anat Physiol* 175–200.
- Weaver B. P., Y. M. Weaver, S. Mitani, and M. Han, 2017 Coupled Caspase and N-End Rule Ligase Activities Allow Recognition and Degradation of Pluripotency Factor LIN-28 during Non-Apoptotic Development. *Dev. Cell.* <https://doi.org/10.1016/j.devcel.2017.05.013>
- Wei H., B. Yan, J. Gagneur, and B. Conradt, 2017 *Caenorhabditis elegans* CES-1 snail represses Pig-1 MELK expression to control asymmetric cell division. *Genetics* 206: 2069–2084. <https://doi.org/10.1534/genetics.117.202754>
- Wilcoxon F., 1945 Individual Comparisons by Ranking Methods. *Biometrics Bull.* <https://doi.org/10.2307/3001968>

- Xue D., S. Shaham, and H. R. Horvitz, 1996 The *Caenorhabditis elegans* cell-death protein CED-3 is a cysteine protease with substrate specificities similar to those of the human CPP32 protease. *Genes Dev.* <https://doi.org/10.1101/gad.10.9.1073>
- Yan N., J. Chai, S. L. Eui, L. Gu, Q. Liu, *et al.*, 2005 Structure of the CED-4-CED-9 complex provides insights into programmed cell death in *Caenorhabditis elegans*. *Nature.* <https://doi.org/10.1038/nature04002>
- Yee C., W. Yang, and S. Hekimi, 2014 The intrinsic apoptosis pathway mediates the pro-longevity response to mitochondrial ROS in *C. elegans*. *Cell.* <https://doi.org/10.1016/j.cell.2014.02.055>
- Yu X., N. Lu, and Z. Zhou, 2008 Phagocytic receptor CED-1 initiates a signaling pathway for degrading engulfed apoptotic cells. *PLoS Biol.* 6: 0581–0600. <https://doi.org/10.1371/journal.pbio.0060061>
- Yuan J., and H. R. Horvitz, 1992 The *Caenorhabditis elegans* cell death gene *ced-4* encodes a novel protein and is expressed during the period of extensive programmed cell death. *Development.*
- Yuan J., S. Shaham, S. Ledoux, H. M. Ellis, and H. R. Horvitz, 1993 The *C. elegans* cell death gene *ced-3* encodes a protein similar to mammalian interleukin-1 β -converting enzyme. *Cell.* [https://doi.org/10.1016/0092-8674\(93\)90485-9](https://doi.org/10.1016/0092-8674(93)90485-9)
- Zhong W., and P. W. Sternberg, 2006 Genome-wide prediction of *C. elegans* genetic interactions. *Science* (80-.). <https://doi.org/10.1126/science.1123287>
- Zhou Z., E. Caron, E. Hartweg, A. Hall, and H. R. Horvitz, 2001a The *C. elegans* PH Domain Protein CED-12 Regulates Cytoskeletal Reorganization via a Rho/Rac GTPase Signaling Pathway. *Dev. Cell.* [https://doi.org/10.1016/S1534-5807\(01\)00058-2](https://doi.org/10.1016/S1534-5807(01)00058-2)
- Zhou Z., E. Hartweg, and H. R. Horvitz, 2001b CED-1 is a transmembrane receptor that mediates cell corpse engulfment in *C. elegans*. *Cell.* [https://doi.org/10.1016/S0092-8674\(01\)00190-8](https://doi.org/10.1016/S0092-8674(01)00190-8)

CURRICULUM VITAE

NIKHIL MISHRA

Doctoral student, Conradt lab
Cell and Developmental Biology
LMU Biocenter, Grosshaderner strasse 2
Planegg-Martinsried
Bavaria-82152, Germany
Office: +49 89 2180 74220
E-mail: mishra@bio.lmu.de

Education

2015-present Ph.D. Biology | Ludwig-Maximilian-University | Munich, Germany
2014 M.Sc. Biology (by research) | Tata Institute of Fundamental Research | Mumbai, India
2011 B.Sc. Biotechnology | University of Mumbai | Mumbai, India

Scientific Training

➤ *Ludwig-Maximilians-University, Munich, Germany*

Doctoral candidate with Prof. Barbara Conradt

02/2015 - present

Investigation of non-apoptotic roles of the central apoptotic pathway in regulation of asymmetric cell divisions during *C. elegans* development

- Described a novel role of the central apoptotic pathway in promoting asymmetry in cell divisions during *C. elegans* postembryonic development.
- Showed that proapoptotic genes control both the size and the contents of cells programmed to die by acting in their mothers.
- Preliminary analyses suggest that the apoptotic genes accomplish this by influencing the Rho-GEF ECT-2, which is a key regulator of cytokinesis.

Technical skills: Single cell imaging, long-term live imaging, quantitative confocal microscopy, 4-D microscopy, cloning and DNA manipulations, genetics

Managerial skills: Mentorship, team interaction, project management

➤ *Tata Institute of Fundamental Research*

Masters (by research) student with Prof. Sandhya Koushika and Dr. V. Sriram

07/2011 - 07/2014

Investigation of the mechanism through which UNC-16, a JNK-interacting protein, limits mitochondrial density in *C. elegans* neuronal processes and the study of mitochondrial dynamics in *Drosophila melanogaster*

- Showed that UNC-16 is essential to maintain a fine balance between Kinesin-1 and Dynein motor levels available for anterograde and retrograde mitochondrial transport, respectively.

- Carried out a biochemical characterization of mitochondrial SNARE proteins and their interactions with Rab32, a small GTPase.

Technical skills: Live imaging, subcellular fractionation and mitochondria isolation, western blotting, genetics, dissection of *Drosophila* third instar larvae to obtain haemocytes, mitochondrial staining in haemocytes.

Managerial skills: Team interaction, project management, mentorship

Publications

- **Mishra, N.**, Wei, H. and Conradt, B. (2018). *Caenorhabditis elegans ced-3* Caspase is required for asymmetric divisions that generate cells programmed to die. *GENETICS*.
- Sure, G., Chatterjee, A., **Mishra, N.**, Sabharwal, V., Devireddy, S., Awasthi, A., Mohan, S. and Koushika, S. (2018). UNC-16/JIP3 and UNC-76/FEZ1 limit the density of mitochondria in *C. elegans* neurons by maintaining the balance of anterograde and retrograde mitochondrial transport. *Scientific Reports*.

Professional Experience

- Freelance editor at Cactus Communications Pvt. Ltd. 01/2017 – 02/2018

My job entailed editing scientific documents (manuscripts, theses, etc.) from clients all over the world in order to ensure that they were free of language or scientific errors and were presentable.

Fellowships

- Secured a fellowship from Studienstiftung des Deutschen Volkes to conduct my doctoral research at LMU, Munich, Germany. 09/2016 – 08/2019
- Was awarded a scholarship by the Government of India to carry out my masters' research at Tata Institute of Fundamental Research, Mumbai, India. 07/2011 – 07/2014

Achievements

- One among only 12 candidates selected for the unique M.Sc. (by research) program at the prestigious Tata Institute of Fundamental Research. The selection process involved a nationwide entrance examination (with several thousand candidates) followed by two rounds of interviews with the faculty.
- Selected for M.Sc. Biology at Jawaharlal Nehru University after a nationwide entrance examination.
- Shortlisted for interviews at the National Center for Biological Sciences to enter its integrated M.Sc.-Ph.D. program.

Experience with model organisms

- *Caenorhabditis elegans* - >7 years 07/2012 - present
- *Drosophila melanogaster* - 1 year 07/2011 – 07/2012
- Basic skills in microbiology

Other skills

- Basic familiarity with R programming language

Presentations at conferences

➤ *Oral presentations*

- Cell Polarity Signaling (Gordon Research Seminar), 2018
- Cell Polarity Signaling (Gordon Research Conference), 2018 [short talk]
- Cell Polarity and Membrane Dynamics (EMBO), 2017 [short talk]

➤ *Poster presentations*

- Bridging cell and tissue mechanics to fate specification in development (EMBO workshop), 2019, Chile
- Cell Polarity Signaling (Gordon Research Seminar), 2018, USA
- Cell Polarity Signaling (Gordon Research Conference), 2018, USA
- Cell Polarity and Membrane Dynamics (EMBO), 2017, Spain
- Cell Polarity Signaling (Gordon Research Seminar), 2016, USA
- Cell Polarity Signaling (Gordon Research Conference), 2016, USA
- Axonal Transport and Neurological Disorders, 2013, India

Mentorship and teaching

- Assisted a practical course in cell biology for B.Sc. students at LMU, Munich. 10/2018
- Mentored M.Sc. rotation students at LMU, Munich. 02/2015 – 10/2018
 - Samantha Martin (M.Sc. rotation student)
 - Samyuktha Suresh (M.Sc. rotation student)
 - Arun Kumar Sundaramurthy (M.Sc. rotation student)
 - Iulia Sorescu (M.Sc. rotation student)
 - Madeleine Premm (M.Sc. rotation student)
 - Ioannis Segos
- Mentored M.Sc. students and a Ph.D. rotation student at TIFR, Mumbai 07/2012 – 12/2014
 - Kanika Sharma (M.Sc. student)
 - Madhushree Kamak (M.Sc. student)
 - Anusheela Chatterjee (M.Sc. student)
 - Sudeepa Nandi (Ph.D. rotation student)

Voluntary service

- Volunteered to teach underprivileged high school students in Mumbai. 07/2014 – 12/2014
- Mentored underprivileged children (New Delhi, India) through Freedom English Academy, an India-based organization. 04/2019 – 08/2019

